IONIZATION IN ATMOSPHERES OF BROWN DWARFS AND GIANT GAS PLANETS

María Isabel Rodríguez Barrera

A Thesis Submitted for the Degree of PhD
at the
University of St Andrews

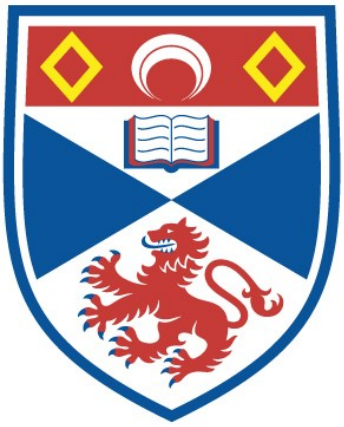

2017

Ionization in Atmospheres of Brown Dwarfs and Giant Gas Planets

by

María Isabel Rodríguez Barrera

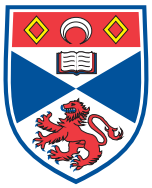

University
of
St Andrews

This thesis is submitted in partial fulfilment for the degree of Doctor of Philosophy in Astrophysics at the University of St Andrews

31th August 2016

Declaration

I, María isabel Rodríguez Barrera hereby certify that this thesis, which is approximately 18601 words in length, has been written by me, and that it is the record of work carried out by me, or principally by myself in collaboration with others as acknowledged, and that it has not been submitted in any previous application for a higher degree.

I was admitted as a research student in July 2012 and as a candidate for the degree of PhD in September 2012; the higher study for which this is a record was carried out in the University of St Andrews between 2012 and 2016.

Date Signature of candidate

I hereby certify that the candidate has fulfilled the conditions of the Resolution and Regulations appropriate for the degree of PhD in the University of St Andrews and that the candidate is qualified to submit this thesis in application for that degree.

Date Signature of supervisor

Copyright Agreement

In submitting this thesis to the University of St Andrews I understand that I am giving permission for it to be made available for use in accordance with the regulations of the University Library for the time being in force, subject to any copyright vested in the work not being affected thereby. I also understand that the title and the abstract will be published, and that a copy of the work may be made and supplied to any bona fide library or research worker, that my thesis will be electronically accessible for personal or research use unless exempt by award of an embargo as requested below, and that the library has the right to migrate my thesis into new electronic forms as required to ensure continued access to the thesis. I have obtained any third-party copyright permissions that may be required in order to allow such access and migration, or have requested the appropriate embargo below.

The following is an agreed request by candidate and supervisor regarding the electronic publication of this thesis: Access to Printed copy and electronic publication of thesis through the University of St Andrews.

Date Signature of candidate

Date Signature of supervisor

Acknowledgements

I would like to dedicate this work to parents, mostly to my father, who was close to me until the last day of his life and who always took care of me and my daughter and who taught me to be strong and perseverant.

Also I want to dedicate this thesis to my partner who has been supporting me, loving me, listening to me and giving me the strength to persevere and to believe in myself during all this time.

I would like to hugely thank my supervisor Christiane Helling who gave me the opportunity to do a PhD and start a new chapter of my life here, in Scotland. Thanks for her support, for her help and her many tips received, not only on academics issues but also on personal matters.

Thank you to the members of the LEAP group: Gabriella, Graham, Paul, Craig, Irena who helped me with my theoretical background in my first years, by giving me good feedback on my work and helping and supporting me in different ways. Thank you also to Irina Leonhardt for the time and the help that she offered to me when I needed it.

Thank you to Kenny for giving the chance to use his code (MCRT) for my research and also for his help and support.

Thank you to Jane Brooks from the IELS for her support as my English tutor and also for her unconditional listening. Thank you to Aleks for his suggestions on my thesis.

Thank you to my office mates: William, Laura, Romas, Gerardo, Milena and Graham to make everyday work so pleasant.

Thank you to Sergio Fonti, Keith Horne, Martin Dominic, HongSheng Zhao and Donald McEwan for their support during the last few years.

I am very grateful to my entire beloved family, in Tenerife and in Italy, who have always supported me specially for the last few years, caring and loving me.

Thank you to little angel, my daughter Laura, who has given me the strength to go on. I

wanted to show her that we have to move on despite the obstacles we can find along our way. She has taught me how to be a better person and a better mum.

A huge thank you to Aurora, Laura, Milena and Gabi for their unconditional friendship, help and support with my daughter and myself. They made my everyday life a little easier during the most difficult moments.

I would like to extend my gratitude to Scott, Barbara and David Ross for their pleasant conversations, and to all other people who, in one or another way, have helped to make my stay in St Andrews nicer.

To all people who care about me : THANK YOU SO MUCH !!!!

Abstract

Recent observations of ultra-cool objects suggest that the gas in their uppermost atmospheres is heated, ionised and magnetised to levels that radio and X-ray emission is possible. *The aim of this work is to identify which low mass objects are most susceptible to plasma and magnetic processes by the effect of thermal ionisation and Lyman continuum photoionisation from the irradiation of external sources in different environments.* I focus my work on very low mass, ultra-cool objects (late M-dwarfs, brown dwarfs and giant gas planets: $T_{eff} = 1000 \ldots 3000\,K$) to analyse the electrostatic and magnetic character of these atmosphere. This work has been carried out in two distinct parts:

a) A reference study to identify which ultra-cool objects are most susceptible to plasma and magnetic processes considering the thermal ionisation as the only mechanism to ionise the atmospheric gas. This presents a theoretical framework using a set of fundamental parameters to analyse the ionisation and magnetic coupling state of objects with ultra-cool atmospheres. The DRIFT-PHOENIX model atmosphere simulations are used to determine the local gas properties T_{gas} [K], p_{gas} [bar], p_e [bar] of the atmospheres structures from the global parameters T_{eff} [K], log(g) [$cm\,s^{-2}$] and [M/H]. Electrostatics interactions dominance over electron-neutral interactions increases as T_{eff} increases: throughout the M-dwarf atmospheres, almost for the whole brown dwarf atmospheres and only giant gas planets with T_{eff}=1200 K, log(g)=3.0, [M/H]=+0.3 fulfil that criterion at the most deeper atmosphere. A magnetised gas is found for M-dwarfs, brown dwarfs and giant gas planet atmospheres even for those with a small degree of ionisation except to the most deeper atmospheric regions. Hence, the upper atmosphere of all of studied objects can be magnetically coupled. A large fraction of the atmospheric volume of M-dwarfs and of early spectral subtypes of brown dwarfs is found to occur plasma processes and magnetised gas, and are therefore the best candidates to emit in H_α and radio wavelengths.

b) An analysis of how the Lyman continuum external irradiation effect the plasma and magnetic state of an ultra-cool atmospheres in additional thermal ionisation. The Monte Carlo radiative transfer code simulations provide the atmospheric ionisation structure

due to photoionisation. Three different cases are studied to see the effect of the Lyman continuum irradiation given by an external source: free-floating ultra-cool objects irradiated by Lyman continuum photons from the interstellar medium (dominated by Galactic O and B stars), brown dwarfs in star forming regions irradiated by a nearby (few parsecs) O star and binary systems where a brown dwarf atmosphere is photoionised by a companion white dwarf. The effect of Lyman continuum irradiation from external sources greatly increases the level of ionisation in the uppermost atmospheric regions. Brown dwarfs in star forming regions and brown dwarfs in binary systems with a companion white dwarf have upper atmospheres that are close to being fully ionised. Adopting temperatures typical for a chromosphere or a corona, the resulting free-free X-ray luminosities are found to be comparable with those observed from brown dwarfs in star forming regions. The results of this study show that it is not unreasonable to expect powerful energy emissions from brown dwarf atmospheres.

The conclusions of this study are that the thermal ionisation allows the establishment of a magnetised plasma in brown dwarf atmospheres as in particular the rarefied upper parts of the atmospheres despite having low degrees of thermal gas ionisation and that the Lyman continuum photoionisation allows to argue for a chromosphere/corona on brown dwarfs and for X-ray emissions from ultra-cool objects. However, other mechanisms, like Alfvén wave heating, are needed to occur which then lead to rise the local gas temperature in the chromosphere/corona on brown dwarfs.

Contents

1

Introduction

Powerful emissions (radio, H_α and X-ray) have been observed in low mass objects like brown dwarfs, despite their low effective temperatures. The mechanisms that lead to those observations are not well understood yet. The presence of a chromosphere could explain such emissions. *The aim of this work is to identify which low mass objects are most susceptible to plasma and magnetic processes by the effect of thermal ionisation and Lyman continuum photoionisation from the irradiation of external sources in different environments.* This study consists of two distinct parts: a) A reference study where a theoretical framework is developed to assess the plasma and magnetic parameters in M-dwarfs, brown dwarfs and giant gas planets assuming that the thermal ionisation is the only mechanism to ionise the atmospheric gas (Chapter 2). b) The study of the effect of Lyman continuum photoionisation on M-dwarfs, brown dwarfs and giant gas planets (Chapter 3) applying the same frame work developed in Chapter 2. The possibly resulting free-free X-ray luminosities are calculated. A comparison between the effect of thermal ionisation and Lyman continuum photoionisation is studied in Chapter 3.

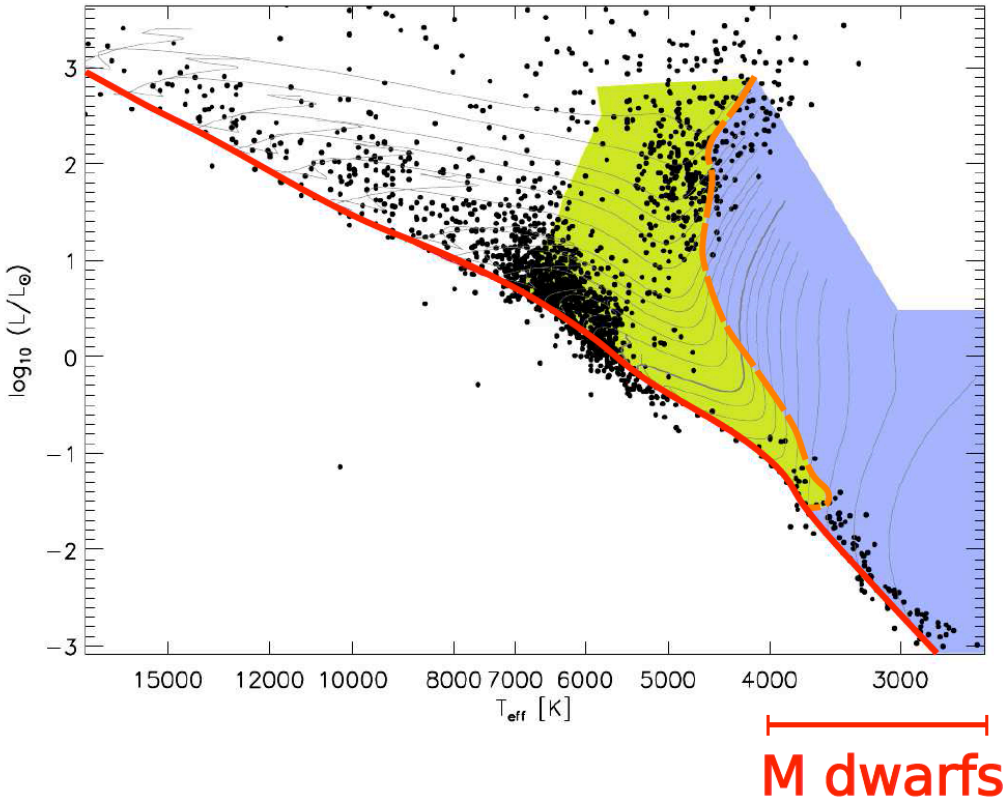

Figure 1.1: Hertzsprung Russell diagram representing the evolutionary tracks of pre-main sequence stars for masses between 7.0 . . . 0.1 M⊙ and for solar composition (black dots) (Siess, Dufour & Forestini 2000). The boundary for a fully-convective zone starts at T_{eff}= 4.100 K. The green zone represents cool stars partly convective; the blue one fully convective objects. M-dwarfs are located at the end of the main sequence (Morin 2012).

1.1 Low mass and ultra-cool objects

This work focuses on low mass objects as M-dwarfs, brown dwarfs and giant gas planets. Brown dwarfs evolve from young objects with an effective temperature between $T_{eff} \approx 3000$ K (M-dwarfs) and $T_{eff} \approx 500$ K (giant gas planets) with a surface gravity of $\log(g)$=3.0 . . . 5.0 cm s^{-2} (see Sec. 5.1). They are placed in the lower right corner of the Hertzsprung Russell diagram (Fig. 1.1). High energy events have been observed in their spectra but, the mechanisms that generates such powerful emissions are not known yet. In Figure 1.1, M-dwarfs are represented as fully-convective objects. Brown dwarfs are also fully-convective objects but, are not included in this diagram. The spectra of very low-mass objects with low temperature and high surface gravity shows a complex chemistry: high surface gravity increases the probability for collision of particles and therefore the formation of molecules as CH_4; low temperatures favour the recombination reactions of the many different chemical elements present in the

atmospheric gas. For example, in the atmospheres[1] of T-dwarfs the alkali metals like K, Na, Cs and molecules as CO or H_2O are predominant (Burrows et al. 2001). Therefore, M-dwarfs, brown dwarfs and giant gas planets are classified through different spectral types that depend not only on the effective temperature but, also on the surface gravity and on the metallicity.

Brown dwarfs and giant gas planets form clouds in their atmospheres which have strong feedback onto the atmospheric structure due to element depletion and due to a high opacity (Helling & Casewell 2014 and references there in). Observations by Buenzli et al. (2014), Crossfield et al. (2014) and Biller et al. (2013) for example, suggest that brown dwarf atmospheres show a patchy cloud coverage. Transit spectroscopy from extrasolar planets suggest that giant gas planets are covered in hazes and clouds too (Pont et al. 2008; Gibson et al. 2012; Sing et al. 2014). Also model simulations suggest that cloud formation prevails for a large range of effective temperatures up to 2800 K, and for metallicities as low as $[\mathrm{M/H}] = -5.0$ (Witte, Helling & Hauschildt, 2009). Helling et al. (2013) suggest that a significant volume of these clouds is susceptible to local discharge events: large-scale discharges in the upper cloud regions and corona-like small-scale discharges in the inner, denser part of the cloud. These local discharge events may generate atmospheric electrical storms. At the same time, storms may ionise the local gas. For example, Luque et al. (2014) model the ionosphere of Saturn and Jupiter finding that the atmospheric electrical storms may produce up to 10^3 cm^{-3} of free electrons below the ionosphere. Brown dwarfs are complex objects with an interplay between gas and cloud chemistry and large-scale processes like magnetic coupling and electric activity.

1.1.1 M-dwarfs

Late M-dwarfs are considered the lowest limit of hydrogen burning stars ($\sim 0.08\,\mathrm{M}\odot$). The M-dwarfs have effective temperatures of $4000 \ldots 2000$ K, surface gravity values of $3.0 \ldots 4.0$ $\mathrm{cm\,s}^{-2}$ and masses of approximately between $0.6 \ldots 0.08\,\mathrm{M}_\odot$ (Reid & Hawley, 2000) and are located at the bottom-right position the Hertzsprung-Russell diagram due to low luminosity and temperature (see Fig. 1.1). M-dwarfs have TiO and VO bands which dominate the optical spectra and also are used to characterise their atmospheres. The transition between M-dwarf and L-dwarf (brown dwarfs) regime is characterised by the lack of metal oxide bands and the presence of metal hybrid bands in their spectra (Berger et al. 2008). The transition M-L dwarfs

[1]The brown dwarf atmosphere is define based on the concept of optical depth (τ): the top of the atmosphere is set up with an optical depth of $\tau = 0$ and the bottom with τ=1.

have effective temperatures between 2000 K-1400 K, surface gravity values of $\log(g)$= 3.0-5.0 cm s^{-2} and masses of 0.1M$_\odot$ ... 0.08M$_\odot$ (Reid & Hawley 2000). M-dwarfs are considered fully convective: the energy produced in their interior is transported by convection process to higher layers.

1.1.2 Brown dwarfs: L, T and Y type dwarfs

The term 'Brown dwarfs' was introduced by Tarter (1975). It was used to name low-mass objects with properties intermediate between 'black dwarfs' (the last stage of white dwarf cooling) and 'red dwarfs' (bright in IR). The term of 'brown dwarf' was used to describe objects with very low luminosity and mass, unable to burn hydrogen. Indeed, two decades later the first brown dwarf, Gliese229B as a T6.5 dwarf was discovered by Nakajima et al. (1995) followed by Teide 1 classified as an M8 dwarf by Rebolo, Zapatero Osorio & Martín (1995). It is well known that Sun like stars were formed by gravitational collapse of molecular clouds and planets from the residue of this process (circumstellar disk of the protostellar nebula). Brown dwarfs likely were formed like stars, however, very low mass brown dwarfs could have masses and effective temperatures similar to high mass giant gas planets (Oppenheimer, Kulkarni & Stauffer 2000). Also the possibility that massive protoplanetary disks could form brown dwarfs in a planet-way has not been excluded (Boss 2011). Brown dwarfs are considered the link between stars and planets, however, the formation process of brown dwarfs and planets marks the difference between both objects: different chemical composition, initial mass function and orbital eccentricities (Reid & Hawley 2000). The spectral type classification of brown dwarfs involves L, T and Y dwarfs. The last two ones may have similar planetary regime characteristics: effective temperatures varying between T_{eff}=2000 ... 500 K and masses between 0.08 ... 0.01M$_\odot$ (Reid & Hawley, 2000). Brown dwarfs are characterised with a magnetic flux strength of B$\approx 10^3$ G (0.1 T) (Shulyak et al. 2011). Young brown dwarfs spectra show a strong Li absorption lines. This feature is a well defined indicator of a young brown dwarf candidates (Reid & Hawley, 2000).

High energy emissions from brown dwarfs have been reported in the last few years (see Sec. 1.2), many of those emissions are at radio wavelengths, even for ultra cool brown dwarfs (T-dwarfs) (Route & Wolszczan 2016, Berger 2002), however, the emission at X-ray wavelengths start to decline for L-type dwarfs (Williams et al. 2014). The evidence of high energy emissions suggest that a chromosphere and magnetised plasma must be present (Schmidt

et al. 2015; Rodríguez-Barrera et al. 2015; Sorahana, Suzuki & Yamamura 2014). The atmospheric gas needs to be fully or partly ionised to reach the criteria to be a plasma (Sec 2.2) and the plasma needs to be magnetised (see Sec. 2.4) to explain such emission from brown dwarfs. A plasma is a gas that can be partial or fully ionised but, retains the overall quasi-neutral balance of the charges which exhibits collective behaviour. Young brown dwarfs are more active than older ones as it happens for M-type dwarfs.

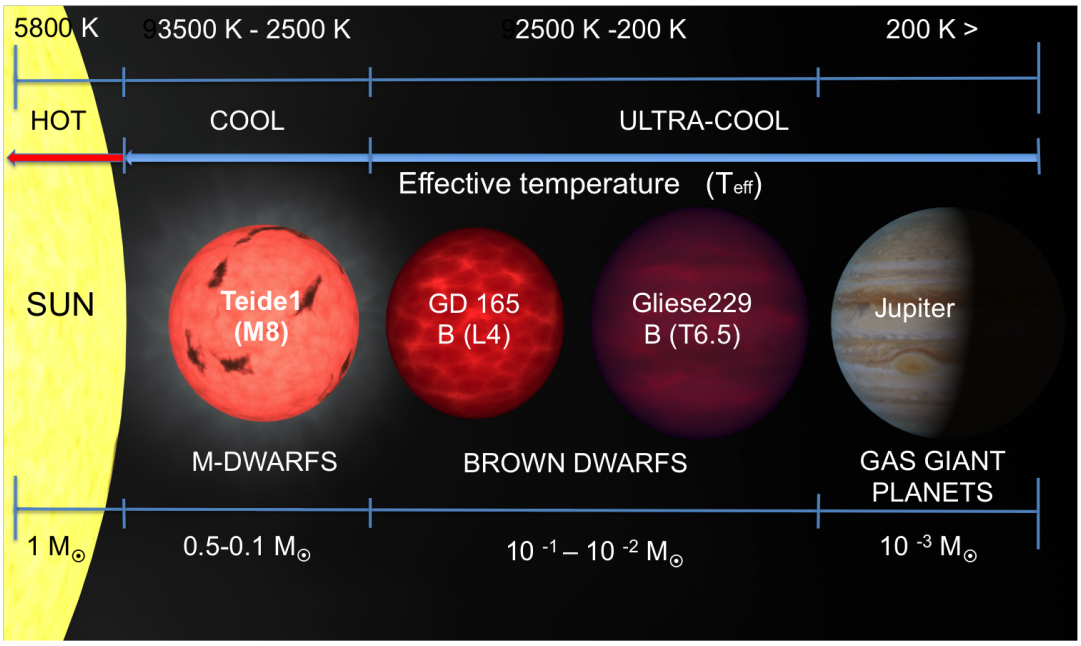

Figure 1.2: The effective temperature versus mass. The objects represented in this figure cover objects from Sun-like to giant gas planets. This picture has been built by Isabel Rodríguez-Barrera based on an artist's conception by NASA/ARC/Robert Hurt.

Hydrogen fusion in brown dwarfs: young brown dwarfs might be confused with old low mass stars that remain stable in the main sequence phase. Brown dwarfs cool down with time reaching effective temperatures similar or below that of the old low-mass stars have in the later stages of their life. Brown dwarfs have masses below the hydrogen-burning limit of ~ 0.08 $M_\odot$ and temperatures below 3000 K (e.g. Burrows et al. 2001) not having sufficient mass to achieve the required core temperature to provide a steady rate of nuclear hydrogen fusion. The nuclear reactions take place in the core of the stars at temperatures of $T_{gas} \approx 2 \cdot 10^7$ K. For a mass of M= 0.08 $M_\odot$ the core temperature is $T_c = 6.4 \cdot 10^6$ K ($\sim$1 Gyr)(Burrows et al. 2001). This temperature is not enough to achieve hydrogen fusion in the core of a L-dwarf with M= 0.08 $M_\odot$. However, brown dwarfs may have thermonuclear

reactions for a short time. Objects with M $\geq 0.01 M_{\odot}$ will burn deuterium and objects with M $\geq 0.06 M_{\odot}$ will burn lithium via absorption of a proton (Burrows et al. 2001):

- Deuterium : $p + d \rightarrow \gamma + {}^{3}He$
- Lithium: $p + {}^{7}Li \rightarrow 2\alpha$ and $p + {}^{6}Li \rightarrow \alpha + {}^{3}He$

As a consequence, the gravitational collapse provides the only energy source for most of the brown dwarf's lifetime. Cooling and contracting during their entire life, brown dwarfs cannot compensate for the radiative losses by thermonuclear processes.

1.1.2.1 L-dwarfs

L-dwarfs have effective temperatures between 2100 ... 1150 K, log(g)= 4.5-5.5 cm s^{-2} and masses between 0.08 ... 0.06$M_{\odot}$ (Reid & Hawley, 2000). L-dwarfs show metal hydride bands due to CaH, FeH, CrH and MgH in their spectra. Absorption lines from CO and H_2O, neutral alkali metals such as K, Na or molecules such as CsI and RbI are observed as well. The presence of CO and water indicates that L-dwarf atmospheres are very cool. Dust grains are formed from different materials like Mg_2SiO_4[s], SiO_2[s], Al_2O_3[s], Fe[s], TiO_2[s] among others raising the opacity index. The composition of some gaseous species as TiO and VO are reduced by the dust formation process increasing the opacity of the gas (Helling, Woitke & Thi 2008; Helling & Woitke 2006). A strong feature of mid L-dwarfs is the influence of the dust clouds on the atmosphere's structure (Witte et al. 2011). The presence of FeH and H_2O absorption bands lines is stronger than in late-L and T-dwarfs. L-T dwarfs transition stars have effective temperatures between 1400 ... 900 K, surface gravity between 4.5 ... 5.0 cm s^{-2} and masses between 0.075 ... 0.06$M_{\odot}$. This transition is characterised by the occurrence of CH_4 absorption lines at near-infrared.

1.1.2.2 T and Y-dwarfs

T-dwarfs are extremely cool with effective temperatures between 900 ... 500 K, very low luminosities, log(g)= 4.0-3.0 cm s^{-2} and masses between 0.06 ... 0.01$M_{\odot}$. Spectral lines of CH_4, KI, NaI, CrI, CsI and H_2O have been detected. T-dwarf characteristics can be similar to giant gas planets in our Solar system (Reid & Hawley 2000). Y-dwarfs are the coolest dwarfs that have been found to date, with effective temperatures around T_{eff}= 300-200 K. Also the spectra of Y-dwarfs is very similar to Jupiter like with NH_3 features. Also it could be possible

also to find a weak Na I and K I resonance lines (Cushing 2014).

1.2 Observations of High Energy Emissions from Brown dwarfs

Improved instruments have made possible the observations of even lower-mass objects in the last decade. For example, the Infrared Array Camera (IRAC) on board the Spitzer Space Telescope (Fazio et al. 2004) and the Wide-Field Infrared Survey Explorer (WISE) that detected one of the coolest brown dwarfs in 2011 (CFBDSIR 1458+1013) (Wright et al. 2011).

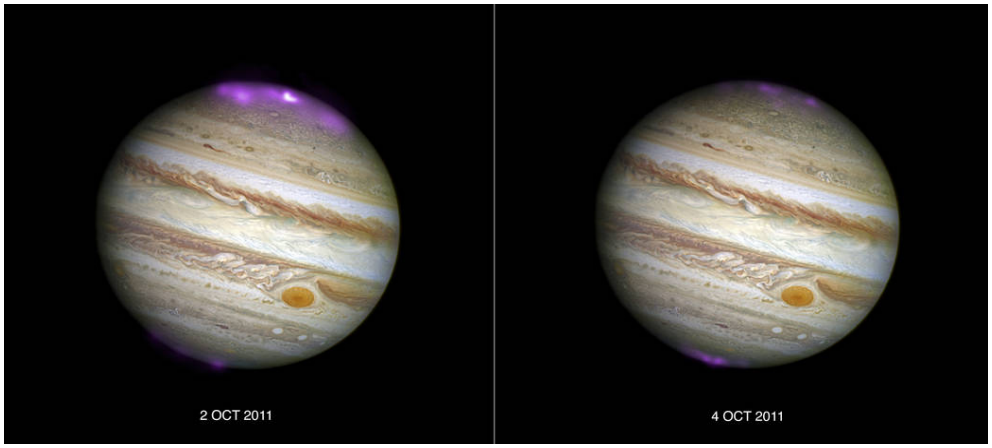

(a) Jupiter's polar aurorae produced by Solar storms. The solar wind is much stronger as it is usual compressing the Jupiter's magnetosphere boundary and trigger to the aurorae phenomena. (Image credit: X-ray: NASA/CXC/UCL/W.Dunn et al, Optical: NASA/STScI)

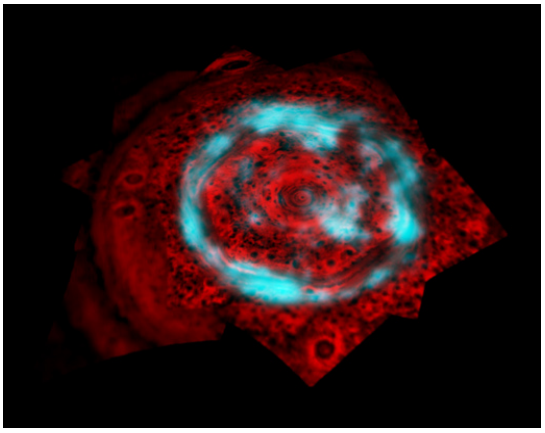

(b) The northern polar region of Saturn shows the aurora and underlying atmosphere, observed at different wavelengths (IR) captured by the Cassini spacecraft. (Image credit: NASA/JPL/University of Arizona)

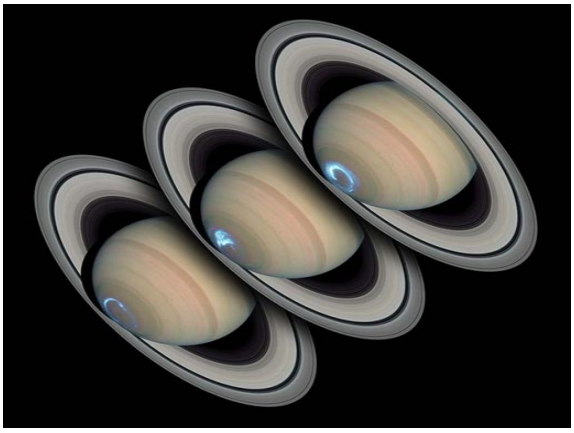

(c) Saturn's polar aurorae produced by the disturbance of the solar wind into the magnetosphere. The observations have been taken by NASA's Hubble Space Telescope during a joint campaign with NASA's Cassini spacecraft. (Image credit: NASA/Hubble/Z. Levay and J. Clarke)

Figure 1.3: Magnetic phenomena on Jupiter and Saturn.

1.2.1 Evidence of radio, H_α and X-ray emissions

Observations in radio[2], H_α[3] and X-ray[4] wavelengths from brown dwarfs have been observed and are not well explained yet, however, they indicate the existence of mechanisms that lead to the formation of a chromosphere[5]/corona[6] and that generate a large-scale magnetic field. Such observations are very common in our solar system. In the Sun, the existence of a ionised gas that leads to a plasma and the coupling with a large-scale background magnetic field sustain very high energy and violent phenomena like flares[7] and coronal mass ejection[8] in the solar chromosphere and corona (where the density is low and the temperature is high: $T_{gas}=10^5 \ldots 10^6$ K). Also aurorae and flashes happen inside the atmosphere of Jupiter, Saturn, Venus and Uranus for example. Figure 1.3 shows flashes of light and polar aurora observed in the atmosphere of Jupiter and Saturn respectively. White-flare[9] observations by Schmidt et al. (2016) (ASASSN-16ae) and Gizis et al. (2013) (W1906+40) suggest that stellar-type activity is present also in the ultra-cool stellar regime (L-dwarfs with $T_{eff} \approx 2300$ K). Pineda et al. (2016) have extracted the spectra at the optical range of 29 brown dwarfs (L4-T8 spectral type) to look for H_α lines. Radio and X-ray emission from ultra-cool dwarfs have been established, for example: the T6.5 2MASS J10475385+212423 by Route & Wolszczan (2016, 2012); brown dwarfs from M6.5 to M9.5 by Williams et al. (2014) and 2MASS J1315-2649AB by Burgasser et al. (2013). Williams et al. (2014) show that ultra-cool objects do not follow the classical Güdel-Benz relation. The Güdel-Benz relationship (GBR) (see Fig. 1.4) is the correlation between the X-ray and the radio luminosity of the coronae of different active stars (Güdel & Benz 1993). This relation was shown to persist for solar flares and active rotating binaries (Benz & Güdel 1994). The deviation of

[2]Radio emission is an electromagnetic radiation with wavelengths in the electromagnetic spectrum longer than infrared light ($\lambda > 10^{-3}$ m).

[3]H_α line: It is a Balmer serie line produced by the emission of a photon when a hydrogen electron decays from the third (n=3) to second energy level (n=2) at the red optical range (λ=656.28 nm).

[4]X-ray emission is a form of electromagnetic radiation covering a wavelength range of λ=0.01 ... 10 nm ($\lambda=10^{-11} \ldots 10^{-8}$ m) and corresponding to energies in the range 100 eV ... 100 keV.

[5]The chromosphere is a layer placed above the photosphere and less dense than it. The chromosphere can rise temperatures between $10^3 \ldots 10^4$ K. At these higher temperatures, the ambient gas can emit at wavelengths that gives off a reddish color (H_α emission or even more energetic).

[6]The corona is a layer above of the chromosphere. The high stages of ionisation of the gas in the corona indicate a plasma temperature around 10^6 K. The density of the gas could be 10^{-12} times as dense as the photosphere as happens in the corona solar).

[7]The flares are a sudden release of magnetic energy from the deeper convective layers.

[8]A coronal mass ejection (CME) is a large release of plasma and magnetic field from the solar corona. It is very common after the occurrence of a CME the ejection of a flare.

[9]White-light flares are events visible in the optical continuum that can contain very small flare kernels being the hallmark of those flares events as occur in the Sun (Jess et al. 2008). The white-light emission is generated by hydrogen recombination radiation and is correlated with hard X-ray emission (Reid & Hawley 2000).

ultra-cool stars beyond of M5 dwarfs may suggest a change in the dynamo mechanism that produces a large-scale magnetic field in such ultra-cool objects (Cook, Williams & Berger 2014). Preibisch et al. (2005b) study the X-ray properties of some brown dwarfs between M6-M9 placed in the core of the Orion Nebula Cluster (their Table 2) with a resulting X-ray luminosity of $\log L_x \approx$28.1-28.7 erg s^{-1}. Tsuboi et al. (2003) report X-ray emission during 3 hr of observation (0.1 ... 10 KeV) from the $\sim$M9 brown dwarf (T_{eff}=2500 K) as a part of a binary system (TWA 5AB) with a resulting X-ray luminosity of $L_x \approx 10^{27}$ erg s^{-1} and with plasma temperature of $T_{gas} \approx 10^6$ K. Those characteristics are common in the solar corona. They suggest that as TWA 5B is not too far away to be between the brown dwarfs and massive planets (considering the masses), it might be possible observe X-ray emissions from massive planets in their youth stages. Feigelson et al. (2003) detected 525 objects in a massive cluster (Orion nebula cluster) at the energies of 0.5 ... 8 KeV (X-rays); 144 of those objects observed are cataloged as M-dwarfs and brown dwarfs: log $(M/M_\odot) \leq$ - 0.2 (their Table 1). Also X-ray emission from very low mass brown dwarfs is reported by Feigelson et al. (2002) in the Orion nebula cluster (their Table 6). Their lowest emitting mass is >0.02 $M_\odot$ (L-T dwarfs) with a X-ray luminosity of $\log_{10} L_x$=28.9 erg s^{-1} and a plasma energy of *KT*=2.4 KeV ($\approx 2.8 \cdot 10^7$ K).

Berger (2002) observed twelve sources in radio, X-ray and H_α emission between the spectral types M8 and L3.5. Poppenhaeger, Robrade & Schmitt (2010) have analysed a sample of 72 stars within 30 pc and provided the X-ray luminosities (0.1 ... 2.4 keV). Some of those analysed objects are late M-dwarfs: VB10 with $\log_{10} L_x$=26.3 erg s^{-1} and τ Boo with $\log_{10} L_x$=28.94 erg s^{-1}. Sicilia-Aguilar et al. (2008) and Forbrich & Preibisch (2007) show that brown dwarfs in star forming regions emit X-ray luminosity of the order of $\approx 10^{28}$ erg s^{-1}. Flaccomio et al. (2003) present the mean and median of the X-ray luminosity versus the mass for stars and brown dwarfs (their Fig. 7) in the Orion Nebula Cluster showing that brown dwarfs of M=0.01 M$\odot$ have X-ray luminosity of $\approx 10^{28}$ erg s^{-1}. Kashyap, Drake & Saar (2008) present X-ray observations from stars hosting giant gas planets. Some of the objects are M-dwarfs and brown dwarfs covering M2 ... M8.5 with a X-ray luminosities of $\log_{10} L_x$=26.36 ... 31.22 erg s^{-1}. According with Flaccomio et al. (2003), X-ray emissions are increased if the mass of the object increases and for younger objects, for example in young low mass stars ($\sim$1 Myr). It is reasonable to expect that young low mass stars could be accreting objects and also have a disk but, *Could the accreting material on the surface and/or the presence of a disk in young stars emit at X-ray energies and hence, interfere with coronal X-ray emissions?*.

The accreting material on the surface of a star produces strong optical and UV emissions and might some soft X-ray (Preibisch et al. 2005a). However, Jardine et al. (2006) suggest that the presence of a disk in low mass stars reduces the magnitude of the X-ray emissions due to the crushing of the outer coronal. Also Flaccomio et al. (2003) suggest that the accreting stars have higher X-ray extinction than it is expected. In this study I am not considered accreting objects therefore, the resulting X-ray luminosity from the objects of my study is originated by the chromosphere/corona heating. If the atmospheric gas can couple to the strong magnetic field in brown dwarfs, the kinetic energy carried by large-scale convective motions may be transported to the top of the atmosphere and released.

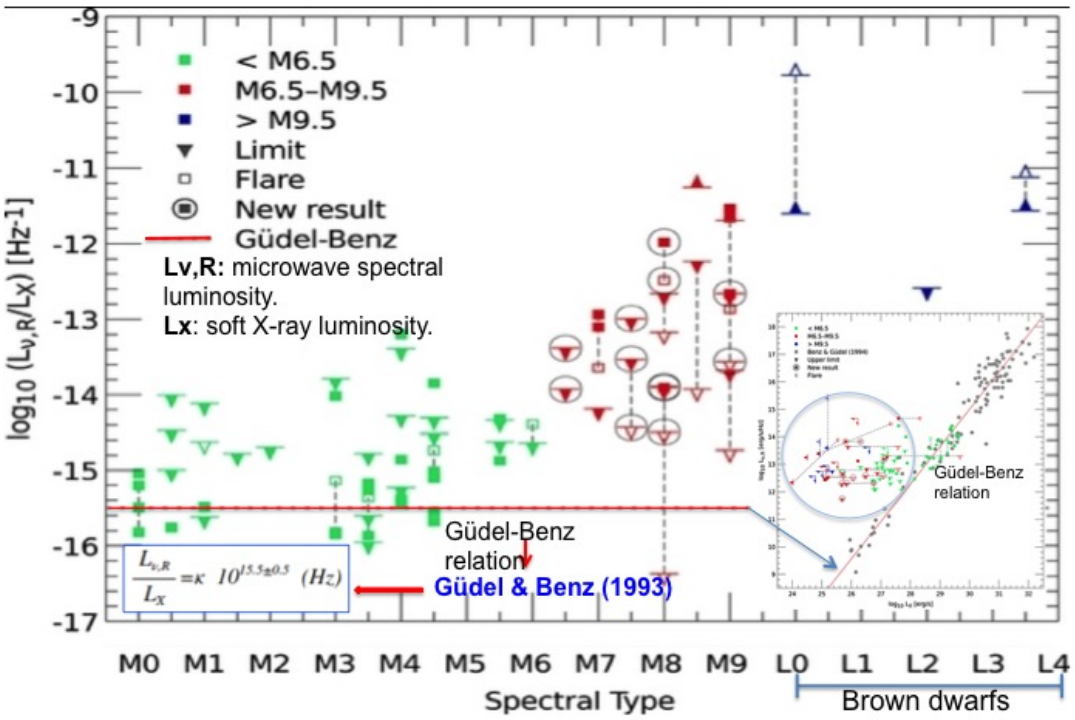

Figure 1.4: Radio luminosity plotted as function of X-ray luminosity. **Red solid line** – the Güdel-Benz relationship (GBR), **Squares** – Quiescent emission, **Asterisks** – Flares, **Inverted triangles** –upper limits. This picture has been built by Isabel Rodríguez-Barrera based on the Fig. 6 and 9 by Williams et al. (2014).

1.2.2 Chromosphere/corona and the magnetic coupling

The solar chromosphere and corona are heated by hydrodynamic and magnetic mechanisms reaching temperatures of the local gas of 10^5 K and 10^6 K respectively (Ulmschneider & Musielak 2003). The high temperatures reached in those atmospheric layers could contribute to the ionisation of the gas and to allow a magnetic coupling between the plasma and the background magnetic field or maybe the magnetic coupling is that allows the high increase of the gas

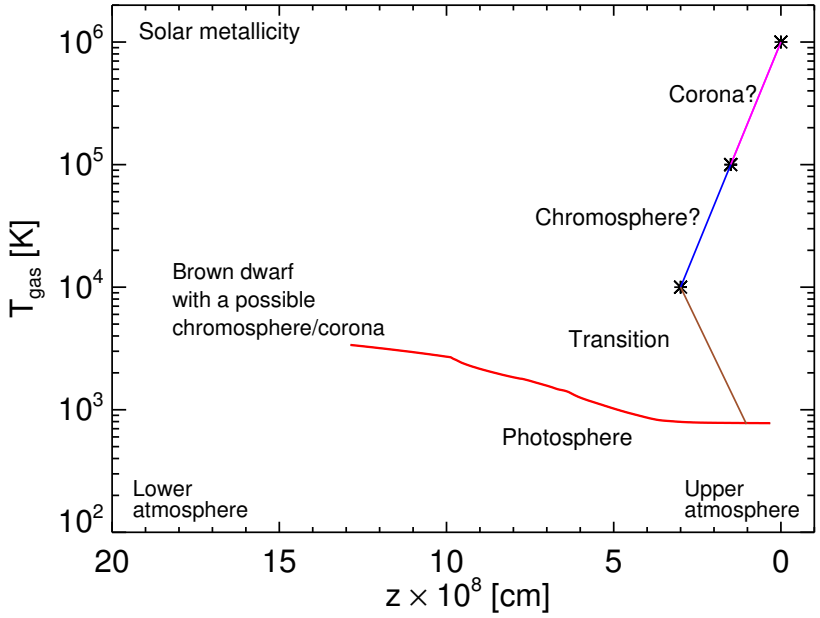

Figure 1.5: (T_{gas}-z) input structure from the DRIFT-PHOENIX model atmosphere with $T_{eff} = 2400$ K. The temperature of a possible chromosphere/corona formed has been plotted.

temperature. The presence of a magnetised atmospheric plasma is required to allow the formation of a chromosphere through MHD processes like e.g. Alfvén wave [10] heating similar to the Sun (Mullan & MacDonald 2016; Reep & Russell 2016; Brady & Arber 2016). Osten et al. (2009) have pointed out that the cyclotron maser emission observed on the M8 dwarf LP 349-25 requires a continuous supply of electrons at high latitudes. In Sec. 2.3.1 is shown that thermal ionisation is sufficient to produce a partially ionised gas in cool brown dwarfs and giant gas planets and a highly ionised gas in the younger brown dwarfs or M-dwarfs. However, for low effective temperatures and high surface gravity, additional mechanisms are required to ionise the upper atmosphere to a degree that radio and X-ray observation become feasible. Sorahana, Suzuki & Yamamura (2014) present mid-IR AKARI observations which suggest the presence of chromospheric activity in brown dwarfs. They model the spectra of three brown dwarfs (with H_α emissions) assuming a chromosphere temperature. This model fits very well with the AKARI observations. Schmidt et al. (2015) derive a rise in magnetic activity (in the form of Hα emission) from SDSS spectra from 2% for early M-dwarfs to 88% early L-dwarfs (the 39% of the L-dwarfs are suggested to be variable) and suggest that the presence of a magnetised atmospheric plasma is required to allow the formation of a chromosphere. Figure 1.5 shows the (T_{gas}-z) profile for the atmosphere structure with $T_{eff} = 2400$ K (see Table 2.1) and the possible chromosphere/corona according to the results of Chapter 3.

[10] An Alfvén wave is a low-frequency magnetohydrodynamic wave produced by the oscillations of the ions in a plasma in response of a restoring force due to the tension on the magnetic field lines.

Such observations indicate that an appropriately ionised gas is present in the atmospheres of such cool objects allowing some kind of chromospheric heating. The prevailing question is how much of such a cool, cloud-forming atmosphere needs to be ionised in order to form a chromosphere. Tanaka, Suzuki & Inutsuka (2014) study the mass loss of hot Jupiters through waves under MHD regime suggesting the formation of a chromosphere by Alfvén wave heating. They observed that the gas does not need to be fully ionised (i.e. degree of ionisation $f_e < 1$). The magnetic field strength of brown dwarfs is as high as 10^3G (Kuzmychov, Berdyugina & Harrington 2015; Lynch, Mutel & Güdel 2015; Shulyak et al. 2011). Kuzmychov, Berdyugina & Harrington (2015) analyse the Stokes spectrum of the CrH molecule under the effect of a magnetic field by a spectropolarimetric techniques showing that the brown dwarf LSR J18353790+3259545 (M8.5) has magnetic flux density of 2-3 kG; the same value is found for the double system GJ 2005 (M5.5/6) by Shulyak et al. (2011). Lynch, Mutel & Güdel (2015) suggest field strength of $\sim 2.2 \ldots 2.5$ kG for the surface field on TVLM 0513-46 (M9) and 2M 0746+20 (L0) in a rotating magnetospheric model. A correlation between radio activity and rotation has not been settled for brown dwarfs given the wide parameter range occupied by these objects (McLean, Berger & Reiners 2012; Antonova et al. 2013). Mohanty et al. (2002) analysed the magnetic Reynolds number that depends on the degree of ionisation ($R_m \propto f_e$) for a set of model atmospheres to show why the chromospheric H_α activity should be low in rapid rotating brown dwarfs with $T_{eff} \geq 1500$K and solar metallicity. The works by Schmidt et al. (2015) and Sorahana, Suzuki & Yamamura (2014) suggest that L-dwarfs should have a chromosphere (but with a reduced filling factor) despite having low magnetic Reynolds numbers.

1.2.3 Generation of the magnetic field in brown dwarf atmopshere

It has been shown that low mass objects as M-dwarfs and brown dwarfs can emit at X-ray wavelengths. Therefore, a mechanism that generates and supplies a large-scale magnetic field in brown dwarf must exist to explain the observations described above. It is well known that in the Sun the generation of a large-scale magnetic field occurs by differential rotation between the convective zone and the radiative core (Parker 1975). However, in fully convective objects as brown dwarfs, is thought that the turbulent motions of the flow at the convective zone can produce a magnetic field (Parker 1955) in the same way that a magnetic field is

generated in a rotating sphere of conducting fluid. However, that turbulent field can generate a short-scale magnetic field at the lower convective zone of the fully convective objects (Durney, De Young & Roxburgh (1993)) that is not sufficient to explain the emissions in radio and X-ray wavelengths observed in brown dwarfs. The latter assumption is also supported by the decrease of the conductivity of the flow in the lower atmosphere of brown dwarfs (see Fig. 2.13). Hence, it is reasonable to expect the generation of the magnetic field by another mechanism. According to Chabrier & Küker (2006) the rotation of the object increases the generation rate of a large-scale magnetic field by the α^2-dynamo [11] that generates and amplifies the already created short-scale magnetic field by the turbulent field of the flow. In fully convective objects is considered that the large-scale α^2-dynamo process is a good candidate to explain the high levels of activity observed in brown dwarfs (Chabrier & Küker 2006).

[11] The α^2-effect is the combination of the α-effect and the Ω-effect: the toroidal component of the magnetic field is created mostly by the poloidal component (Ω-effect); the poloidal component is created due to the Coriolis force that deflects and twists the convective motions (Morin 2012).

Table 1.1: **Properties of M , L , T and Y - dwarfs:**

Properties	M	M-L transition	L	L-T transition	T	Y
$T_{\rm eff}$	3500 . . . 2000K (Reid & Hawley 2000)	2000 . . . 1400K (Reid & Hawley 2000)	2100 . . . 1150K (Reid & Hawley 2000)	1400 . . . 900K (Reid & Hawley 2000)	700 . . . 500K (Reid & Hawley 2000)	300 . . . 200K (Reid & Hawley 2000)
Log(g)	3 . . . 4 4.65 . . . 5.4 (Reid & Hawley 2000)	3 . . . 5	4.5 . . . 5.5	4 . . . 5.5 4.5 . . . 5 (Burgasser & Putman 2005)		
Mass	0.6- 0.1 M⊙ (Mohanty et al. 2002)	0.1- 0.08 M⊙	0.08 - 0.06 M⊙ (Reid & Hawley 2000)	0.06 - 0.075 M⊙ (Reid & Hawley 2000)	0.06 - 0.01 M⊙ (Reid & Hawley 2000)	M < 0.01 M⊙
Opacity	H_2O, CO, silicate grains, TiO(g), VO(g) (Burrows et al. 2001)	H_2O, CO, silicate grains (Burrows et al. 2001)	Strong due to CH_4, also H_2O, NH_3, H_2, alkali metals DUST CLOUDS (Burrows et al. 2001)	Strong due to CH_4 also H_2O, NH_3, H_2, alkali metals DUST CLOUDS (Burrows et al. 2001)	CH_4, NH_3, H_2O clouds above photosphere (Burrows et al. 2001)	CH_4, NH_3, H_2O clouds above photosphere (Burrows et al. 2001)
$\|\vec{B}\|$	M5-M9 ∼2-3 kG radio measurements polarimetry (Kuzmychov, Berdyugina & Harrington 2015)	M7-M9.5 1-4 kG magnetic splitting FeH line (Reiners & Basri 2010)	L0 ∼2.2-2.5 kG radio measurements polarimetry (Lynch, Mutel & Güdel 2015)	∼ 0.07 M⊙ dynamo's surface t≤ 1 Gyr 0.1-1 kG (Reiners & Christensen 2010)	∼ 0.07 M⊙ dynamo's surface t≤ 1 Gyr 0.1-1 kG (Reiners & Christensen 2010)	∼ 0.001 M⊙ dynamo's surface 4.6 Gyr 9 G radio measurements (Reiners & Christensen 2010)
X-ray	M2-M8.5 $\log_{10}L_x$=26.36 erg s^{-1} (Poppenhaeger, Robrade & Schmitt 2010) (Kashyap, Drake & Saar 2008)	$L_X/L_{bol} < 10^{-5.7}$ (Williams, Berger & Zauderer 2013) $L_x \sim 10^{27}$ erg s^{-1} (Tsuboi et al. 2003)	$\log_{10}L_x$=28.5-28.9 erg s^{-1} (Feigelson et al. 2003)	$L_x \sim 10^{28}$ erg s^{-1} (Feigelson et al. 2002) (Flaccomio et al. 2003)	$L_x \sim 10^{28}$ erg s^{-1} (Feigelson et al. 2002) (Flaccomio et al. 2003)	
H_α	$L_{H_\alpha}/L_{bol} \sim 10^{-4}$ (Berger et al. 2010)	$L_{H_\alpha}/L_{bol} \sim 10^{-4.4} - 10^{-4.9}$ $L_{H_\alpha}/L_{bol} \sim (1 - 3.5)10^{-4.4}$ (Williams, Berger & Zauderer 2013)	$L_{H_\alpha}/L_{bol} < -5.2$ (Berger 2002)	$L_{H_\alpha}/L_{bol} < -5.3$ (Berger 2002) (Burgasser et al. 2000)	$L_{H_\alpha}/L_{bol} < -5.3$ (Berger 2002)	
Radio	$\nu L_{\nu,R}/L_{bol} \sim 10^{-8}$ (Berger 2002)	$\nu L_{\nu,R}/L_{bol} \sim 10^{7.5}$ $L_R/L_X \sim 10^{-11.3}$ (Mohanty et al. 2002) (Williams, Berger & Zauderer 2013)	$L_R/L_{bol} \sim 10^{-6}$ (Berger 2002)	$L_R/L_{bol} \sim 10^{-7} - 10^{-8}$ (Berger 2002)	$L_R/L_{bol} \sim 10^{-8}$ (Berger 2002)	

2

Reference study of electrostatic and magnetic characteristics across the star-planet transition regime for thermal ionisation

Radio and X-ray emissions have been observed from low mass objects (see Sec. 1.2). To explain this high energy emission, an ionised gas coupled with the magnetic field present in the atmosphere of the objects must exist. This assumption is the prelude to the necessary existence of a chromosphere/corona in brown dwarf atmospheres. This chapter introduces a framework to analyse the electrostatic and magnetic character of an atmospheric gas identifying at which local gas pressure values of the ultra-cool atmospheres the gas behaves as a plasma (see Sec. 2.3), if is magnetised (see Sec. 2.4) how this depends on the global parameters like T_{eff}, $\log(g)$, [M/H]. In this chapter, only the effect of thermal ionisation is considered. It is shown that the local degree of ionisation varies largely amongst the objects (e.g. T_{eff}=1000 K... 3000 K, $\log(g)$=3.0, 4.0, 5.0 and metallicity [M/H]=-0.6, -0.3, 0.0, +0.3 and

throughout the atmospheres: while late M-dwarfs have a considerable degree of ionisation throughout the atmosphere, the degree of thermal ionisation for a L-dwarf is rather low, however, it has also been demonstrated that a magnetic coupling between the atmospheric gas and the background magnetic field can be possible in L-dwarfs (do have rather strong magnetic fields). This study also supports the suggestion made by Mullan & MacDonald (2016), Schmidt et al. (2015) and Sorahana, Suzuki & Yamamura (2014) that cool objects as brown dwarfs could have a chromosphere (Sec. 1.2.2). In Sec. 2.2 a definition of plasma and the definition of the relevant plasma parameters are provided. Section 2.3 shows where electromagnetic interactions can dominate over electron-neutral interactions also in regions with a very low degree of ionisation.

2.1 Approach

I aim to assemble a theoretical framework that allows to assess the plasma and magnetic character in atmospheres of objects across the stellar-planetary boundary, namely for M-dwarfs, brown dwarfs and giant gas planets. The approach of this theoretical framework is not limited to these objects as the plasma parameters used are fundamental properties of a gas rather than of a particular object (see Sec. 2.2).

2.1.1 The model atmosphere grid DRIFT-PHOENIX

The grid of DRIFT-PHOENIX model atmosphere structures is used in order to quantify the plasma and magnetic characteristics. DRIFT-PHOENIX determines the thermodynamic structure of the atmosphere (local gas temperature T_{gas} [K], local gas pressure p_{gas} [bar] and local electronic pressure p_e [bar]) from fundamental stellar parameters (effective temperature T_{eff} [K], surface gravity $\log(g)$ [$\mathrm{cm\,s^{-2}}$] and metallicity [M/H]). DRIFT-PHOENIX is a combination of two complementary codes, DRIFT and PHOENIX (Witte et al. 2011; Witte, Helling & Hauschildt 2009; Helling et al. 2008). The DRIFT code (Helling et al. 2008; Woitke & Helling 2004) solves a system of equations that describes the stationary dust formation process of mineral clouds (seed formation, growth, evaporation, sedimentation, element depletion) and interaction between the dust grains and gas (Helling, Woitke & Thi 2008; Helling & Woitke 2006; Woitke & Helling 2004, 2003). PHOENIX is a hydrostatic radiative transfer model atmosphere code (Hauschildt & Baron 1999) that solves the radiation transfer equation, the equation of motion in hydrostatic equilibrium and the gas-phase composition by assuming chemical equi-

Table 2.1: DRIFT-PHOENIX atmosphere structures used (Fig. 2.1):
Group 1: giant gas planets and young brown dwarfs.
Group 2: dependence on log(g).
Group 3: dependence on metallicity.

	$T_{\rm eff}$ [K]	log(g)	[M/H]
Group 1	1000-3000	3.0	0.0
Group 2	1000 2000 2800	3.0, 4.0, 5.0	0.0
Group 3	1000 2000 2800	3.0	-0.6, -0.3, 0.0, +0.3

librium. DRIFT-PHOENIX, as the result of combining PHOENIX with DRIFT, is a self-consistent atmospheric model that takes into account cloud formation and its impact on the thermodynamic structure and the resulting spectral energy distribution. The degree of ionisation of the atmospheric gas, the plasma and magnetic parameters are evaluated using DRIFT-PHOENIX atmospheric models with a range of effective temperatures ($T_{\rm eff} = 1000\,{\rm K}...3000\,{\rm K}$), surface gravity (log($g$)=3.0, 4.0, 5.0) and metallicity ([M/H]= -0.6, -0.3, 0.0 +0.3).

2.1.1.1 Models to study

The DRIFT-PHOENIX atmosphere structures are grouped into three groups for an easier presentation of the results (Table 2.1). These groups (Fig. 2.1), defined by a range of global parameters, cover giant gas planets, old and young brown dwarfs and M-dwarfs. Figure 2.1 shows the thermodynamic profiles ($T_{\rm gas}$, $p_{\rm gas}$) for each of these groups. The thermodynamic gas temperature of the atmosphere increases and the formation of dust clouds decreases as:

- the effective temperature is increased for a given log(g) and [M/H].

- the surface gravity is decreased for a given $T_{\rm eff}$ and [M/H].

- the metallicity is increased for a given $T_{\rm eff}$ and log(g).

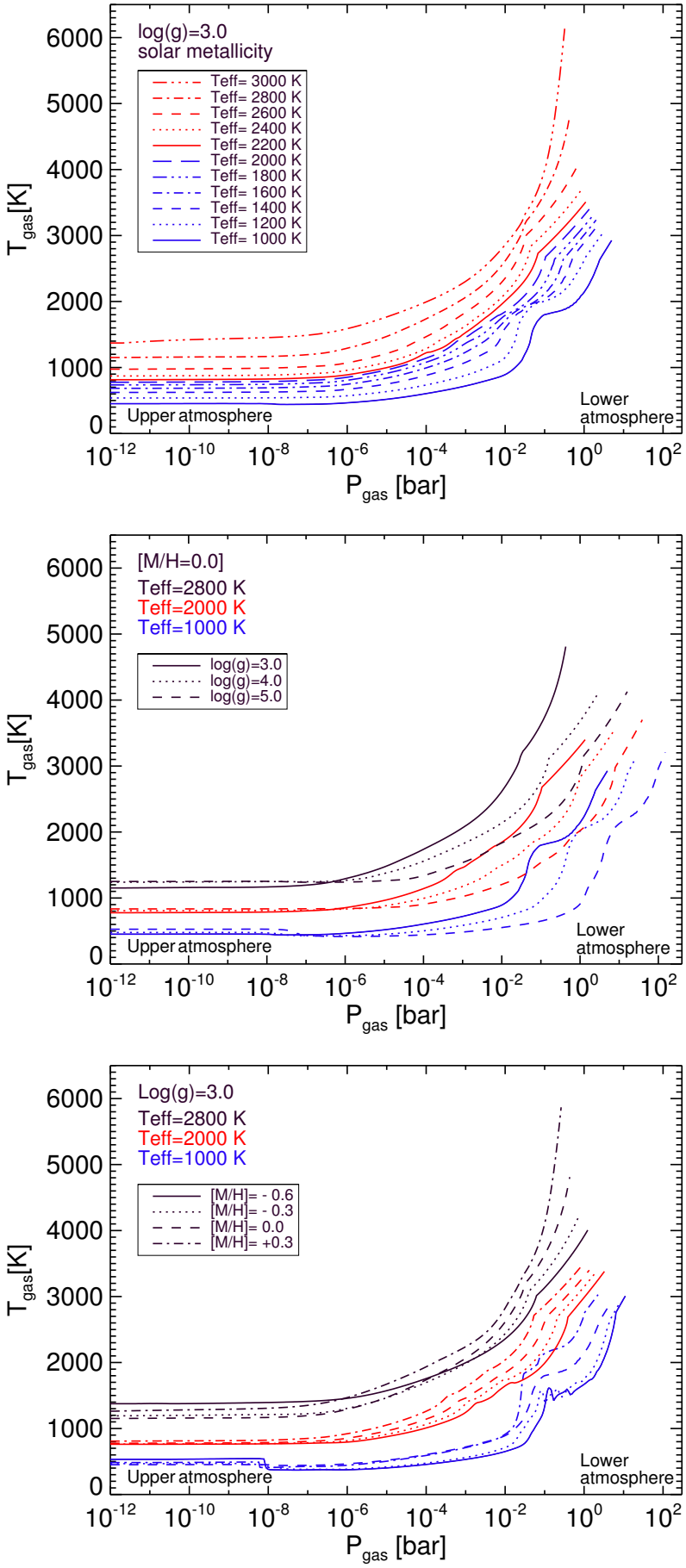

Figure 2.1: (T_{gas}-p_{gas}) input structure from the DRIFT-PHOENIX model atmosphere grid. The hottest models represent M-dwarf atmospheres or atmospheres of young brown dwarfs. The coolest models represent atmospheres in the planetary regime. **Top:** Group 1. **Middle:** Group 2. **Bottom:** Group 3.

2.2 Plasma definition and basic plasma parameters

A qualitative definition of plasma can be found in Chen (1983): "A plasma is a quasi neutral gas of charged and neutral particles which exhibits collective behaviour". According to this definition, the plasma can be partially or fully ionised but, retains the overall quasi-neutral balance of the charges. Collective behaviour means that the local conditions influences the plasma as a whole. This is a consequence of the long range electromagnetic interactions (Coulomb forces), that can dominate over particle collisions. A plasma can fulfil the approximation of local thermodynamic equilibrium (LTE) if the temperature of the plasma particles is approximately the same ($T_e \approx T_{ion} \approx T_{gas}$). A plasma that does not satisfy the above criteria (e.g. $T_e \gg T_{ion,gas}$) is dubbed a non-local thermal equilibrium (NLTE)(Zohm 2005). All calculations in this study have been made under the approximation of local thermodynamic equilibrium (LTE). In the following section, the plasma of an atmospheric environment is characterised based on its electrostatic and magnetostatic behaviour. This is inspired by the wealth of radio and X-ray observations of substellar objects (Berger 2002; Berger et al. 2010; Route & Wolszczan 2012; Burgasser et al. 2013; Williams et al. 2014). These observations suggest that the atmospheric gas must couple with the background magnetic field. As a consequence, free charged particles produced in the atmosphere would be accelerated along magnetic field lines and released into the upper parts of the atmosphere. A magnetic coupling of the local gas would also be required for Alfvén waves to develop and potentially contributing to an acoustic heating of a chromosphere also on such ultra-cool objects (e.g. Testa, Saar & Drake 2015). Note that ideal and non-ideal MHD simulations require a certain degree of ionisation to allow Alfvén wave heating to develop as possible mechanisms for chromospheric heating.

For a plasma to exist, the gas needs to be ionised. The degree of ionisation of the gas, f_e measures the extent to which a gas is ionised (fraction of the free electrons respect to the gas density) and it is defined as

$$f_e = \frac{p_e}{p_e + p_{gas}} , \tag{2.1}$$

where p_{gas} and p_e are the gas and electron pressure respectively, both in [bar]. Once the degree of ionisation of the atmospheric gas depending on the global parameters (T_{eff}, $\log(g)$, [M/H]) is determined, the plasma frequency is evaluated to investigate where in the atmosphere, electromagnetic interactions dominate over kinetic collisions between electrons and

neutrals,

$$\omega_{\mathrm{pe}} \gg \nu_{\mathrm{ne}}. \tag{2.2}$$

where ω_{pe} [rad s^{-1}] is the plasma frequency (dominance of the electrostatics interactions over collisions)) and ν_{ne} [s^{-1}] is the frequency of the collisions between neutral and charged particles. Only if Eq. 2.2 is fulfilled, it can be expected that the ionised gas undergos electromagnetic interactions that could lead, for example, to discharge processes. A more refined insight about electrostatic interactions influencing the atmospheric gas can be gained by determining the length scales beyond which the Coulomb force of a charge does not any more effects its surrounding. On length-scale larger than the Debye length, a gas will be quasi-neutral and no electrostatic forces will effect the gas behaviour. Hence,

$$\lambda_{\mathrm{D}} \ll L \tag{2.3}$$

where λ_{D} is the Debye length (scale length of the electrostatics interactions) and L is the pressure scale height of the considered plasma, both in [m]. Ideally, this would be associated with the atmospheric volume where the ionised gas can couple to an external magnetic field. In the following subsections each of those plasma criteria are defined and evaluated for the DRIFT-PHOENIX atmosphere structures presented in Table 2.1. All equations and natural constants are given in SI units. All results, however, have been converted into cgs units for an easier representation in the astrophysical context.

2.2.1 Plasma Frequency

In a plasma, if electrons are displaced from their equilibrium position (assuming a uniform, stationary ionic background), a charge imbalance is imposed on the plasma, creating a local, restoring electric field. Consequently, the electrons try to re-establish charge neutrality resulting in them oscillating around their equilibrium position with a particular frequency called plasma frequency. The plasma frequency is defined as,

$$\omega_{\mathrm{pe}} = \left(\frac{n_{\mathrm{e}} e^2}{\epsilon_0 m_{\mathrm{e}}} \right)^{1/2}, \tag{2.4}$$

where n_e is the electron number density [m^{-3}], e the electron charge [C], m_e the electron mass [kg] and $\epsilon_0 = 8.85 \cdot 10^{-12}$ [$F\,m^{-1}$]. If the plasma frequency, ω_{pe} is greater than the frequency of collisions between the electrons and neutral particles, ν_{ne} [s^{-1}] , long-range electromagnetic collective effects dominant over short-range binary interactions (see Fig. 2.5). The collision frequency for neutral particles with electrons is given by $\nu_{ne} = \sigma_{gas} n_{gas} \nu_{th,e}$, where $\nu_{th,e}$ is the thermal velocity of electrons given by $\nu_{th,e}=(k_B T_s/m_s)^{1/2}$ [m s^{-1}], m_s the mass of the specie [kg], T_s the temperature of the specie [K], n_{gas} the number gas density and σ_{gas} the collision, or scattering, cross section of particles. The latter is assumed to be $\sigma_{gas} = \pi \cdot r_{gas}^2$ with $r_{gas} = r_{H_2}$ as the atmospheric gas in late M-dwarfs, brown dwarfs and most likely in giant gas planets is composed mostly of molecular hydrogen H_2. Therefore, the collision cross section is approximated by $\sigma_{gas} \approx \sigma_{H_2} \approx \pi \cdot {r_{H_2}}^2 = 5.81 \cdot 10^{-20}$ m^2 ($r_{H_2} = 1.36 \cdot 10^{-10}$ m). If the charged particles collide frequently with the ambient neutral gas ($\omega_{pe}/\nu_{ne} < 1$), their motion will be determined by nearest neighbour interactions and not by collective, long-range electromagnetic interactions.

2.2.2 Debye length

The Debye length, λ_D [m] is the spatial length scale beyond which a plasma can be considered quasi-neutral ($n_e \approx n_i \approx n_{gas}$) (Fig. 2.2). A Debye sphere is a bulk of plasma with radius equal to the Debye length. For length scales less than the Debye length, a test charge will experience the influence of the charge imbalance inside the Debye sphere. The charges are increasingly electrically screened at radius of the bulk of plasma that approaches the Debye length. The Debye length, λ_D result from the solution of the Poisson equation for a non-zero charge density near a test charge, and is defined as

$$\lambda_D = \left(\frac{\epsilon_0 k_B T_e}{n_e e^2} \right)^{1/2}. \tag{2.5}$$

where T_e [K] is the electron temperature and $k_B = 1.38 \cdot 10^{-23}$ [$J\,K^{-1}$]. A plasma is quasi-neutral if

$$\lambda_D \ll L. \tag{2.6}$$

For an ionised gas region to exhibit plasma behaviour, it is required that over the length scale of that region, the electron number density is high enough such that $L \gg \lambda_D$. The typical length scale of the plasma, L , considered in the literature (e.g. Mohanty et al. 2002;

Tanaka, Suzuki & Inutsuka 2014) is the pressure scale height which depends on the local gas properties and varies with $1/g$. Typical values for the pressure scale height are $10^5 \ldots 10^6$ cm for a brown dwarf with $\log(g) = 5$. Tanaka, Suzuki & Inutsuka (2014) base their length scale on the definition of the Alfvén speed that is of the order of the velocity of sound (their Eq.12). Also their approach results in a typical length scale of the order of the pressure scale height. Associate with the Debye length is the number of charges inside a Debye sphere, N_D (Sec. 2.2.3). If $N_D \gg 1$, the ionised gas exhibits plasma behaviour.

2.2.3 Number of particles in a Debye sphere, N_D

A plasma has the capacity to screen a single charged particle placed at any point because, any single charged particle attracts oppositely charged particles producing a screening and repels those who have the same charge. A net space is produced in the neighbourhood of any single charged particle, reducing the electric field generated by it. The effective range of the net force between particles is restricted to the order of the Debye length (see Sec. 2). As a consequence, a test particle in the Debye sphere interacts only with particles that lie within this sphere. N_D measures the efficiency of this screening and allows to calculate how many gas particles are required to fulfil $L \gg \lambda_D$. Therefore, only the charged particles inside the Debye sphere can be considered as electrostatically active. All particles have a thermal velocity due

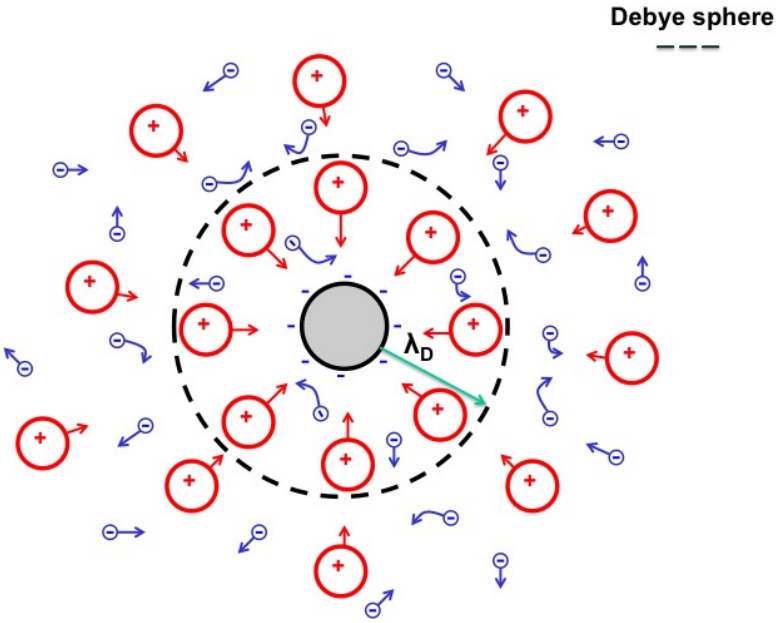

Figure 2.2: The Debye sphere and the Debye length, λ_D. Courtesy of Craig Stark.

to the temperature of the plasma. The deflected angle due to the electrostatic interactions is

bigger if the number of particles around of the screened particle in the Debye sphere is small. The movement of the screened particle will not be smooth, unlike in the situation when the number of particles in the Debye sphere is sufficiently large to reduce it. That is why the Debye length increases as the number of particles in the screened sphere decreases. This is shown in Fig. 2.7 where all Debye length increase with height in the atmosphere, i.e. with the outward decreasing local gas pressure. The change in velocity due to the interactions with the particles produces a non-negligible net electrostatic force inside the Debye sphere. Therefore, large numbers of particles that are uniformly distributed inside the Debye sphere are required to avoid a large-angle deflection on a test particle and hence, the Debye length must be small in comparison to the length scale of the plasma. In this case, the plasma is dominated by many long-range interactions, rather than the short-range binary collisions of a neutral gas. A measure of the efficiency of the screening is the plasma parameter N_D.

The plasma parameter is defined as

$$N_D = (4/3)\pi n_e \lambda_D^3, \tag{2.7}$$

the number of particles in a Debye sphere with radius λ_D and centred on a single charge particle that produced the charge imbalance. When there are many plasma particles in a Debye sphere ($N_D \gg 1$) and long-range collective interactions are dominant over short-range collisions, the plasma frequency is much larger than the electron-ion collision frequency (see Fig. 2.3).

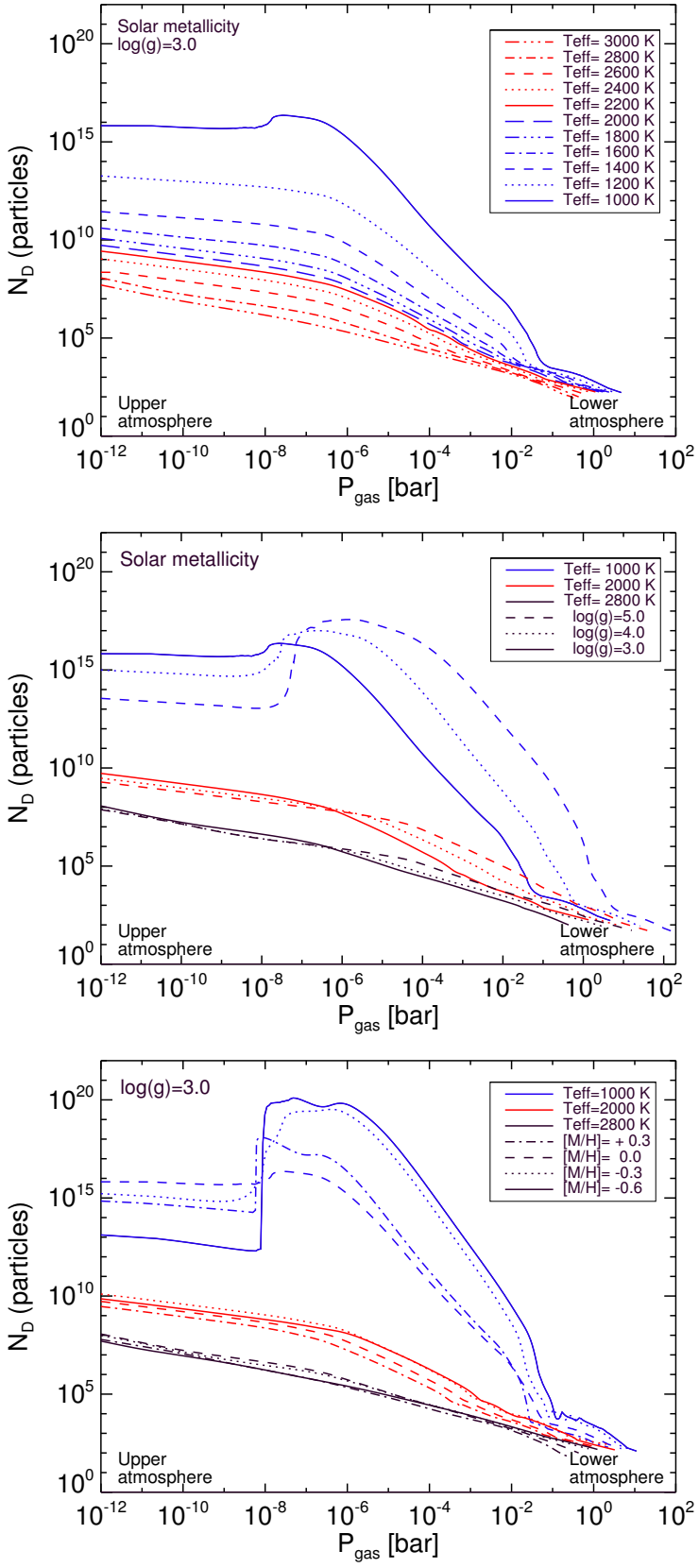

Figure 2.3: Number of particles inside of Debye sphere measure the efficiency of the screening given by the Debye sphere in the plasma. $N_D \gg 1$ results in the collective interactions dominate over short-range collisions in the gas. **Top:** Group 1. **Middle:** Group 2. **Bottom:** Group 3.

2.3 Plasma parameters across the star-planet regime

In the following, the plasma criteria are evaluated for late M-dwarfs, brown dwarfs and giant gas planet atmospheres. All results have been calculated considering thermal ionisation only and compose my reference study against which the need for additional ionisation processes can be derived. First I examine for which global parameters, the gas is ionised above the threshold value of $f_e > 10^{-7}$ (Sec. 2.3.1). In Sec. 2.3.2 it is shown that long-range electromagnetic collective interactions of many charged particles can dominate over short-range binary interactions also in regions of a very low degree of ionisation ($\omega_{pe} \gg \nu_{ne}$). In Sec. 2.3.3, it is shown at which local gas pressure scale, the ultra-cool atmospheres will be affected or not by electrostatic processes ($\lambda_D \ll L$).

2.3.1 Degree of ionisation by thermal processes, f_e

Figure 2.4 shows the degree of thermal ionisation evaluated for the same models represented in Fig. 2.1 (Table 2.1). Guided by these results, I consider $f_e > 10^{-7}$ to be a threshold above which the gas is partially ionised and may exhibit plasma behaviour. The above choice of a threshold value is supported by results from laboratory experiments and laboratory plasma devices (e.g. Tokamak; Diver 2001; Fridman 2008). For a fluorescent tube, the degree of ionisation is $f_e \approx 10^{-5}$ according to Inan & Golkowski (2010). Christophorou & Olthoff (2004) showed that at low temperature ($T_{gas} \approx 300 - 600$ K) and low density ($10^{13} - 10^{16}$ cm^{-3}) the gas is weakly ionised with $f_e \approx 10^{-6} - 10^{-1}$. If the density of the charged particles increases towards $f_e \rightarrow 1$ the gas will be fully ionised. For example, a fully ionised gas is assumed in ideal MHD regime[1]. The threshold mentioned above ($f_e > 10^{-7}$) allows me to derive the atmospheric volume that can be considered as an ionised gas (Sect. 2.3.4, Fig. 2.8). Deriving such atmospheric volume fractions will enable me to compare the results from different plasma criteria (Eqs. 2.2, 2.3) and to show that a gas does not need to be fully ionised in order to exhibit collective plasma effects. In the following, the results for the used DRIFT-PHOENIX atmosphere structures (see Table 2.1) and shown in Fig. 2.4 are:

- **Group 1:** changing $\mathbf{T_{eff}}$ **(Fig. 2.4, top)**
  ($\log(g)$=3.0, [M/H]= 0.0)
  A solar-metallicity M-dwarf with $T_{eff} = 3000$ K achieves $f_e > 10^{-7}$ in almost the entire

[1] In a MHD regime, a fluid approximation can be valid for a plasma. In an ideal MHD the fluid is considered to have a low resistivity and the magnetic field lines are driven by the motion of the flow.

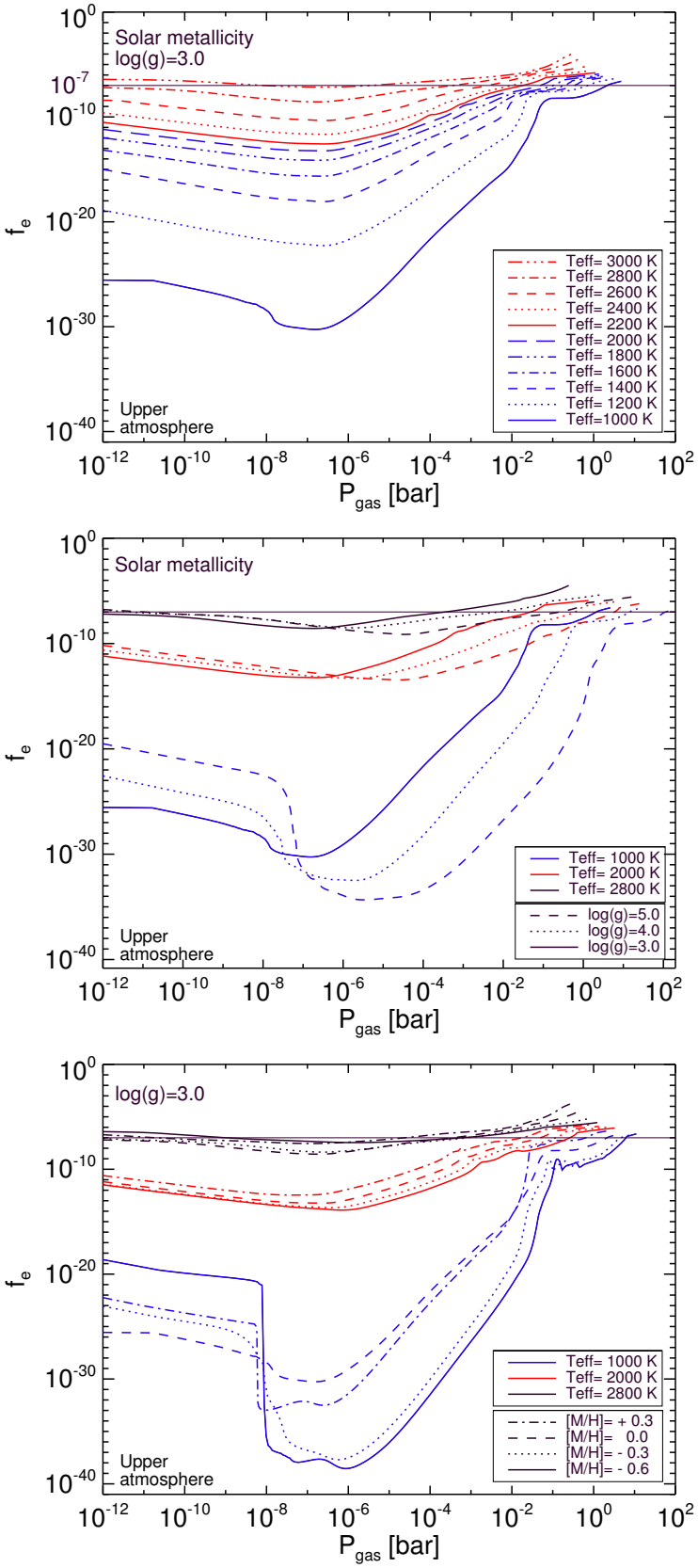

Figure 2.4: The degree of thermal ionisation, $f_e = p_e/(p_e + p_{gas})$ as a measure of free charged particles for M-dwarf, brown dwarf and giant gas planet atmospheres. The M-dwarf atmosphere is easily ionised by thermal processes. Atmosphere of brown dwarfs can only be thermally ionised in deeper layers. **Top:** Group 1. **Middle:** Group 2. **Bottom:** Group 3.

atmosphere. For cooler atmospheres with $T_{eff} \leq 2800$ K, $f_e > 10^{-7}$ is only reached for $p_{gas} > 10^{-4}$ bar. The atmospheric fraction that reached $f_e > 10^{-7}$ increases with increasing T_{eff}.

- **Group 2**: changing **log(g) (Fig. 2.4, middle)**

  ($T_{eff} = 1000$ K, 2000 K, 2800 K , [M/H]= 0.0)

  Values of varying surface gravity log(g)= 3.0, 4.0, 5.0 are studied here. Models with $T_{eff} = 2800$ K reach $f_e > 10^{-7}$ for $p_{gas} > 10^{-4}$ bar; models with $T_{eff} = 2000$ K for $p_{gas} > 10^{-2}$ bar. A small part of the upper atmospheric reaches $f_e > 10^{-7}$ for T_{eff}=2800 K and log(g)=4.0, 5.0. Models with $T_{eff} = 1000$ K have only a small fraction of the atmospheric gas that reaches the $f_e > 10^{-7}$ threshold. This occurs in the deepest layers of the atmosphere $1 < p_{gas} < 10^2$ bar. The atmospheric fraction that reached $f_e > 10^{-7}$ increases with decreasing log(g) at high p_{gas} and with increasing log(g) at low p_{gas}.

- **Group 3**: changing **[M/H]**= 0.0 **(Fig. 2.4, bottom)**

  ($T_{eff} = 1000$ K, 2000 K, 2800 K, log(g))

  Values of varying metallicity $[M/H]$= - 0.6, -0.3, 0.0, +0.3 are analysed. Models with T_{eff}=2800 K and $T_{eff} = 2000$ K satisfy $f_e > 10^{-7}$ for all values of metallicity for $p_{gas} > 10^{-5}$ bar. Models with T_{eff}=1000 K have only a small fraction of the atmospheric gas that can be ionised for $p_{gas} > 10^{-1}$ bar.

All models of non-irradiated atmospheres show a degree of ionisation that increases from a minimum ($p_{gas} \sim 10^{-8} - 10^{-6}$ bar) with increasing local gas pressure values towards the deeper layers of the atmosphere. Atmosphere models with $T_{eff} \leq 2800$ K, log(g)= 3.0, [M/H]= 0.0 can reach $f_e > 10^{-7}$ only for high p_{gas} (inner parts of the atmosphere). Only one model atmosphere achieves $f_e > 10^{-7}$ throughout nearly the entire atmosphere (T_{eff}= 3000 K, log(g)= 3.0, [M/H]= 0.0). For atmospheres of late M-dwarfs, brown dwarfs and giant gas planets for $T_{eff} = 1000 \ldots 3000$ K for varying log(g) and metallicity, I observe that:

- The hottest model has the highest thermal degree of ionisation as the electron density increases as the local gas temperature increases towards the largest effective temperature.

- The lowest value of surface gravity causes an increase of f_e at high p_{gas}, however, the highest value of surface gravity causes an increase of f_e at low p_{gas}. Both trends are for a given T_{eff} and [M/H].

- The highest metallicity values cause an increase of f_e at high p_{gas} compared to the lowest metallicity models. For T_{eff}=2800 K and T_{eff}=1000 K the lowest value of the metallicity causes an increase of f_e at low p_{gas}. Both trends are for a given T_{eff} and log(g).

2.3.2 Dominating electromagnetic interaction

The criterion $\omega_{pe} \gg \nu_{ne}$ is used to derive where in an ultra-cool atmosphere the long-range, electromagnetic, collective interactions of many charged particles dominates over short-range binary interactions in a ionised gas of a certain degree of ionisation. Figure 2.5 shows the results of this criterion for the three groups of model atmosphere structures (Fig. 2.1 and table 2.1). The results are described in the following:

- **Group 1:** changing $\mathbf{T_{eff}}$ **(Fig. 2.5, top)**
  (log(g)=3.0, [M/H]= 0.0)
  As T_{eff} increases, the range of the p_{gas} where $\omega_{pe} \gg \nu_{ne}$ increases too. For models with $T_{eff} \geq 2200$ K the entire atmosphere satisfies this criterion; for $T_{eff} = 2000$ K almost the entire atmosphere; for models with $T_{eff} = 1800 - 1400$ K in the uppermost and for the innermost parts of the atmosphere and for $T_{eff} = 1200$ K only for $10^{-2} < p_{gas} < 10^{-1}$ bar. The model with T_{eff} =1000 K is too cool to fulfill this criterion.

- **Group 2**: changing **log(g) (Fig. 2.5, middle)**
  ($T_{eff} = 1000$ K, 2000 K, 2800 K , [M/H]= 0.0)
  Models with $T_{eff} = 2800$ K satisfy this criterion throughout the whole atmosphere except for log=5.0 at the highest pressures. For $T_{eff} = 2000$ K and log(g)=3.0 almost the entire atmosphere fulfills this criterion; $T_{eff} = 2000$ K and log(g)=4.0 only in the uppermost and for the innermost parts of the atmosphere; for $T_{eff} = 2000$ K and log(g)= 5.0 only for $p_{gas} < 10^{-6}$ bar. Models with $T_{eff} = 1000$ K do not satisfy the criterion.

- **Group 3**: changing **[M/H]**= 0.0 **(Fig. 2.5, bottom)**
  ($T_{eff} = 1000$ K, 2000 K, 2800 K, log(g))
  Models with $T_{eff} = 2800$ K and all value of metallicity and $T_{eff} = 2000$ K with [M/H]= +0.3 satisfy this criterion in the whole atmosphere. For $T_{eff} = 2000$ K and [M/H]= 0.0 almost the entire atmosphere fulfills this criterion. For $T_{eff} = 2000$ K and [M/H]= -0.3, -0.6 only in the uppermost and for the innermost parts of the atmosphere, $10^{-7} >$

$p_{gas} > 10^{-3}$; models with $T_{eff} = 1000$ K and [M/H]$= +0.3$ only for $10^{-2} < p_{gas} < 10^{0}$. Models with $T_{eff} = 1000$ K and [M/H]$= 0.0$, -0.3, -0.6 and do not fulfill this criterion for any atmospheric gas pressure.

Figure 2.5 shows that the collective, long-range electromagnetic interactions dominate over short-range binary interactions in atmospheres of low degrees of ionisations, i.e. for $2800 \geq T_{eff} \geq 2000$ K. As T_{eff} and the metallicity increase, $\omega_{pe} \gg \nu_{ne}$ is easier fulfilled at high p_{gas}, however, as T_{eff} increases and the metallicity decreases, $\omega_{pe} \gg \nu_{ne}$ is easier fulfilled at low p_{gas} for $T_{eff} = 2800$ K, 1000 K. This effect is counteracted by an increase in log(g). The lowest value of $\log(g)$ causes a decrease of ω_{pe}/ν_{ne} in the uppermost parts of the atmosphere and an increase in the innermost parts. Consequently, long-range, electromagnetic, collective interactions of many charged particles do not require a complete ionisation of the atmospheric gas, and a moderate gas ionisation is sufficient.

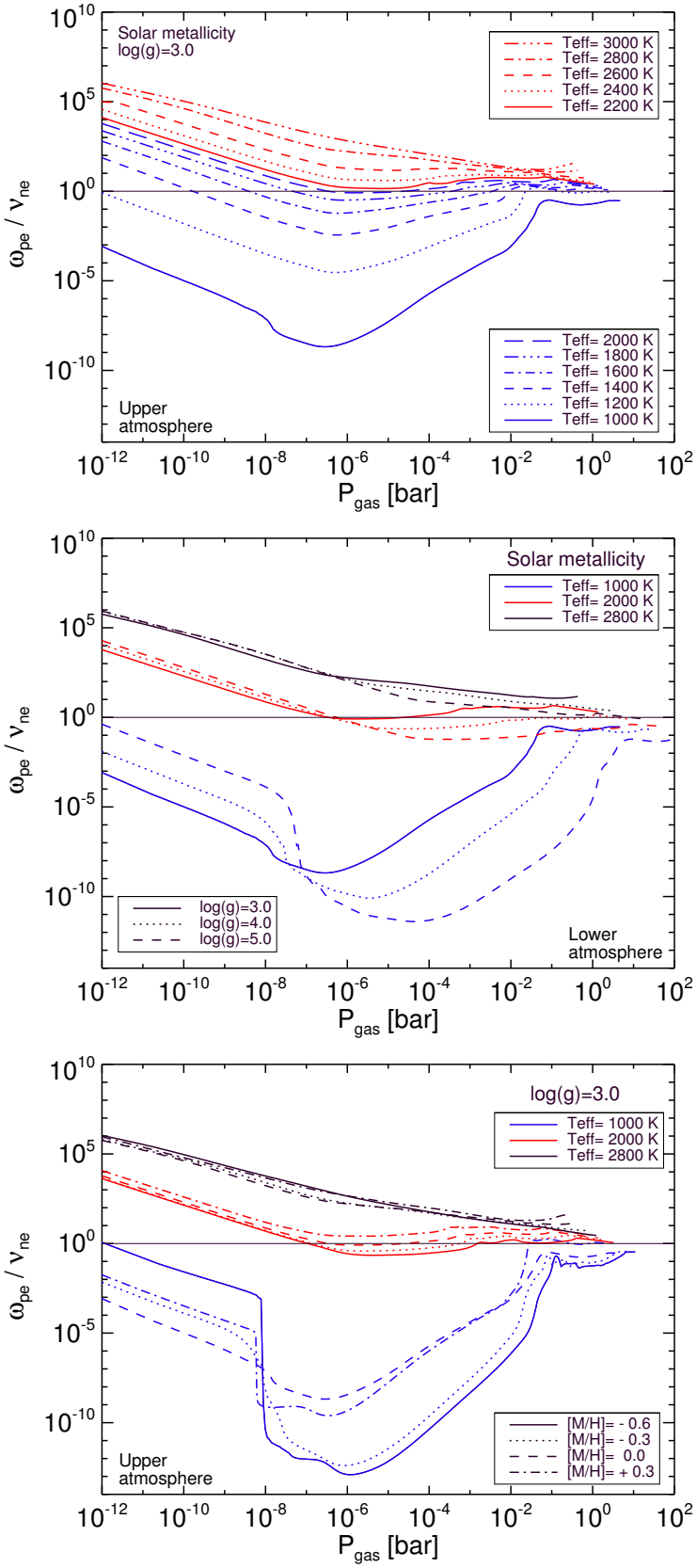

Figure 2.5: Ratio of plasma frequency of the electrons and the frequency of collisions between neutral particles and electrons. Electromagnetic interactions dominate over electron-neutral interactions if $\omega_{pe}/\nu_{ne} \gg 1$. **Top:** Group 1. **Middle:** Group 2. **Bottom:** Group 3.

2.3.3 Electrostatically effected atmospheric length scales

The Debye length, λ_D, is compared to a typical atmospheric length scale of the order of the pressure scale height, L=10^3 m (Helling et al. 2011a). Figure 2.7 shows how the Debye length changes depending on the local atmospheric gas pressure, and where $\lambda_D \ll L$ is fulfilled. In the following, the results for the DRIFT-PHOENIX atmosphere structures used for this study (see Table 2.1) and as shown in Fig. 2.7 are:

- **Group 1**: changing $\mathbf{T_{eff}}$ **(Fig. 2.5, top)**
  ($\log(g)$=3.0, [M/H]= 0.0)
  The criterion $\lambda_D \ll L$ is fulfilled throughout the whole atmosphere for $T_{eff} \geq 1800$ K; only for $T_{eff} = 1600$ K a small atmospheric gas volume for $p_{gas} < 10^{-10}$ bar cannot reach this criterion. For models with $T_{eff} \leq 1400$ K this criterion is fulfilled for $p_{gas} > 10^{-6}$ bar. As T_{eff} increases, the range of p_{gas} where $\lambda_D \ll L$ increases.

- **Group 2**: changing **log(g) (Fig. 2.5, middle)**
  ($T_{eff} = 1000$ K, 2000 K, 2800 K , [M/H]= 0.0)
  Models with $T_{eff} = 2800$ K and 2000 K satisfy this criterion for all surface gravity values and throughout the whole atmosphere. For $T_{eff} = 1000$ K and all surface gravity values then $\lambda_D \ll L$ is fulfilled only for $p_{gas} > 10^{-4}$ bar.

- **Group 3**: changing **[M/H]**= 0.0 **(Fig. 2.5, bottom)**
  ($T_{eff} = 1000$ K, 2000 K, 2800 K, $\log(g)$)
  Models with $T_{eff} = 2800$ K and 2000 K satisfy this criterion for all metallicities and p_{gas}. Models with $T_{eff} = 1000$ K satisfy this criterion in the inner atmospheric regions only where $p_{gas} > 10^{-4}$ bar.

Figure 2.7 shows that the Debye length is generally very large compared to the pressure scale height, L, in the uppermost atmosphere throughout the whole regime of ultra-cool objects, i.e. late M-dwarfs, brown dwarfs and giant gas planets, however, only for objects with $T_{eff} \leq 1600$ K, the criterion $\lambda_D \ll L$ is not fullfilled. In the upper atmosphere the electron density is low causing an increasing Debye length; whereas deeper in the atmosphere the electron number density is high and so the Debye length is relatively lower. The results from the Fig. 2.7 can be compared to the values from some solar system samples: at the top of the Earth's ionosphere the Debye length is $\lambda_D \approx 1$cm for $T_e \approx 10^3$ K and $n_e \approx 10^{11}$cm^{-3} (Cravens

1997); at $\sim$10 R_s of the Saturn's surface with a plasma temperature of T_{gas}=10^8 K and an electron density of $n_e \approx 1\,cm^{-3}$ the Debye length is λ_D=2.2·10^3 cm ; for the solar wind at $\approx$ 1 AU, $\lambda_D \approx$7·10^2 cm ($T_e \approx 10^5$ K, $n_e \approx 10^7\,cm^{-3}$) (Green et al. 2002). Another values of the Debye length are presented in Table 2.2 and in Fig. 2.6: Duru et al. (2008) investigate the electron density in the upper ionosphere of Mars; Trotignon et al. (2001) the interaction of the Martian's atmosphere with the solar wind. Both consider the presence of the dust in the plasma environment; Yaroshenko et al. (2011) model a plasma composed of electrons, water group ions and protons with the presence of photoemission due to the UV radiation; Kremer et al. (2006) work with a pure electron plasma. The results in Fig. 2.7 suggest that the Debye length values are smaller to the value of the Earth's ionosphere at deeper atmosphere; only for the coolest atmospheres (L-T dwarfs and giant gas planets) with local gas temperature $T_{gas} \approx 10^3$ K (Fig. 2.1) and electron density $n_e \leq 10^{10}\,cm^{-3}$, the values of λ_D are comparable to the Earth's ionosphere. However, at the upper atmosphere of objects with $T_{eff} \geq$2600 K (M-dwarfs and early spectral subtypes of brown dwarfs), the Debye length is comparable with those values found for the Martian's atmosphere (Fig. 2.6).

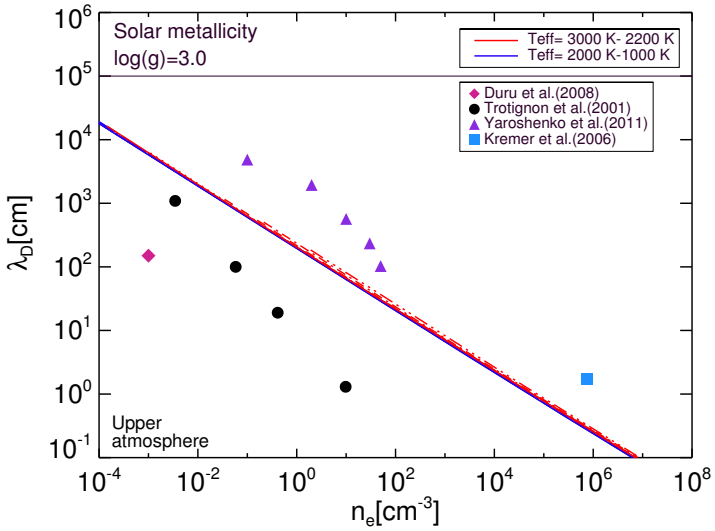

Figure 2.6: Comparison of the Debye length in different astrophysical environments. Group 1 (Table 2.1) is plotted here. The red lines represent T_{eff} = 3000 - 2200 K covering M-dwarfs and young L-dwarfs. Blue lines represent T_{eff} = 2000 -1000 K covering late L-dwarfs and giant gas planets regime. The Debye lengths for Martians atmosphere: **Red diamond** by Duru et al. (2008); **Black circles** by Trotignon et al. (2001). **Light blue squares** - a plasma composed of electrons, water group ions and protons are plotted as violet triangle (Yaroshenko et al. 2011) and a pure electron plasma (Kremer et al. 2006); **Black line**- atmospheric length scale L=10^5 cm (Helling et al. 2011a).

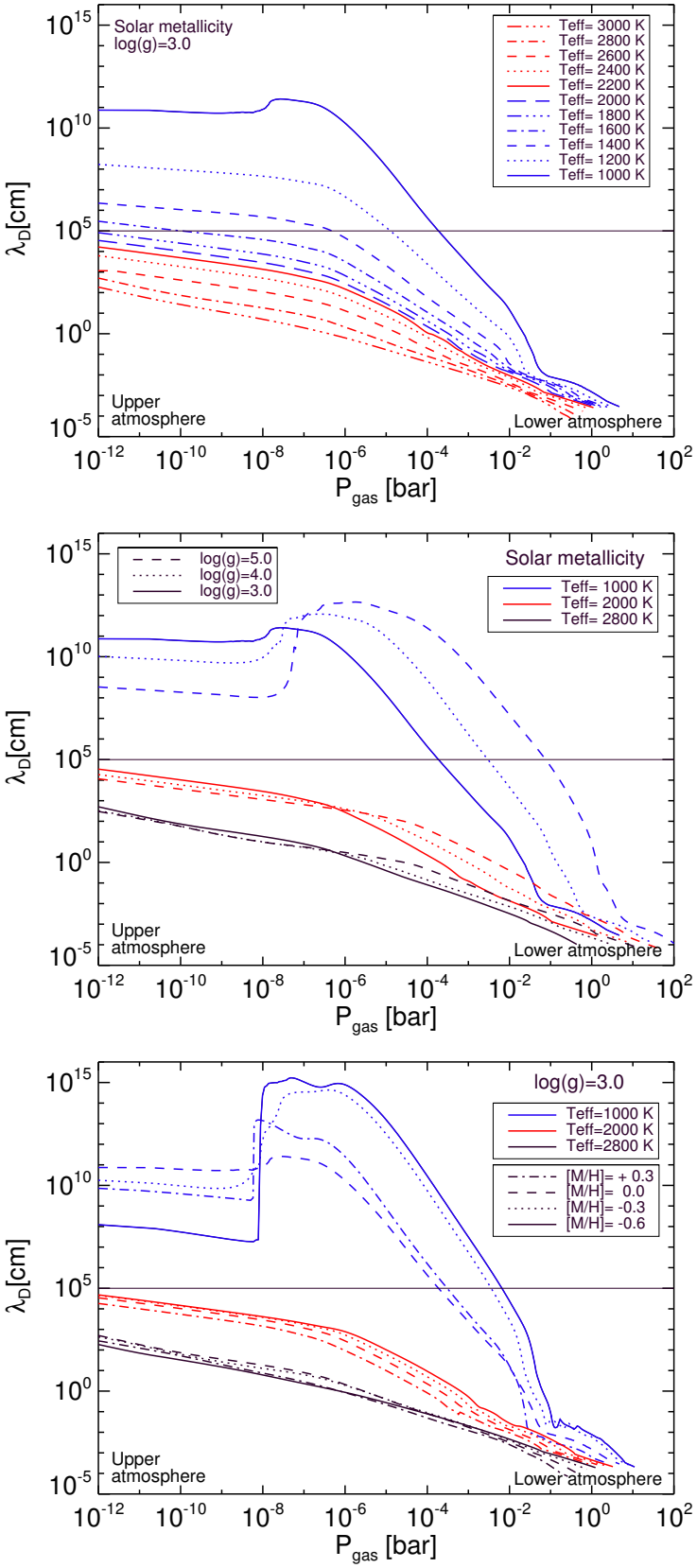

Figure 2.7: Debye length versus the local gas pressure assuming $T_e \approx T_{gas}$. For length scales less than the Debye length, a test charge will experience the influence of the charge imbalance inside the Debye sphere. The horizontal line indicates the typical length scale of the plasma L=10^3m consider in this study (Helling et al. 2011a). **Top:** Group 1. **Middle:** Group 2. **Bottom:** Group 3.

Table 2.2: Debye lengths for different astrophysical environments. Figure 2.6 provides a comparison to results of these papers.

Object	T_e [K]	n_e [cm^{-3}]	$\lambda_D[cm]$	References
Martians Ionosphere	5000	10^{-3}	1.5×10^{2}	Duru et al. (2008) (Martians atmosphere)
Martians Ionosphere	347 3131 12222 86665	9.78 4.12×10^{-1} 5.82×10^{-2} 3.47×10^{-3}	1.3 19 10^{2} 1.1×10^{3}	Trotignon et al. (2001) (Martians atmosphere)
Saturn Orbit Insertion	1.16×10^{4} 3×10^{4} 7×10^{4} 1.7×10^{5} 4×10^{5}	50 30 10 2 0.1	10^{2} 2×10^{2} 5.6×10^{2} 1.9×10^{3} 5×10^{3}	Yaroshenko et al. (2011) (electron, water group ions and protons plasma)
Laboratory Experiments	46418	7.5×10^{6}	1.7	Kremer et al. (2006) (pure electrons plasma)

Section 2.2.3 provides supplementary material about N_D, the average number of charges in the Debye sphere. The values for N_D are $\gg 10^5$ in the rarefied upper part of the atmospheres ($p_{gas} < 10^{-4}$ bar) for all M-dwarf, brown dwarf and giant gas planet model atmospheres investigated here. Values for the above quoted Debye length for the Earth ionosphere and solar wind are $N_D^{ionosphere} = 10^5$ and $N_D^{sunwind} = 10^{10}$. The parameter N_D indicates that the gas is dominated by many long-range interactions of charged particles, rather than the short-range binary interactions. If any charged particle is close enough to others then, it interacts in a collective behaviour, not only with the closest one. This collective behaviour distinguishes a plasma from a kinetic gas. Collective behaviour occurs if $N_D \gg 1$. Figure 2.3 shows that $N_D \gg 1$ is satisfied throughout the whole atmosphere for model atmosphere structures presented in Table 2.1. A substantially higher N_D is required for cooler atmospheres than in atmospheres for higher T_{eff} if thermal ionisation is considered only (i.e. $T_e = T_{gas,LTE}$).

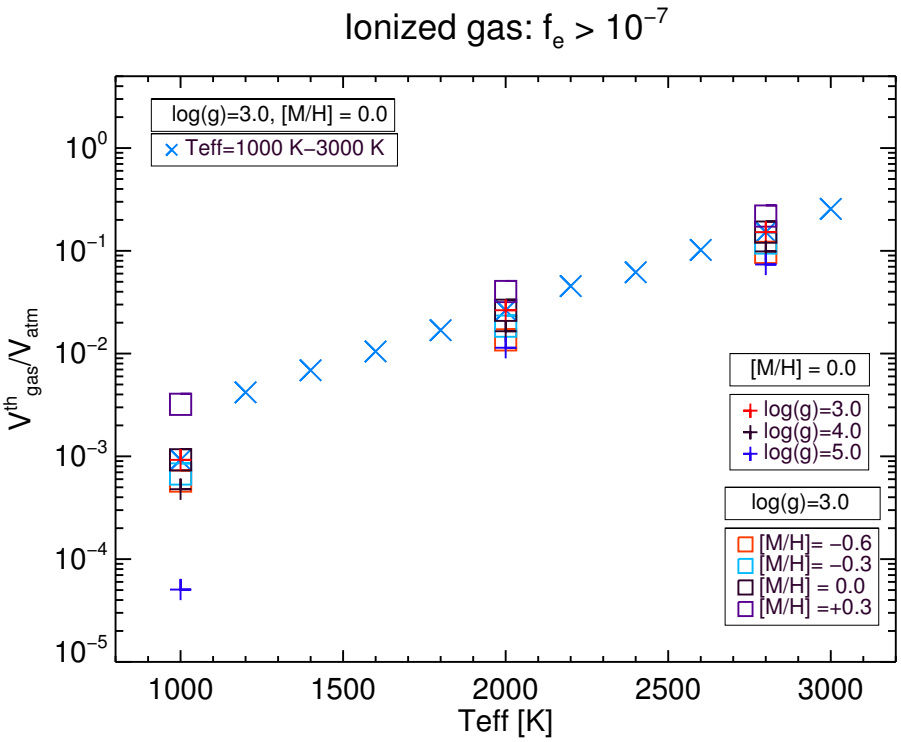

Figure 2.8: The fraction of the thermally ionized atmospheres volume, $V^{\rm th}_{\rm gas}/V_{\rm atm}$, for $f_{\rm e} > 10^{-7}$ and for M-dwarf, brown dwarf and giant gas planet atmospheres.

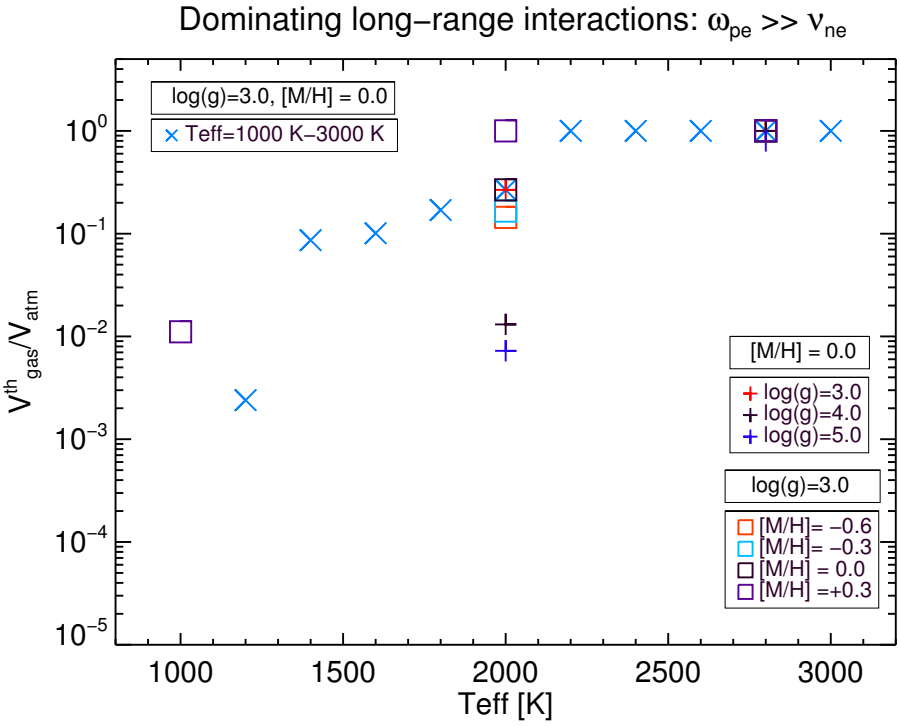

Figure 2.9: The fraction of the thermally ionized atmospheres volume, $V^{\rm th}_{\rm gas}/V_{\rm atm}$ for $\omega_{\rm pe} \gg \nu_{\rm ne}$ for M-dwarf, brown dwarf and giant gas planet atmospheres.

2.3.4 Comparing different plasma criteria

Radio and X-ray observations from low-mass objects suggest that their atmospheres contain enough free charges to constitute a magnetized plasma (Hallinan et al. 2008). From the evaluation of the thermal degree of ionisation (Sec. 2.3.1), I chose a threshold for the degree of ionisation of $f_e > 10^{-7}$ above which an atmospheric gas can be sufficiently ionised that it may exhibit plasma behaviour. In a plasma, electron-electron interactions dominate over collisions between electrons and neutral particles, $\omega_{pe} \gg \nu_{ne}$ (see Sec. 2.3.2). Additionally, for a plasma to be considered magnetized, the magnetic field must be sufficiently strong that it significantly influences the electron and ion dynamics. I address this topic in Chapter 2.4. I now cast the results in terms of atmospheric volumes to allow a comparison between the results for different parameters. Figure 2.8 and 2.9 summarise the findings in terms of the volume fraction, V^{th}_{gas}/V_{atm}, with V^{th}_{gas} the thermally ionised volume of the atmosphere and V_{atm} the total atmospheric volume. V^{th}_{gas} is derived by calculating the fraction of the atmospheric volume for which $f_e > 10^{-7}$ (Fig. 2.8). Figure 2.9 visualises the atmospheric volume fraction where $\omega_{pe} \gg \nu_{ne}$ is fulfilled. The atmosphere volume that reached $f_e > 10^{-7}$ and satisfied $\omega_{pe} \gg \nu_{ne}$ is affected by the global parameters as follows:

- If T_{eff} increases, then the thermally ionised atmospheric volume fraction increases for a given $\log(g)$ and [M/H].

- The V^{th}_{gas}/V_{atm}, that reaches $f_e > 10^{-7}$ and $\omega_{pe} \gg \nu_{ne}$, increases if $\log(g)$ decreases for a given T_{eff} and [M/H].

- Higher values of the metallicity [M/H], cause a larger fraction of the atmosphere volume to have a sufficiently ionised gas that large-scale electromagnetic interactions dominate over electron-neutral collisions for a given T_{eff} and $\log(g)$.

The late M-dwarfs have the largest atmosphere volume fraction, V^{th}_{gas}/V_{atm}, that reached $f_e > 10^{-7}$ that is for model atmosphere structures with $T_{eff} = 2600-3000$ K, $\log(g)$=3.0, [M/H]= 0.0 and $T_{eff} = 2800$ K , $\log(g)$=3.0, [M/H]=+0.3. For late M-dwarfs and brown dwarfs, the atmospheric gas satisfies $f_e > 10^{-7}$ only for half of their atmosphere. For planetary objects the fraction of the volume that reaches $f_e > 10^{-7}$ becomes increasingly small except for those that have the highest value of metallicity and the lowest value of surface gravity.

Models with 2200 K$\leq$ T_{eff} $\leq$ 3000 K, log(g)=3.0, [M/H]= 0.0 have the largest atmosphere volume fraction that reached $\omega_{pe} \gg \nu_{ne}$ for a given log(g) and [M/H]. Models with T_{eff} =2800 K, log(g)=4.0, [M/H]= 0.0; T_{eff} =2800 K, log(g)=3.0, [M/H]= -0.6, -0.3, 0.0, +0.3 and T_{eff} = 2000 K, log(g)=3.0, [M/H]= +0.3 have the largest atmosphere volume fraction that reached $\omega_{pe} \gg \nu_{ne}$ as well. In young brown dwarfs, the atmospheric gas volume that reaches $\omega_{pe} \gg \nu_{ne}$ is more than 50%. The atmospheric gas volume that reaches $\omega_{pe} \gg \nu_{ne}$ for planetary objects is smaller than for the rest of the objects, i.e. for $T_{eff} = 1000$ K, log(g)=3.0, [M/H]= +0.3. The results show that V^{th}_{gas}/V_{atm} ($\omega_{pe} \gg \nu_{ne}$) is larger than $V^{th}_{gas}/V_{atm}(f_e > 10^{-7})$ for 1000 K $\leq$ T_{eff} $\leq$ 3000 K. A general observation is that despite a relatively low degree of ionisation, large-scale electromagnetic interactions can dominate a considerably larger atmospheric volume than a f_e evaluation would suggest for all ultra-cool objects in this sample.

2.3.5 Dominating ions across the late M-dwarf, brown dwarf and planetary regime

The DRIFT-PHOENIX atmosphere structures is used to investigate the atmospheric gas-phase composition for the most abundant local ions to show which ones are the dominating electron donors across the star-planet regime. This study allow to understand which gas-phase species are responsible for increasing the number of free electrons in ultra-cool atmospheres and are ultimately responsible for satisfying the plasma parameters given in Eq. 2.1-2.3 across the star-planet regime. Rodríguez-Barrera et al. (2015) show that K^+, Na^+, Ca^+, Mg^+ and Fe^+ are the dominating thermal electron donors. As their abundances increase, the criteria given by the Eq. 2.1-2.3 are met. *This section was part of a summer student work. The detailed results are not shown here but, in Rodríguez-Barrera et al. (2015), are described in more detail.*

2.4 Basic magnetic parameters of the atmospheric gas across the star-planet regime

In the previous sections it was discussed that a certain degree of ionization ($f_e > 10^{-7}$) is a necessary property of a plasma. The plasma frequency was used to investigate where in the atmosphere, electromagnetic interactions dominate over kinetic collisions between electrons and neutrals. The Debye length provides insight about the length scales at which electrostatic interactions influence the atmospheric gas. It was shown that the atmospheric volume frac-

tion, $V^{\rm th}_{\rm gas}/V_{\rm atm}$ (suspected to show plasma behaviour) varies largely through the M-dwarf to planetary regime. A plasma is considered magnetised when the motion and dynamics of the charged particles are influenced by an ambient magnetic field. This requires that the magnetic field is strong enough to force charged particles to participate on average in at least one Larmor radius[2] (or Larmor orbit) before colliding with a neutral atom or dust particle: frequent collisions with the ambient neutrals would otherwise dominate the dynamical evolution of the plasma particles and the influence of the magnetic field would be negligible. It could happen that the electrons can be magnetised while the ions are not due to the differing mass between them.

In the follow section is discussed the magnetic behaviour of the atmospheric gas in the environment of brown dwarf atmospheres. For magneto-fluid descriptions of plasmas (such as magnetohydrodynamics) both the electrons and ions need to be magnetised. The high energy events in brown dwarfs (Sec. 1.2) suggest that there should be a strong magnetic field and considerable coupling between the magnetic field and the atmospheric gas, either to directly accelerate free electrons or to allow plasma waves to travel into the low-density upper atmosphere and deposit their energy causing a chromosphere to develop. For young brown dwarfs, rapid rotation may favour chromospheric heating by a better coupling to a stronger magnetic field.

2.4.1 Cyclotron frequency versus collisional frequency

A particle with a charge q, velocity v and mass m immersed in a electric a magnetic field is accelerated according the equation of motion for a charged particle and also known as Newton-Lorentz equation[3]. The Lorentz force overcomes the centrifugal force and the particle will describe a spiral orbit along the magnetic field line. The spiral movement is described by a frequency, $\omega_{\rm c,s}$ (the cyclotron frequency) and with a radius, $r_{\rm L,s}$(the Larmor radius) (see Fig. 2.11). The cyclotron frequency is the angular velocity with which the charged particle gyrates around the magnetic field line (Boyd & Sanderson, 2003), $\omega_{\rm c,s} = v_{\perp,\rm s}/r_{\rm L,s} = q_{\rm s}B/m_{\rm s}$ in $[\mathrm{rad\,s^{-1}}]$, where $m_{\rm s}$ [kg], $q_{\rm s}$ [C], B [T] and $v_{\perp,\rm s}$ $[\mathrm{m\,s^{-1}}]$ are the mass of species s, with charge $q_{\rm s}$ and speed perpendicular to the magnetic field $v_{\perp,\rm s}$ respectively; and $|\overrightarrow{B}| = B$ is the magni-

[2]The Larmor radius, $\mathrm{r_{L,s}}$[cm], is the radius of a complete spiral of the movement of a charged particle immersed in a ionised gas around of the magnetic field lines

[3]The equation of motion for a charged particle: $m\dot{\overrightarrow{v}} = q(\overrightarrow{E} + \overrightarrow{v} \times \overrightarrow{B})$ where $\overrightarrow{v}$ is the velocity of the charged particle, $\overrightarrow{E}$ and $\overrightarrow{B}$ the electric and magnetic field present in the environment respectively (Dinklage 2005).

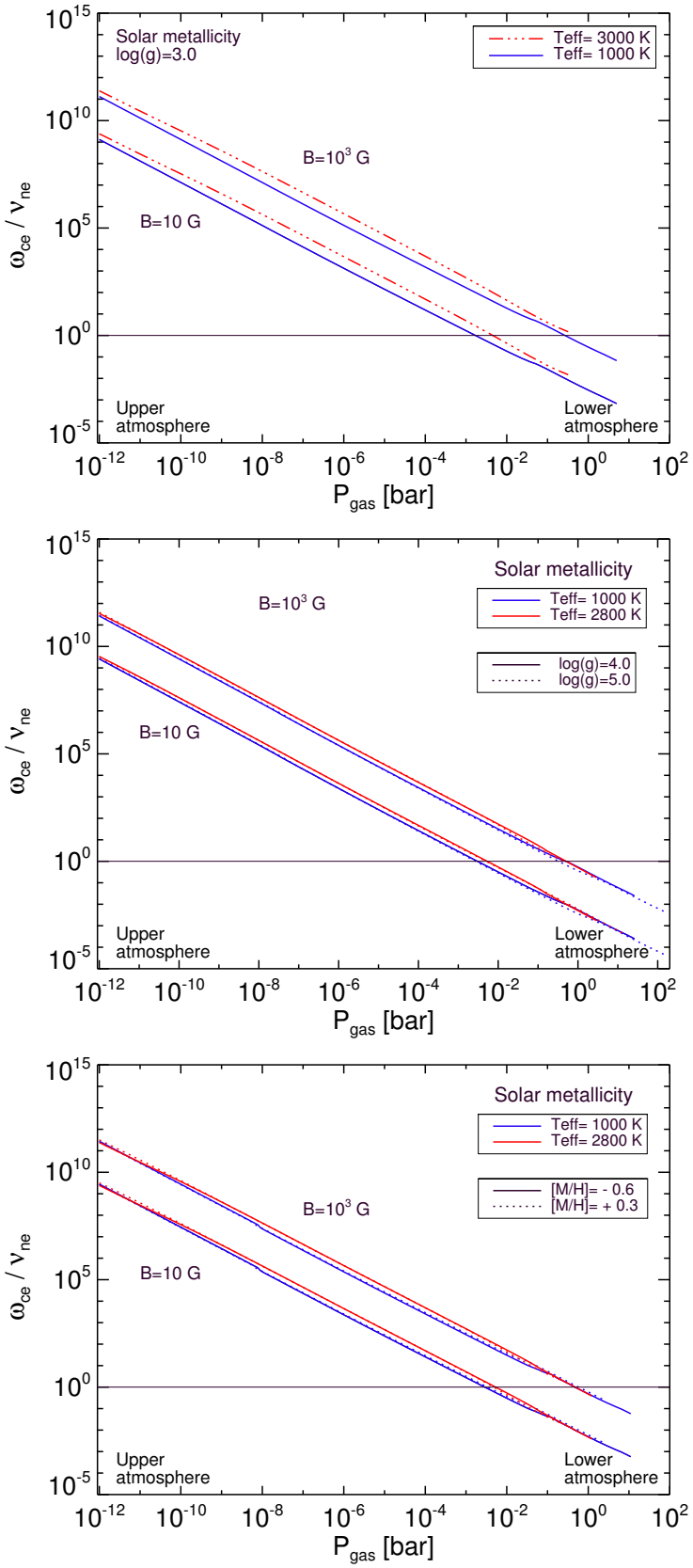

Figure 2.10: Ratio of cyclotron frequency of the electrons and the frequency of collisions between neutral particles and electrons. **Top:** Group 1. **Middle:** Group 2. **Bottom:** Group 3.

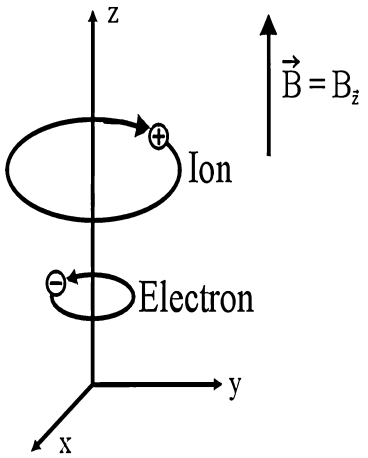

Figure 2.11: The charged particle rotate around the magnetic field line with Larmor radius and a cyclotron frequency (Dinklage 2005).

tude of the external magnetic flux density present in the medium. The synchrotron radiation is defined as the emission of relativistic electrons gyrating in the presence of a magnetic field. The movement of the charged particles are described by the Newton-Lorentz equation but, introducing a relativistic factor, γ. Hence, the synchrotron radiation for particles with charge, q_α and mass m_α is described by a cyclotron frequency $\omega_{c,s} = q_\alpha B/(\gamma m_{\alpha,0})$ and by the Larmour radius $r_{L,s} = \gamma m_{\alpha,0}/(q_\alpha B)$ (Dinklage 2005).

For a charged particle's motion to be dictated by a magnetic field, the particle needs to complete on average one gyration before a collision with a neutral atom. Formally, a magnetised plasma requires

$$\omega_{c,s} \gg \nu_{ns}, \tag{2.8}$$

where ν_{ns} [s^{-1}] is the collision frequency for neutral particles with charged species s. From Eq. 2.8 I obtain the minimum value for the external magnetic field flux, $|\overrightarrow{B}| = B$, that is needed to satisfied this criteria. Figure 2.10 shows that for a $p_{gas} < 10^0$ bar and B= 10^3 G and for a $p_{gas} < 10^{-2}$ bar and B= 10 G , $\omega_{ce} \gg \nu_{ne}$ (horizontal black line) is fullfilled for all model atmosphere structures. There is almost no dependence on T_{eff}, $\log(g)$ and the metallicity [M/H]. Largest values of ω_{ce}/ν_{ne} are reached for B= 10^3 G representative for M-dwarfs or brown dwarfs.

The critical magnetic flux density required for the dynamics of the charged particle to be influenced by the background magnetic field is calculated applying the definitions for $\omega_{c,s}$

and ν_{ns}:

$$\frac{eB}{m_s} \gg \sigma_{gas,e} n_{gas} \nu_s, \tag{2.9}$$

$$\Rightarrow B_s \gg \frac{m_s}{e} \sigma_{gas,e} n_{gas} \left(\frac{k_B T_s}{m_s} \right)^{1/2}, \tag{2.10}$$

where the collision, or scattering, cross section is $\sigma_{gas} = \pi \cdot r_{gas}^2$. The atmospheric gas in late M-dwarfs, brown dwarfs and most likely also in giant gas planets is composed mostly of molecular hydrogen, H_2. The collision cross section is approximated as $\sigma_{gas} \approx \sigma_{H_2} \approx \pi \cdot {r_{H_2}}^2 = 5.81 \cdot 10^{-20}$ m^2 ($r_{H_2} = 1.36 \cdot 10^{-10}$ m).

Taking the electrons and ions as the particles that are influenced by an external magnetic flux density, the Eq. 2.10 becomes

$$B_e \gg \frac{m_e}{e} \sigma_{gas} n_{gas} \left(\frac{k_B T_e}{m_e} \right)^{1/2}, \tag{2.11}$$

$$B_i \gg \frac{m_i}{e} \sigma_{gas} n_{gas} \left(\frac{k_B T_i}{m_i} \right)^{1/2}. \tag{2.12}$$

Grouping the constants the Eqs. 2.11 and 2.12 are rewritten as $B_e \propto n_{gas}(m_e T_e)^{1/2}$ and $B_i \propto n_{gas}(m_i T_i)^{1/2}$, with B_e and B_i as the minimum threshold for the magnetic flux density to ensure that the electrons and ions respectively can be magnetised (see Fig. 2.12). The ion masses m_i are taken to be for K^+, Na^+ Ca^+, Fe^+ and Mg^+ assuming LTE ($T_{gas} \approx T_i \approx T_e$).

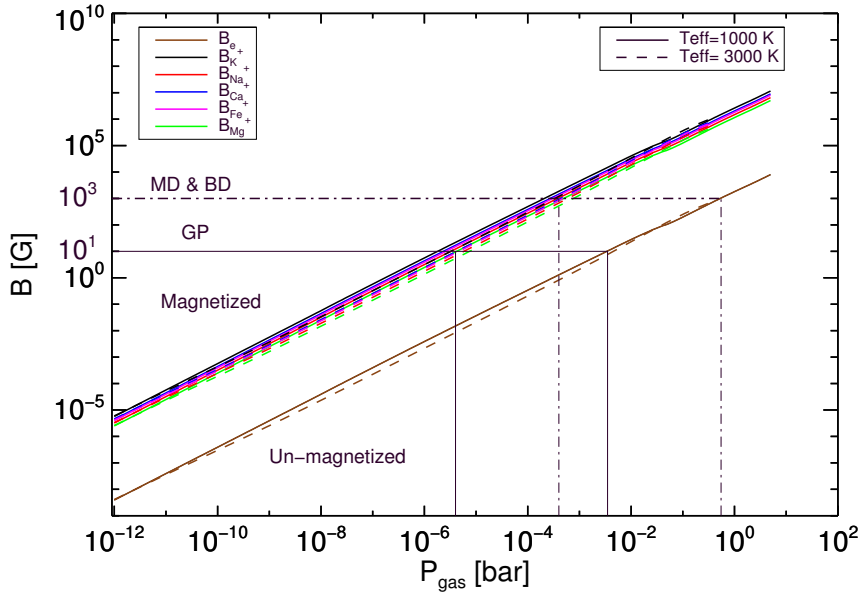

Figure 2.12: Magnetic flux density required for electrons, B_e (lower set of lines), and ions, B_i (upper set of lines), to be magnetically coupled to the magnetic field produced by the object: B=10 G for giant gas planets (GP) (black dash-dot lines) and B= 10^3 G for M-dwarfs (MD) and brown dwarfs (BD) (solid black lines). If $B > B_i$ (or $B > B_e$), $\omega_{c,s} \gg \nu_{ns}$ is fulfiled and the gas is magnetised by the external magnetic field B.

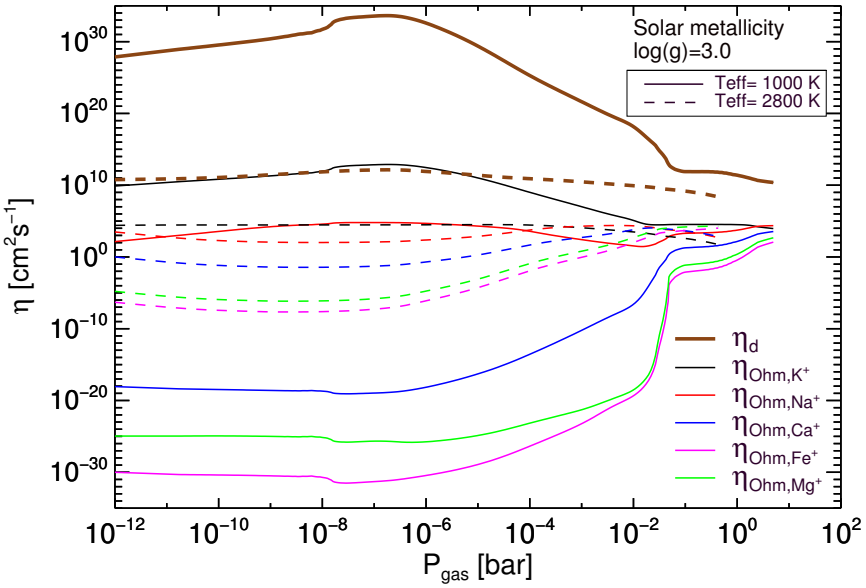

Figure 2.13: Decoupled diffusion coefficient, $\eta_d = c^2\nu_{en}/\omega_{pe}^2$ and the Ohmic diffusion coefficient, $\eta_{ohm} = c^2\nu_{ei}/\omega_{pe}^2$ for the dominating thermal electron donors for $T_{eff} = 1000, 2800$ K, for log(g)=3.0 and solar element abundances; K^+, Na^+, Ca^+, Fe^+ and Mg^+. The Ohmic diffusion coefficient is smaller than the decoupled diffusion coefficient. This result suggest that the binary interactions between the ions and electrons (η_{Ohm}) are not significant compared to the binary interactions between electrons and neutral particles (η_d) in the case of thermal ionisation. *The lines in both temperature sets appear from top to bottom in the order* η_d , η_{Ohm,K^+}, η_{Ohm,Na^+}, η_{Ohm,Ca^+}, η_{Ohm,Mg^+}, η_{Ohm,Fe^+}.

Figure 2.12 shows for which atmospheric gas pressures, p_{gas}, electrons and ions can be magnetised in the atmospheres of M-dwarfs, brown dwarfs and giant gas planets. For M-dwarfs and brown dwarfs, a background magnetic field flux density of B= 10^3 G is large enough to magnetise the charged particles: for electrons at $p_{gas} < 1$ bar and for ions at $p_{gas} < 10^{-3}$ bar. For giant gas planets, the magnetised part of the atmosphere decreases because of a smaller background field (B $\leq$ 10 G) compared to M-dwarfs and brown dwarfs. For electrons this occurs at $p_{gas} < 10^{-2}$ bar and for ions at $p_{gas} < 10^{-5}$ bar.
Figure 2.15 summarises the results on magnetic coupling in term of the affected atmospheric gas volume, V^{th}_{gas}/V_{atm}, that reach $\omega_{c,e} \gg \nu_{ne}$. The magnetically coupled volume of an atmosphere increases if:

- T_{eff} increases for a given log(g) and [M/H].
- log(g) decreases for a given T_{eff} and [M/H].
- the metallicity [M/H] increases for a given T_{eff} and log(g).

For a fixed value of magnetic flux density, M-dwarfs and brown dwarf atmospheres have the largest magnetically coupled volume. Unsurprisingly, a smaller fraction of a giant gas planets atmosphere is magnetically coupled when thermal ionisation is considered as the only source of gas ionisation. However, this fraction can reach 80% also in a planetary atmosphere. The fraction of the atmospheric gas volume, V^{th}_{gas}/V_{atm}, that reaches $f_e > 10^{-7}$ (Fig. 2.8) and $\omega_{pe} \gg \nu_{ne}$ (Fig. 2.9) increases for the same set of global parameters T_{eff}, log(g), [M/H] like the atmospheric gas volume that reaches $\omega_{ce} \gg \nu_{ne}$. Figure 2.15 also shows that a larger atmospheric gas volume can be expected to be more magnetically coupled than the thermal degree of ionisation had initially suggested in Fig. 2.8. Therefore, a partial ionisation of the magnetically coupled gas does not influence the magnetic flux density. This finding is also supported by Donati et al. (2008) that show that partially-convective M-dwarfs host non-axisymmetric poloidal large-scale magnetic fields with a strong toroidal component, while fully convective objects have stronger large-scale field dominated by a mainly axisymmetric poloidal component and its strength increases as the decrease of the mass of the object.

2.4.2 Cyclotron frequency versus frequency of the plasma

Radio emission is thought to be produced by the emission mechanism electron-cyclotron maser instability (ECMI)(Hallinan et al. 2006) which requires that the electron frequency

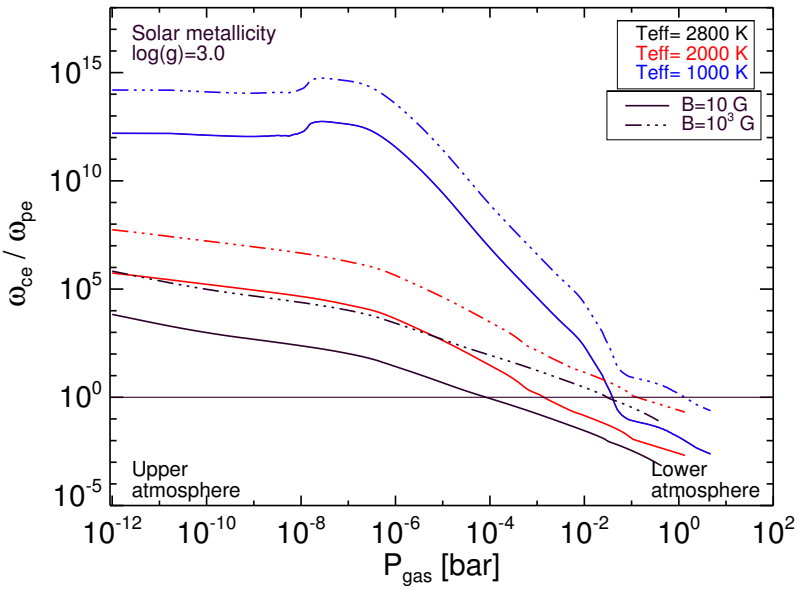

Figure 2.14: Ratio of the cyclotron frequency and the plasma frequency of the electrons, required condition for the electron-cyclotron maser instability as the possible dominant mechanism to produce the radio emission in the magnetospheres of ultracool dwarfs.

much be greater than the plasma frequency of the electrons, $\omega_{c,e} \gg \omega_{p,e}$. Figure 2.14 shows that $\omega_{c,e} \gg \omega_{p,e}$ is fulfilled at $p_{gas} < 10^{-4}$ bar for T_{eff}=2800 K and $p_{gas} < 10^{-1}$ bar for T_{eff}=1000 K.

2.4.3 Magnetic Reynolds Number, R_m

The previous sections outlined the framework quantifying when an ionised gas in a substellar atmosphere behaves like a magnetised plasma. The magnetic Reynolds, R_m, number is an easy to use measure of a potentially magnetically coupled ionised gas. Within the context of MHD, R_m is the ratio of the convective and diffusive terms from the magnetic field induction equation. It quantifies whether the MHD plasma is in the ideal or resistive regimes. When the magnetic Reynolds number is very large (i.e. in the limit of large length scales), the MHD plasma is in the ideal MHD regime and the convective term has the dominant influence. In this regime the motion of the plasma fluid is determined by the magnetic field and viceversa. In the resistive MHD regime, the diffusive term is important and dissipative processes as Ohmic dissipation (Huang & Cumming 2012; Perna, Menou & Rauscher 2010) become significant. The magnetic Reynolds number is defined through the induction equation

$$\frac{\partial \vec{B}}{\partial t} = \nabla \times (\vec{u} \times \vec{B}) + \eta \nabla^2 B \tag{2.13}$$

where $|\overrightarrow{B}| = B\ [T]$ is the magnetic flux density, u is the flow velocity (formed by electrons and ions), and $\sigma\ [\mathrm{S\,m^{-1}}]$ is the electric conductivity. The magnetic diffusivity, η, is linked to the conductivity by $\eta = 1/\sigma$ in $[\mathrm{m^2\,s^{-1}}]$ and represents the diffusion of the magnetic field, a measure of the effect of collisions between the electrons and the neutral particles on the magnetic field. The collisions between the neutral particles and the charged particles (electrons or ions) have an influence on the diffusivity of the magnetic field. If the effect of the collisions is sufficient to displace them away from the magnetic lines, the coupling between the magnetic field and the fluid may be not effective. Therefore, the diffusion of the magnetic field depends on the frequency of the collisions between neutral particles and charged particles.

The magnetic Reynolds number, $\mathrm{R_m}$ can be defined as the ratio between the diffusive term and the advective term of the induction equation. It can be used as a measure of the magnetic coupling calling the plasma coupled to the magnetic field if $R_\mathrm{m} \geq 1$, with

$$R_m = \frac{|\nabla \times (\vec{u} \times \vec{B})|}{\eta\,|\nabla^2 B|}. \tag{2.14}$$

Applying a dimensional analysis, the Eq. 2.16 is reduced to

$$R_m \approx \frac{vB/L}{\eta B/L^2} = \frac{vL}{\eta}, \tag{2.15}$$

where L [cm] is the pressure scale length of the plasma over which $|\overrightarrow{B}| = B$ varies through a hydrodynamic motion of a velocity $|\overrightarrow{v}|$ and it can be approximated by L=10^3 [m] according to Helling et al. (2011a). The diffusion coefficient, η, can be approximated by $\eta \approx \eta_\mathrm{d}$ (Fig. 2.13). The diffusion coefficient used in Eq. 2.15 is given by $\eta = \eta_\mathrm{d} + \eta_\mathrm{ohm}$ being $\eta_\mathrm{d} = c^2\nu_\mathrm{ne}/\omega_\mathrm{pe}^2$ as the decoupled diffusion coefficient and $\eta_\mathrm{ohm} = c^2\nu_\mathrm{ei}/\omega_\mathrm{pe}^2$ as the Ohmic diffusion coefficient being satisfied that $\eta_\mathrm{d} \gg \eta_\mathrm{ohm}$ (see Fig. 2.13). Both measure the degree of the dominance of the collisions between electrons-neutral particles and electrons-ions respectively over long-range electromagnetic collective interactions. It is easy to relate η_d with

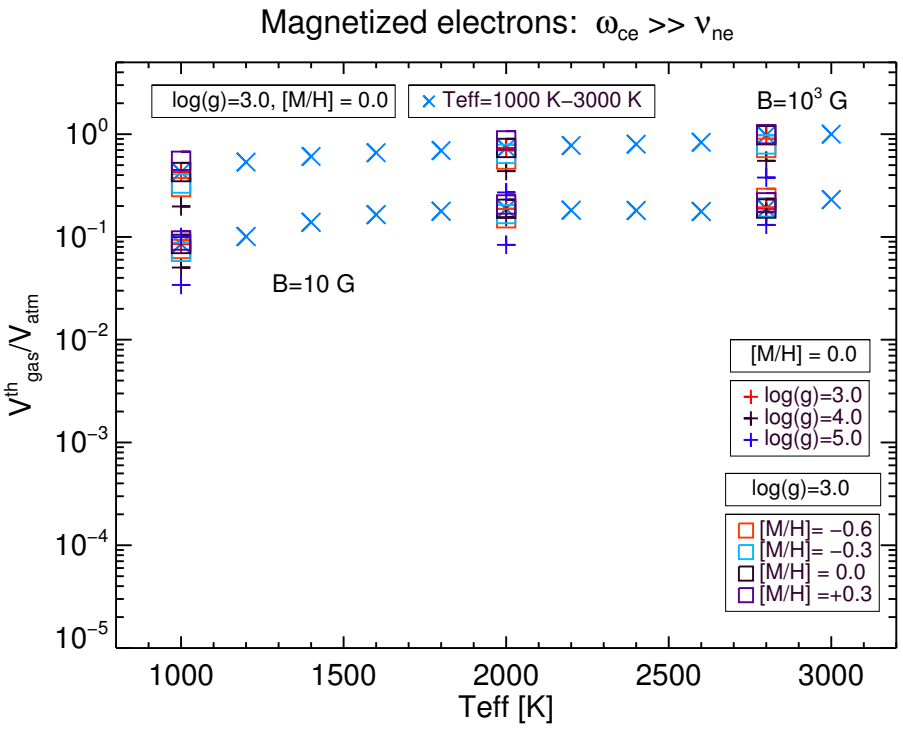

Figure 2.15: The fraction of the atmospheric volume, $V^{\rm th}_{\rm gas}/V_{\rm atm}$, where $\omega_{\rm ce} \gg \nu_{\rm ne}$ for M-dwarf, brown dwarf and giant gas planet atmospheres. M-dwarfs and brown dwarfs are represented by B= 10^3 G and giant gas planets for B= 10 G.

$\omega_{\rm pe}/\nu_{\rm ne}$ (see Fig. 2.5). If the latter increase, the diffusion coefficient decrease and the magnetic field may be generated and transported by fluid motions allowing the magnetic energy to be released into upper layers of the atmosphere as radio, X-ray and H_α emissions.

Therefore, the expression for the magnetic Reynolds number is rewritten as

$$R_{\rm m} \approx 10^{-4} \cdot v_{\rm flow} \left(\frac{n_{\rm e}}{n_{\rm gas} T_{\rm e}^{1/2}} \right). \tag{2.16}$$

The values for the flow velocity chosen are $v_{\rm flow}$= 10^4 cm s^{-1} and $v_{\rm flow}$= 10^6 cm s^{-1} guided by values of circulation models (Cooper & Showman 2005; Menou & Rauscher 2009; Rauscher & Menou 2013; Heng & Showman 2014; Rauscher & Kempton 2014). Figure 2.16 represents the magnetic Reynolds number for the DRIFT-PHOENIX model atmosphere structures which are comparable to the earlier results by Mohanty et al. (2002) that were based on DUSTY- and COND-PHOENIX. The Reynolds number increases as:

- T_{eff} increases for a given $\log(g)$ and [M/H] due to the increasing of n_e/n_{gas} in globally and locally hotter atmospheres (see Sec. 2.3.1). The highest R_m is reached for T_{eff}= 3000 K, $\log(g)$= 3.0, [M/H]= 0.0, v_{flow}= 10^6 cm s^{-1}.

- $\log(g)$ decreases in the inner, high-density atmosphere for a given T_{eff} and [M/H].

- $\log(g)$ increases in the outer, low-density atmosphere for a given T_{eff} and [M/H].

- [M/H] increases at high p_{gas} (inner atmosphere, high density) for a given T_{eff} and $\log(g)$.

- [M/H] decreases at low p_{gas} (outer atmosphere, low density) for a given T_{eff} and $\log(g)$ for low effective temperatures (i.e planet or T- and Y-dwarf atmospheres).

The results suggest that an ideal MHD regime, where a fully ionised gas is assumed, is best suited for models atmospheres with $T_{eff} \geq 3000$ K which includes M-dwarfs and young brown dwarfs. For cooler brown dwarfs and planetary regime objects only a small fraction of their atmosphere can be considered in ideal MHD regime.

2.4.4 Searching for a magnetized plasma

The study of the plasma parameters in late M-dwarfs, brown dwarfs and giant gas planets suggests that late M-dwarfs with T_{eff}=3000 K and brown dwarfs with T_{eff}=2800 K and [M/H]=+0.3 have a large atmosphere volume where the ambient gas is ionised. Another important result is that the whole atmosphere of a wide variety of studied objects fulfill that the electrostatics interactions dominate over the collisions between electron-neutral particles: from late-M-dwarfs until brown dwarfs with T_{eff}=2000 K and [M/H]=+0.3. This latter result suggests that cool brown dwarf atmospheres with supermetallicity are good candidates to host a plasma despite the fact that they have less ionised gas volume than late M-dwarfs and early brown dwarfs. In the other side, giant gas planets are so cool to apply for a plasma at upper part of the atmosphere: only for the deeper atmospheres the gas leads to be a plasma.

In terms of magnetic parameters, late M-dwarfs and brown dwarf atmospheres have the largest atmosphere gas volume that is coupled with the magnetic field. As it can be conclude form the previous paragraph, cool brown dwarf atmospheres have a low fraction of the ionised atmosphere gas, however, that does not affect to the coupling between the present magnetic field and the gas. Giant gas planets have a smaller fraction of atmosphere volume magnetically coupled. Another relevant parameter that measure the magnetic coupling is the magnetic Reynolds number that increases as T_{eff} increases: late M-dwarf atmosphere with T_{eff}= 3000 K are completely coupled with the gas; at the upper atmosphere only for early brown dwarf atmospheres the gas is coupled with the magnetic field (T_{eff}= 2800 K, log(g)= 5.0, [M/H]= 0.0); for late brown dwarfs and giant gas planets the coupling is reached at the deeper atmosphere.

Summarising, I can conclude that a magnetised plasma is reached considering only thermal ionisation as the only mechanism to ionise the atmosphere gas for:

- late M-dwarfs throughout the whole atmosphere.
- early brown dwarfs at the upper atmosphere.
- late brown dwarfs and giant gas planets and the deeper atmosphere.

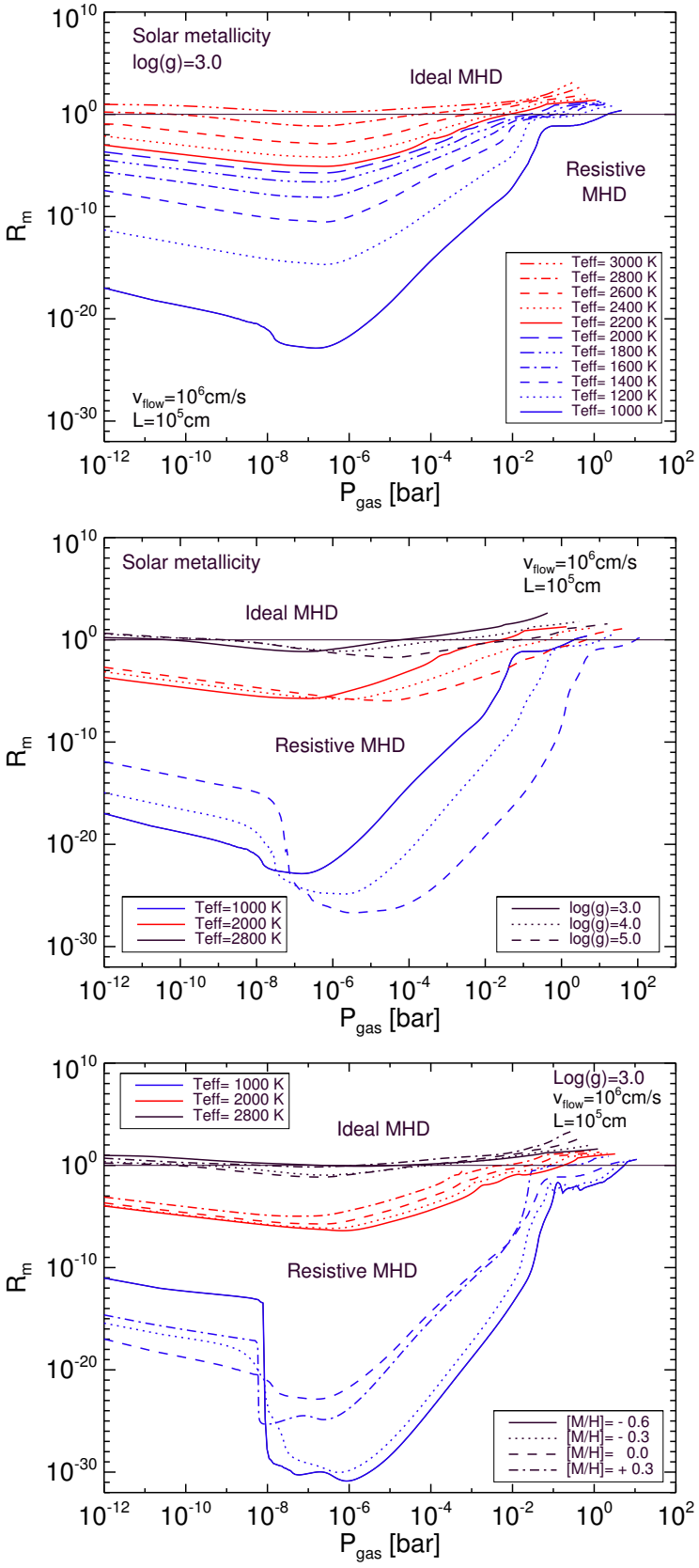

Figure 2.16: Magnetic Reynolds number R_m for the three different model atmosphere structure groups described in Sec 2.1. R_m is calculated for a flow speed of $v_{flow} = 10^6$ cm s^{-1}. If the flow speed increases, then R_m increases. **Top:** Group 1. **Middle:** Group 2. **Bottom:** Group 3.

3

Environmental effects on brown dwarf atmospheres through Lyman continuum irradiation in the ISM, in star forming regions and in white dwarf - brown dwarf binaries.

Chapter 2 has shown that thermal ionisation produces a partially ionised gas in cool brown dwarfs and giant gas planets and a highly ionised gas in the hotter/younger brown dwarfs or M-dwarfs but, for low effective temperatures and high surface gravity, an additional mechanism is needed to ionise the upper atmosphere of those objects. Chapter 3 investigates the effect of Lyman continuum irradiation compared to thermal ionisation on the ionisation structure of brown dwarf and giant gas planet atmospheres with different global (T_{eff}, $\log(g)$, [M/H]) parameters. The effect of external Lyman continuum irradiation is evaluated in the follow scenarios:

a) Young brown dwarf in an environment with strong radiation field, namely in star forming regions with O and B stars.

b) Old brown dwarf as companion of a white dwarf.

c) Free floating ultra-cool object in the ISM.

Section 3.3.2 and 3.3.3 apply the same methodology as Chapter 2 to study the local degree of ionisation, the dominance of the electromagnetic interactions over electron-neutral interactions, the magnetic Reynolds number and the required magnetic flux density to magnetise the electrons in objects irradiated by OB stars and by a white dwarf in a binary system respectively. Section 3.3.2.5 and 3.3.3.4 discuss the effect of photoionisation by Lyman continuum irradiation in conjunction with a chromosphere/corona on the production of observable X-ray luminosity from brown dwarfs.

3.1 Approach

The 3D Monte Carlo photoionisation code (Wood & Loeb 2000a) is used to determine the ionisation structure of the upper atmosphere of a low-mass, ultra-cool object, which is irradiated from an external source of Lyman continuum photons. In this study the photoionisation simulation is set up to be a 1D plane parallel atmosphere. Photons may therefore only exit the simulation via the upper and lower z faces, thus simulating a semi-infinite plane parallel atmosphere. The z direction traces the vertical 1D atmosphere profile where T_{gas}, p_{gas}, and ρ_{gas} increase inwards with increasing z (Fig. 2.1). By adopting a static plane parallel 1D atmosphere I determine the depth dependent ionisation structure in z-direction only. The z component of this simulation is represented by results from 1D DRIFT-PHOENIX model atmosphere simulations ($T_{gas}(z)$, $p_{gas}(z)$, $p_e(z)$).

3.1.1 Physical background of the Monte Carlo Radiative Transfer code

A bright source is emitting photons that travel some distance and interact with the material in the path of the photon (Lyman continuum photons or irradiation). The photons are scattered, absorbed or re-emitted. The scattering is considered isotropic and every single absorption is assumed to be followed by an immediately re-emission. The photon interaction with the material can heat it, changing the level populations of its components. Hence, the ionised balance of the material is disturbed producing a change of the opacity. The main goal of this study is to quantify the effect of an external radiation field of varying source strengths. The

photon energy, E=h·ν, is given by the simulation of the physical interactions of packets of photons through this medium, which contain the same energy (frequency).

3.1.2 Modelling approach

Young brown dwarfs are considered in an environment of strong radiation field, namely in star forming regions that host high-mass O and B stars that produce a substantial fraction of high-energy radiation compared to other less massive stars in the same region, old brown dwarfs as companions to white dwarfs, and a free floating ultra-cool objects in the ISM. Given the external radiation field originating from an O or a B star, the white dwarf, and as a reference from the ISM, the radiation energy E > 13.6 eV is assumed to be sufficient to ionise the H_2 which leaves the gas in the upper atmosphere to be dominated by the atomic hydrogen. The Monte Carlo radiative transfer (MCRT) technique is applied to investigate the ionised atomic hydrogen structure (photoionisation by Lyman continuum irradiation). This approach is guided by studies of the ionisation of photo-dissociation regions (PDRs). For interstellar photodissociation regions (PDRs), Hollenbach & Tielens (1999) demonstrate in their Fig. 3 that the interstellar radiation field (ISRF) ionises the gas until the gas reaches a column density $N_{gas}^{col} = 2\times10^{21}\,cm^{-2}$. For column densities $> 2\times10^{21}\,cm^{-2}$ the gas remains molecular. Hence, for column densities $< 2\times10^{21}\ cm^{-2}$, all H_2 has been converted into atomic hydrogen. The Monte Carlo code is applied to calculate the abundance of H^+ and therefore, the number of electrons originated by Lyman continuum irradiation. This approach is supported by Rimmer & Helling (2015) (their Fig. 9) which shows that $H_2 \rightarrow H$ in the uppermost atmospheric layers of an irradiated planet. In the upper atmosphere, free-free emission[1] from an optically thin gas may lead to observable X-ray emission.

3.1.3 Structure of the Monte Carlo photoionisation code

The Monte Carlo photoionisation code tracks the random walk of ionising photons on a 3D linear Cartesian grid and computes the 3D ionisation structure of hydrogen assuming a constant temperature and two frequency approximation for the ionising radiation, however, in this work, only a 1D ionisation structure of hydrogen is set up. What the ionisation code does is to emit photons that ionise the neutral gas. The ionised gas has a smaller opacity

[1]The free-free emission, also called thermal Bremsstrahlung radiation, is the process by which a rapid charged particle emits radiation when is accelerated due to the proximity of an atom, molecule or ion. The free-bound emission in that is the process by which a photon is emitted when an electron is recombined with an ion but, is not taken in account in this work.

than neutral gas, so photons can penetrate further and ionise a larger volume. To get the resulting ionisation structure, the code iterates several times until the ionisation structure does not change from iteration to iteration. At each iteration, the MCRT code computes, in each cell, the number of photoionisation events. The code balances the photoionisation event with radiative recombinations by the ionisation equilibrium equation in each cell to get a new ionisation structure (changing the H^+ abundance in each cell),

$$n(H^o)\int_{\nu_o}^{\infty}\frac{4\pi J_\nu}{h\nu}a_\nu(H^o)d\nu = n_e n_p \alpha(H^o,T), \tag{3.1}$$

where n(H^o) is the neutral atom density [cm^{-3}], J_ν is the mean intensity [$erg\,cm^{-2}\,s^{-1}\,Hz^{-1}$], $a_\nu(H^o)$ [cm^2] is the ionisation cross section for the hydrogen with E > $h\nu_o$ (E > 13.6 eV), $\alpha(H^o,T)$ is the recombination coefficient [$cm^3\,s^{-1}$] and n_e and n_p [cm^{-3}] is the electron and proton density respectively. The opacity changes as the ionisation structure changes: the photon population changes in each interaction and they interact with the material heating it. The Monte Carlo code follows the random walks within the photoionised region in each cell for both, the direct ionising photons from the source(s) and diffuse photons produced by radiative recombinations direct to the ground state of hydrogen within the photoionised region.

Two frequency approximations are applied:

a) *The direct photons* are assigned a cross section $\sigma = 2.77\times10^{-18}$ cm^2 corresponding to an energy of 18 eV, thus making the approximation that the dominating ionising photons from the source are emitted at a single frequency.

b) *The diffuse photons* are assigned a cross section $\sigma = 6.3\times10^{-18}\,cm^3$ and an energy of 13.6 eV from recombinations to the ground state of the hydrogen atom.

During the Monte Carlo radiation transfer simulation direct ionising photons are converted to diffuse photons with a probability $\alpha_1/\ \alpha_A$, where α_1 is the hydrogen recombination coefficient direct to the ground state and α_A is the recombination coefficient to all levels. For photoionized gas at a temperature of 10^4 K this ratio is $\alpha_1\ /\ \alpha_A = 0.38$ (Osterbrock & Ferland 2006).

3.1.3.1 Input

A) *Model atmospheres input*

DRIFT-PHOENIX atmosphere structures with effective temperatures of $T_{eff} = 2800$ K, 2000 K, 1000 K, surface gravities of $\log(g) = 3.0$, 5.0 and metallicity of [M/H]=0.0 are used to describe atmospheres of young and old brown dwarfs (see Fig. 2.1 and Fig. 3.1). The local gas output by DRIFT-PHOENIX, $T_{gas}(z)[K]$, $p_{gas}(z)[bar]$ and $p_e(z)[bar]$ (or $n_e(z)[cm^{-3}]$), for a given global parameters as T_{eff} [K], $\log(g)$ [cm s^{-2}] and [M/H], change with the geometrical vertical coordinate z (see Fig. 2.1, Fig. 3.1 and Fig. 3.4) and also are used as part of the input for the Monte Carlo radiative transfer photoionisation code. The ($T_{gas}(z)$, $p_{gas}(z)$)-structures also allow to study where, in a brown dwarf atmosphere, the threshold of N_{col}=2·10^{21} cm^{-2} for H_2 ionisation may be reached. Figure 3.2 shows the column densities ($N_{col} = \int_{z_{min}}^{z_{max}} n < H > (z) z\, dz$ [cm^{-2}]) for the atmosphere models utilised in this paper: old brown dwarfs ($\log(g)$=5.0 lower panel); giant gas planets and young brown dwarfs ($\log(g)$=3.0, upper panel). Also Fig. 3.2 shows that the atmosphere column density is $< 2 \times 10^{21}$ cm^{-2} in the upper atmosphere (where the effect of Lyman continuum irradiation on the atmosphere ionisation is investigated) and means that all H_2 has been converted into atomic hydrogen. For the deeper atmosphere (where the ionising photons from an external source do not penetrate), the column densities is $> 2 \times 10^{21}$ cm^{-2}. That means that the atmospheric gas start to remain in form of molecular hydrogen.

B) *Lyman continuum irradiation input*

The Lyman continuum irradiation is formed of photons from high-mass stars, like O and B stars in a galaxy (Wood & Loeb 2000b), from a white dwarf (Casewell et al. (2012); Hills (1973)) or from the interstellar medium for example (massive hot stars as O and B provide important amounts of energy into the interstellar medium: Sternberg, Hoffmann & Pauldrach 2003; Reynolds 1984) that are emitted with energies above the Lyman limit. The Lyman limit, $E_\nu = h\nu$>13.6 eV is the required energy that an electron, at the ground state, must possess to escape from the electrostatic potential of the hydrogen atom. The ionising photons from the high-mass stars produce a free-free continuum fluxes (Sternberg, Hoffmann & Pauldrach 2003). High-mass stars often form clusters as the OB1 association in the Orion Nebula Cluster. That association could be formed by tens to hundred of individual

OB stars within small volumes (Feigelson et al. 2003). The effect of the Lyman continuum irradiation on the ionised structure of brown dwarfs by photoionisation of a hydrogen-rich gas is determined using the Monte Carlo radiative transfer code (Sec. 3.1.2) and the model atmosphere simulations DRIFT-PHOENIX (Sec. 3.1.3.1). A key parameter (input of the MCRT code) to get the ionised structure of the hydrogen gas is the number of ionising photons per second that a bulk volume of the irradiated object is receiving from the external source that is given by $Q = N_{LyC} \cdot A$ [photons s^{-1}] where N_{LyC} [photons $cm^{-2}\,s^{-1}$] is the rate of emission of Lyman continuum photons per unit of time and area from the external source and A [cm] is the surface area of the irradiated object. Table 3.1 shows the rate of emission of Lyman continuum photons, N_{LyC}, from different sources of radiation (OB stars, a white dwarf and the ISM).

Table 3.1: Lyman continuum flux emitted from an OB star, from a white dwarf and from the ISM. The emitted Lyman continuum flux of the external sources has been taken from: ISM from Reynolds (1984); for O3 and B0 from Sternberg, Hoffmann & Pauldrach (2003); for WD from Casewell et al. (2012) and Hills (1973).

Source	T_{eff} [K]	Q [photons s^{-1}]	d	N_{LyC} [photons s^{-1} cm^{-2}]
O3	51230	$7.41 \cdot 10^{49}$	0.5 pc	$3.11 \cdot 10^{13}$
B0	33340	$1.05 \cdot 10^{48}$	0.5 pc	$4.42 \cdot 10^{11}$
WD	14748	$2.75 \cdot 10^{41}$	0.006 AU	$3.41 \cdot 10^{9}$
ISM	———	———	———	$3 \cdot 10^{7}$

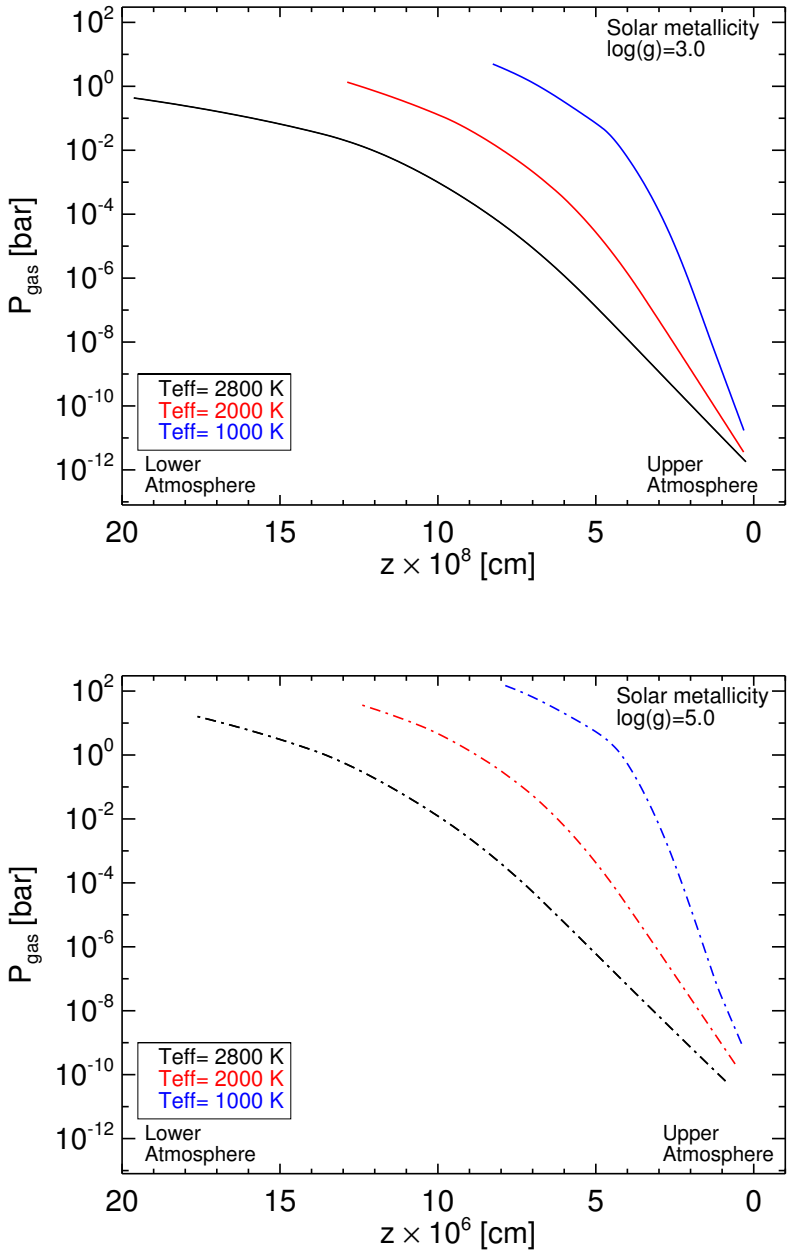

Figure 3.1: Local gas pressure, P_{gas} [bar] as function of vertical geometrical extension of the atmosphere, z [cm] given by model atmosphere simulations DRIFT-PHOENIX. **Top:** Young brown dwarf atmospheres **Bottom:** Old brown dwarf atmospheres.

3.1.3.2 Output

The Monte Carlo radiative transfer code provides the fraction of the molecular hydrogen, n_{frac}, present in the atmosphere of the studied objects (Wood & Loeb 2000a). From the fraction of the neutral gas, the fraction of free electrons given by the degree of ionisation, f_e, and the electron density, n_e [cm^{-3}], are calculated.

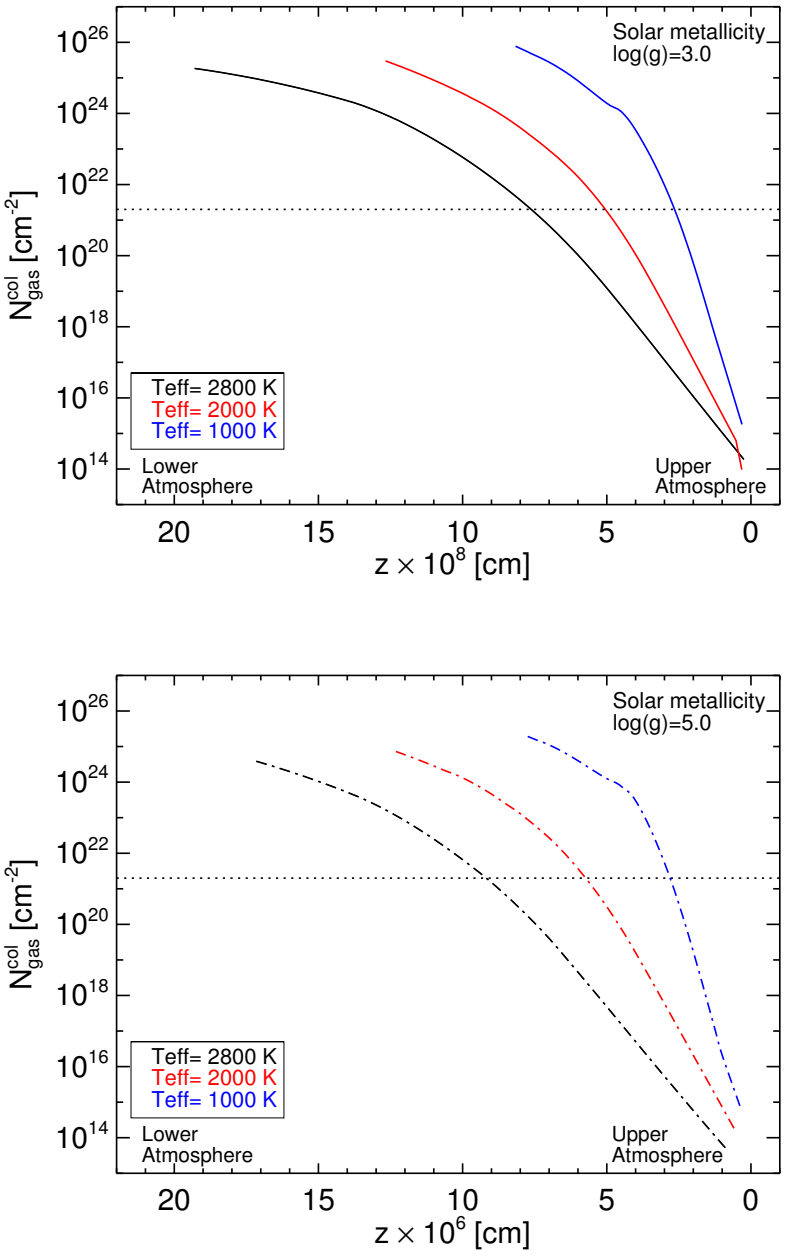

Figure 3.2: The column density, N_{gas}^{col} [cm^{-2}] as function of vertical geometrical extension of the atmosphere, z [cm]; **Top:** Young brown dwarf atmospheres **Bottom:** Old brown dwarf atmospheres. This value is represented as horizontal dash line.

3.2 Lyman continuum irradiation

The resulting luminosity from free-free emission is calculated applying the Eq. 3.2 if the ionised gas is optically thin,

$$L^{ff}(z) = 4\pi\,(R + (z_{max} - z_i))^2\,\epsilon_\nu^{ff}\,\delta(z), \tag{3.2}$$

with R [cm] the radius of the irradiated object, z_{max} [cm] the maximum value of the vertical geometrical extension of the atmosphere, z_i [cm] the value of the vertical geometrical extension of a particular shell of the atmosphere, $\delta(z) = z_{i+1} - z_i$ [cm] the vertical geometrical separation between two adjacent shells of the atmosphere. The volume emissivity or the total free-free emission power that a gas can emit per unit of volume, per solid angle and per unit of frequency, ϵ_ν^{ff} [erg cm^{-3} s^{-1}], of an optically thin gas integrated over a range of energy (Osterbrock & Ferland 2006; Lang 1974) is given by the follow equation

$$\epsilon^{ff} = 5.44 \cdot 10^{-39}\,T_{gas}^{1/2}\,n_e n_i\,\overline{g}_B \frac{1}{h}\int_{h\nu_1}^{h\nu_2} e^{-\frac{h\nu}{k_B T}}\,d(h\nu)\,[cm^{-3}]\,. \tag{3.3}$$

The resulting luminosity from free-free emission calculated for each shell of the atmosphere, L_{tot}^{ff} [erg s^{-1}], is given by the Eq. 3.4,

$$L_{tot}^{ff} = \sum_z L^{ff}(z), \tag{3.4}$$

where $L^{ff}(z)$ is given by the Eq. 3.2. The electron density, n_e [cm^{-3}] is calculated from the ionisation fraction of the hydrogen-rich atmosphere gas that is given by the Montecarlo transfer radiative code. The local gas temperature, T_{gas} [K] in Eq. 3.3 is assumed to be chromospheric/corona temperature only for the calculation of $L^{ff}(z)$ (Eq. 3.2), k_B is the Boltzamnn constant in [eV K^{-1}], h is the Planck constant in [eV s] and $\overline{g}_B$=1.2 is the Gaunt factor for a hydrogen plasma (Osterbrock & Ferland 2006). The Gaunt factor is a multiplicative factor that correct the calculations of continuous absorption or emission when a classical method is used rather than a quantum one. The integration boundaries $h\nu_1$=0.5 KeV and $h\nu_2$= 8 KeV correspond to X-ray range of the electromagnetic spectra.

3.3 Results

In this section, it is evaluated the effect of Lyman continuum photoionisation in the follow scenarios: a) In a *star forming region:* free-floating ultra-cool objects like brown dwarfs and planets receiving the Lyman continuum irradiation from massive stars like O3/B0 stars; b) In a *white dwarf - brown dwarf* binary system: a white dwarf irradiating its companion; c) In the *ISM:* old brown dwarfs or free floating planets irradiated from the interstellar medium.

Case a) and b) are studied in separate sections with respect to effect of Lyman continuum irradiation on the electrostatic character and regarding the potential magnetic coupling of the atmosphere. Case c), however, will only shortly be summarised and then used as a lower-limit reference for Lyman continuum irradiation on ultra-cool atmospheres. This evaluation follows the same framework introduced in Chapter 2. In Fig. 3.3 is represented the effect of Lyman continuum irradiation in the upper atmosphere of brown dwarfs. As I have metioned in Sec. 3.1.3.1, the column density threshold to ionise the H_2 is for $N_{col}=2{\cdot}10^{21}$ cm^{-2}. This threshold is always met in the upper atmosphere of brown dwarfs where the dominant ionising mechanism is Lyman continuum irradiation in the present investigation (rather than thermal ionisation) (Fig. 3.2).

3.3.1 Effect of the radiation field emitted from the interstellar medium (ISM)

The interstellar radiation field (ISRF) that is emitted from the ISM can be considered as a lower limit for high-energy irradiation of an old brown dwarf without a companion. It has been considered a Flux=$3{\cdot}10^7$ photons s^{-1} cm^{-2} (Reynolds 1984) from the ISM (Table 3.1). The effect of the ISRF on the structure atmosphere of brown dwarfs is shown in Fig. 3.3. The ISM can ionise the upper most part of ultracool objects covering late M-dwarfs, young and old brown dwarfs and hot objects in a planetary regime.

3.3.2 Application to star forming regions

In this section, I study the effect of Lyman continuum irradiation from OB stars on a brown dwarf atmosphere as a part of a star forming region. Their effect is expected to be considerably larger than that for brown dwarfs in the ISM (see Table 3.1). I have chosen an O3 and a B0 star at a distance to the brown dwarf of d=0.5 pc. The chosen O3 star allows to explore an upper limit of the irradiation effect, while B stars are more common members of star forming

regions, like e.g. in the Orion OB1 stellar association in the Orion constellation which contains 4 OB associations with 21 B-stars. The core of the Orion Nebula (M42 or NGC 1976) forms part of the Orion OB1 association and has been object of numerous observational studies (e.g. Feigelson et al. 2003). In the heart of the Orion Nebula (M42) is placed a strong star forming region (McCaughrean, Rayner & Zinnecker 1994) that reveals thermal radio sources being likely a circumstellar disks around young low-mass stars produced by the ionization from the irradiation of nearby OB stars. The Coronet cluster contains two, rather late-type B stars, only (e.g. Sicilia-Aguilar et al. 2008). As those young low-mass stars in the Orion Nebula (M42) are irradiated by OB stars, maybe the upper atmosphere gas could be ionised enough to emit powerful energy emissions at X-ray wavelengths. *The main observable implication of the effect of Lyman continuum irradiation from OB stars on a brown dwarf atmosphere is that the probability of having a larger volume susceptible to emit at high energy levels (e.g at X-ray energies) has considerably increased*.

3.3.2.1 Degree of ionisation

As it was defined in Chapter 2, the degree of the ionisation, f_e, quantifies of number of free electrons given by a particular ionising mechanism on a particular gas. Figure 3.3 represents the degree of ionisation of the atmosphere gas generated from thermal ionisation as result of the DRIFT-PHOENIX simulations and from Lyman continuum irradiation (LyC) as result of the MCRT code. Figure 3.3 shows that at the upper atmosphere of different objects, the predominant ionising mechanism is Lyman continuum photoionisation. However, the effect of the Lyman continuum irradiation cannot penetrate below a certain atmospheric depth below which other mechanisms are required to ionise the atmosphere. The thermal ionisation starts to dominate the ionisation of the atmosphere at $z \geq 10^9$ cm for atmosphere structures with $\log(g) = 3.0$ cm s^{-2} and at $z \geq 10^7$ cm for $\log(g) = 5.0$ cm s^{-2}. Therefore, the atmospheric gas of brown dwarfs, even with low effective temperature, is almost fully ionised under the effect of Lyman continuum irradiation for the upper atmosphere. The threshold $f_e > 10^{-7}$ marks the point above the atmospheric gas starts to be partially ionised and a plasma may be found (Rodríguez-Barrera et al. 2015). Figure 3.3 furthermore compares the location of the cloud in terms of cloud particles number density, n_d [cm^{-3}] (open triangles in Fig. 3.3) with the penetration depth of the effect of gas ionisation from LyC. Only the outermost cloud layer would be affected from the LyC, either by the high-energy photon directly interacting with

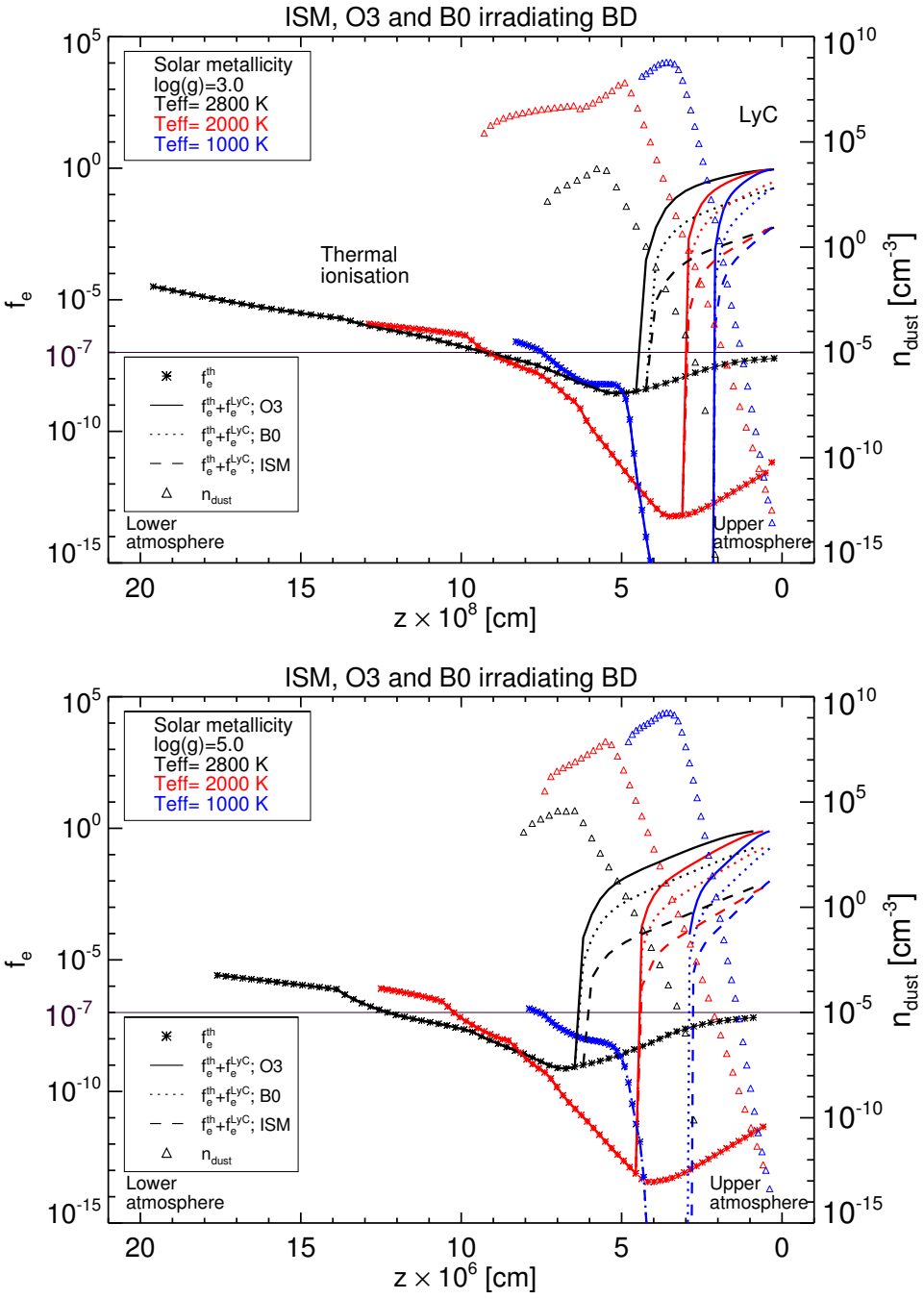

Figure 3.3: Effect of Lyman continuum irradiation from an O3 and a B0 star at a distance of 0.5 pc and from the ISM compared to the effect of the thermal ionisation on a) **Top**: giant gas planet or young brown dwarf atmospheres , b) **Bottom**: old brown dwarf atmospheres. The threshold $f_e > 10^{-7}$ (**thin solid black line**) marks the point above which the atmospheric gas starts to be partially ionised and a plasma may be found. The dust density, n_{dust} [cm^{-3}], is plotted here showing where the cloud layer is located inside the atmospheres as result of the kinetic cloud formation model using in this study.

the cloud particle surface or from the ionised gas depositing on the cloud particle surface. Both processes can cause an ionisation of the cloud particles as long as the cloud particles remain stable against electrostatic disruption. Helling et al. (2016) present a first consideration showing that electrostatic disruption occurs only for ionisation sources leading to $f_e \sim 1$ like in the case of Alfvén ionisation.

3.3.2.2 The effect of Lyman continuum irradiation on the atmospheric electron budget

Figure 3.4 and Table 3.2 show the resulting electron density, n_e [cm^{-3}] for substellar objects irradiated from an OB star in a star forming region in comparison to objects irradiated from the ISRF. Table 3.2 shows that the effect of Lyman continuum irradiation from an OB star is considerably larger than for the ISM. Therefore, brown dwarfs in star forming regions could emit from this upper, highly ionised atmosphere in free-free emission. The electron density from the irradiation of an O3 star is three orders of magnitude larger than that from the ISM on brown dwarf atmospheres with log(g)=3.0 and two orders of magnitude larger on brown dwarf atmospheres with log(g)=5.0. However, type B0 stars produce one and two orders of magnitude (depend on the atmosphere) more electrons than the effect of the irradiation from the ISM for brown dwarfs (log(g)=3.0, 5.0).

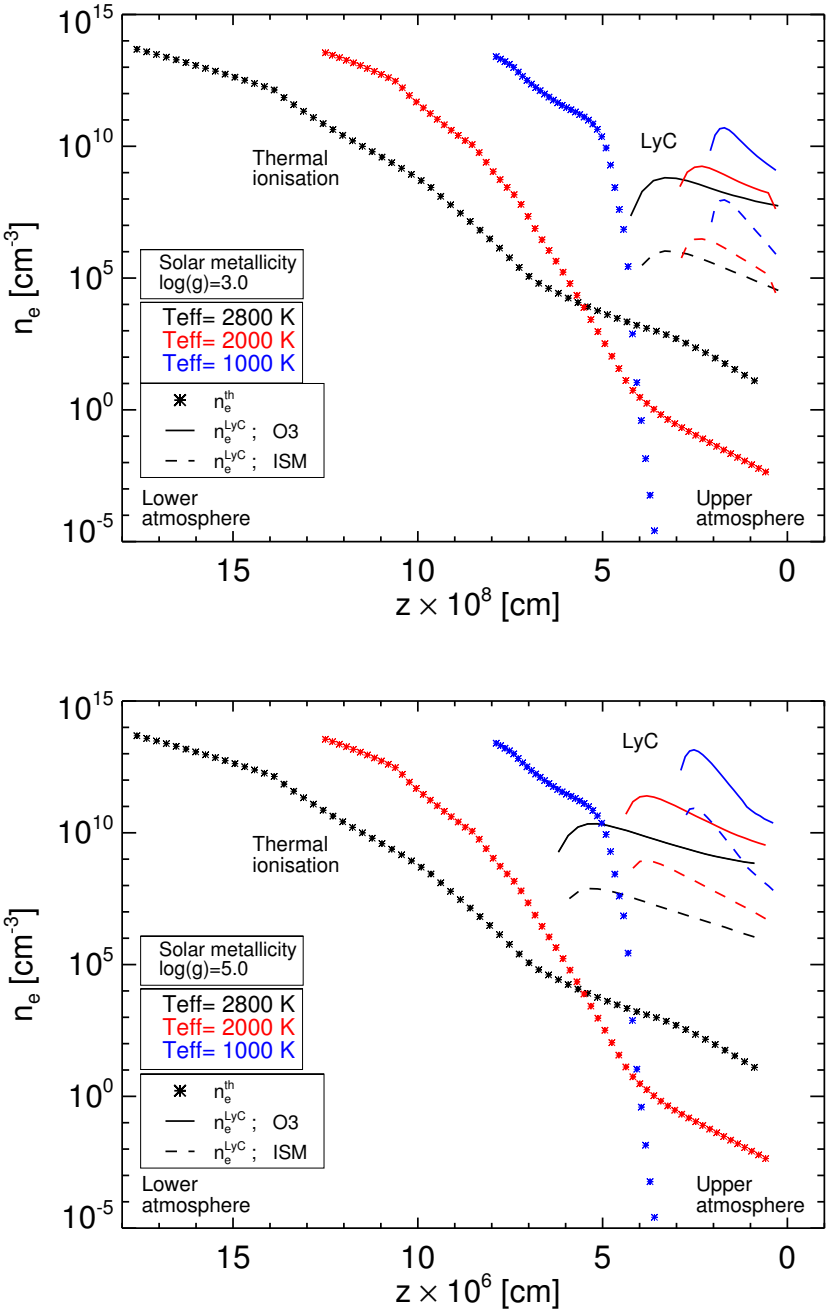

Figure 3.4: The electron density as a function of vertical geometrical extension of the atmosphere, z [cm], generated by Lyman continuum irradiation in a star forming region compared to the effect of thermal ionisation: **Solid lines** – Lyman continuum irradiation from an O3 star at a distance of 0.5 pc, **Dashed Lines** – Lyman continuum irradiation from ISM, **Asterisks** – Thermal ionisation. **Top:** Young brown dwarf atmospheres **Bottom:** Old brown dwarf atmospheres. The effect of Lyman continuum ionisation increases the electron density at outer parts of the atmosphere compared to the effect of thermal ionisation.

Table 3.2: The maximum of the electron number density, n_e [cm^{-3}] as result of the effect of Lyman continuum irradiation from an O3 and a B0 star at a distance of 0.5 pc in a star forming region and for the irradiation from the ISM. The atmosphere models studied here are for T_{eff}=2800 K, 2000 K, 1000 K; log(g)=3.0 (young brown dwarfs) and log(g)=5.0 (old brown dwarfs).

Source	T_{eff} [K] log(g) = 3.0	n_e [cm^{-3}] max value
O3	2800	$3.26 \cdot 10^{8}$
	2000	$1.75 \cdot 10^{9}$
	1000	$5.04 \cdot 10^{10}$
B0	2800	$3.52 \cdot 10^{7}$
	2000	$1.81 \cdot 10^{8}$
	1000	$3.03 \cdot 10^{9}$
ISM	2800	$1.06 \cdot 10^{6}$
	2000	$3.04 \cdot 10^{6}$
	1000	$9.22 \cdot 10^{7}$
Source	T_{eff} [K] log(g) = 5.0	n_e [cm^{-3}] max value
O3	2800	$2.19 \cdot 10^{10}$
	2000	$2.51 \cdot 10^{11}$
	1000	$1.41 \cdot 10^{13}$
B0	2800	$2.58 \cdot 10^{9}$
	2000	$2.97 \cdot 10^{10}$
	1000	$1.58 \cdot 10^{12}$
ISM	2800	$7.65 \cdot 10^{7}$
	2000	$8.81 \cdot 10^{8}$
	1000	$4.77 \cdot 10^{10}$

3.3.2.3 Plasma parameter

The plasma frequency, ω_{pe}, quantifies the electrostatic character of the gas (see Chapter 2). The criterion $\omega_{pe} \gg \nu_{ne}$ represents the dominance of the long-range charged particles interactions (electrostatics) over short-range interactions (electron-neutral collisions). If $\omega_{pe}/\nu_{ne} \gg 1$, the free electrons in the plasma are re-established to their equilibrium position against to the collision between electrons and neutral particles. The effect of Lyman continuum irradiation from an O3 type star at a distance of d=0.5 pc in a star forming region is studied here and compared to the effect of thermal ionisation. Figure 3.5 suggests that the criterion $\omega_{pe} \gg \nu_{ne}$ is fulfilled for atmospheres with:

- T_{eff}=2800 K and log(g)=3.0, 5.0 along of their local gas pressure scale except for a little fraction of the atmospheric gas ($p_{gas} \geq 10^{0}$ bar) for the atmosphere log(g)=5.0.
- T_{eff}=2000 K and log(g)=3.0 for $p_{gas} \leq 5 \cdot 10^{-8}$ bar and $p_{gas} \geq 10^{-5}$ bar.
- T_{eff}=2000 K and log(g)=5.0 for $p_{gas} \leq 5 \cdot 10^{-4}$ bar.
- T_{eff}=1000 K and log(g)=3.0 for $p_{gas} \leq 10^{-6}$ bar.
- T_{eff}=1000 K and log(g)=5.0 for $p_{gas} < 10^{-2}$ bar.

These results suggest that:

- for the hottest atmosphere and for the atmosphere with T_{eff}=2000 K and log(g)=3.0 the collective long-range electromagnetic interactions dominate over the collisions between electrons and neutral particles throughout the whole atmosphere.

- for the coldest atmosphere with T_{eff}=1000 K and log(g)=3.0, almost in the whole atmosphere collective long-range electromagnetic interactions dominate over the collisions.

Figure 3.3 and Fig. 3.5 show where the atmospheric gas can be treated as a plasma. This study demonstrates that Lyman continuum irradiation increases the atmospheric volume where the collective long-range electromagnetic interactions dominate in comparison with the calculations done in Chapter 2: two orders of magnitude more (in terms of local gas pressure) are obtained under the effect of LyC than by thermal ionisation (therefore, a considerably larger atmospheric volume is affected). Figure 3.5 suggests that there is not a strong dependence on T_{eff} and log(g) which is similar to the calculations done in Chapter 2 for the thermal ionisation.

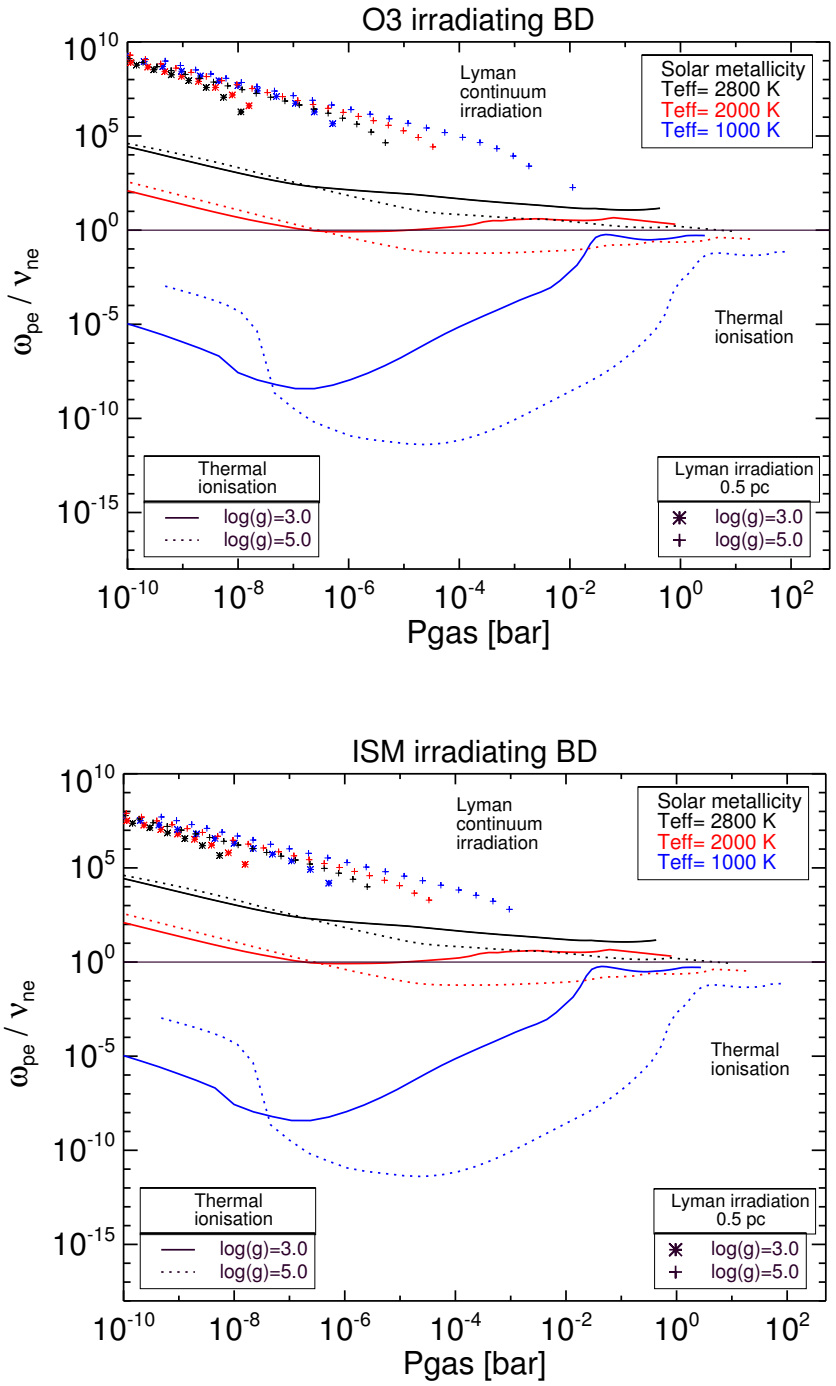

Figure 3.5: The ratio of plasma frequency of the electrons and the frequency of the collisions between neutral and electrons under the effect of Lyman continuum irradiation compared to the effect of thermal ionisation on brown dwarf atmospheres for different T_{eff}. **Top:** An O3 star irradiating a BD at a distance of 0.5 pc (star forming region). **Bottom:** The ISRF irradiating a BD. In both panels young brown dwarf atmospheres (log(g)=3.0) and old brown dwarf atmospheres (log(g)=5.0) are plotted.

3.3.2.4 Magnetic parameters

In previous sections, the degree of ionisation and the plasma frequency have been quantified and shown how they are affected by the Lyman continuum irradiation compared to thermal ionisation in a substellar atmosphere. In this section, I show if and how the magnetic coupling changes due to photoionisation from an external Lyman continuum irradiation. In Chapter 2 it was affirmed that for a gas to be magnetised, the cyclotron frequency, $\omega_{c,s}$ needs to be larger than the collisional frequency, $\nu_{n,s}$. For fulfilling this criterion, $\omega_{c,s} \gg \nu_{n,s}$, a critical magnetic flux is required that is given by Eq. 2.10. Figure 3.6 shows that electrons can be magnetised under the effect of the Lyman continuum irradiation from an O3 star compared to the effect of thermal ionisation in the upper M-dwarf, brown dwarf and giant gas planet atmospheres which confirms the results seen in Chapter 2:

- For atmospheres with T_{eff}=2800 K (M-dwarfs and young brown dwarfs) the background magnetic field flux B= 10^3 G can magnetise the ambient electrons at $p_{gas} < 5 \cdot 10^0$ bar.
- For atmospheres with T_{eff}=1000 K (giant gas planets) the background magnetic field flux B= 10^0 G can magnetise the electrons at $p_{gas} < 5 \cdot 10^{-2}$ bar (z $< 4 \cdot 10^8$ cm).

The magnetic Reynolds number provides a measurement of the diffusivity of the magnetic field in a given atmospheric gas (see Eq. 2.16). Figure 3.7 shows the magnetic Reynolds number as the result of the thermal ionisation plus the photoionisation by Lyman continuum irradiation from an O3 star and from the ISM. The results from Fig. 3.7 suggest that:

- A decrease of T_{eff}, for a given $\log(g)$ and [M/H], causes a decreasing of z where $R_m \gg 1$ is fulfilled, hence a smaller atmospheric volume.

- An ideal MHD behaviour ($R_m \gg 1$) can be considered in the upper atmosphere due to the significant increase of the electron density ($R_m \propto n_e$) by the effect of the Lyman continuum irradiation compared to the effect of thermal ionisation (deeper atmosphere) (see Fig. 3.4).

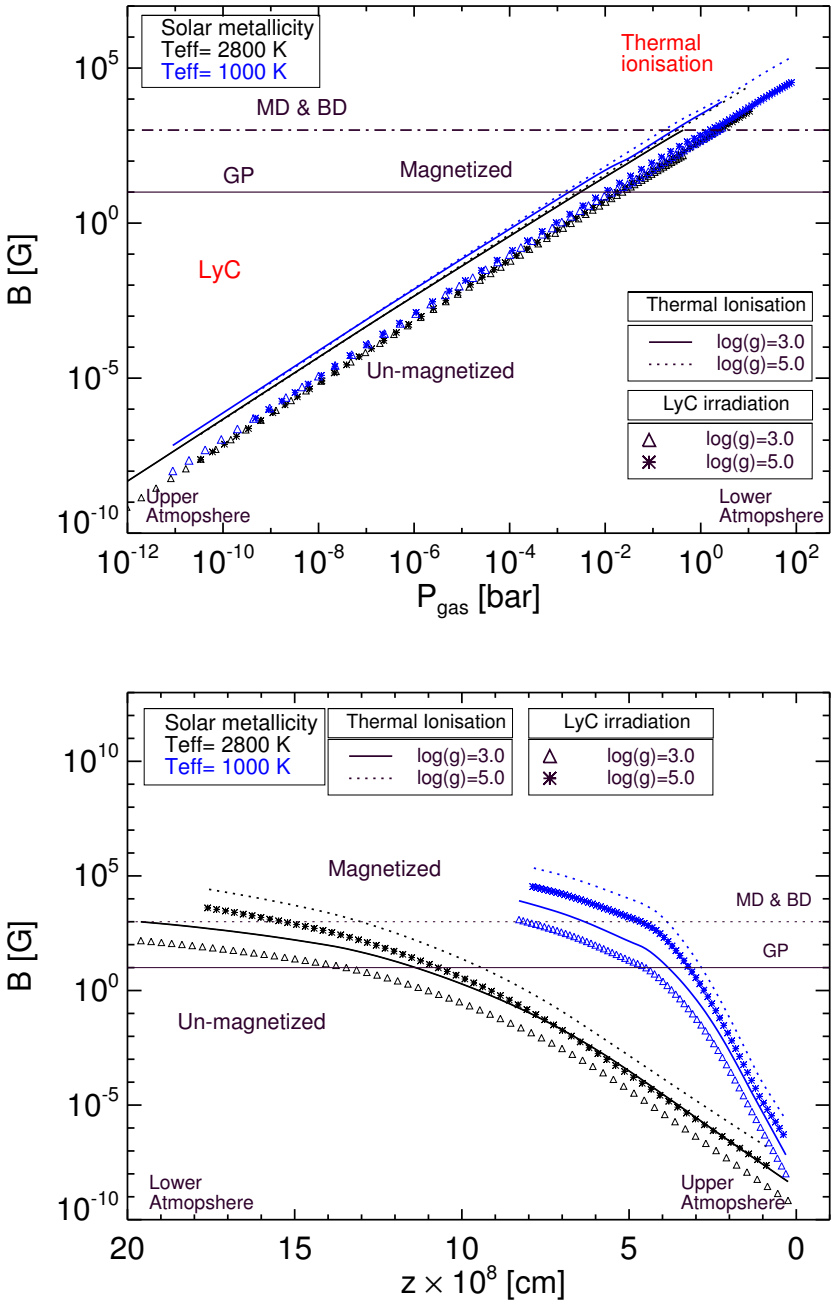

Figure 3.6: The magnetic flux density required for the electrons to be coupled with the background magnetic field in the atmosphere as a function of the local gas pressure, p_{gas} (**top**) and of the geometrical vertical coordinate, z (**bottom**). The effect of Lyman continuum irradiation (**Asterisks** – late M-dwarfs and young brown dwarf atmospheres, log(g)=3.0; **Triangle** – old brown dwarfs, log(g)=5.0) is compared to the effect of the thermal ionisation (**Solid line** – log(g)=3.0; **Dot line** – log(g)=5.0). Brown dwarfs are irradiated from an O3 star at a distance of 0.5 pc in a star forming region.

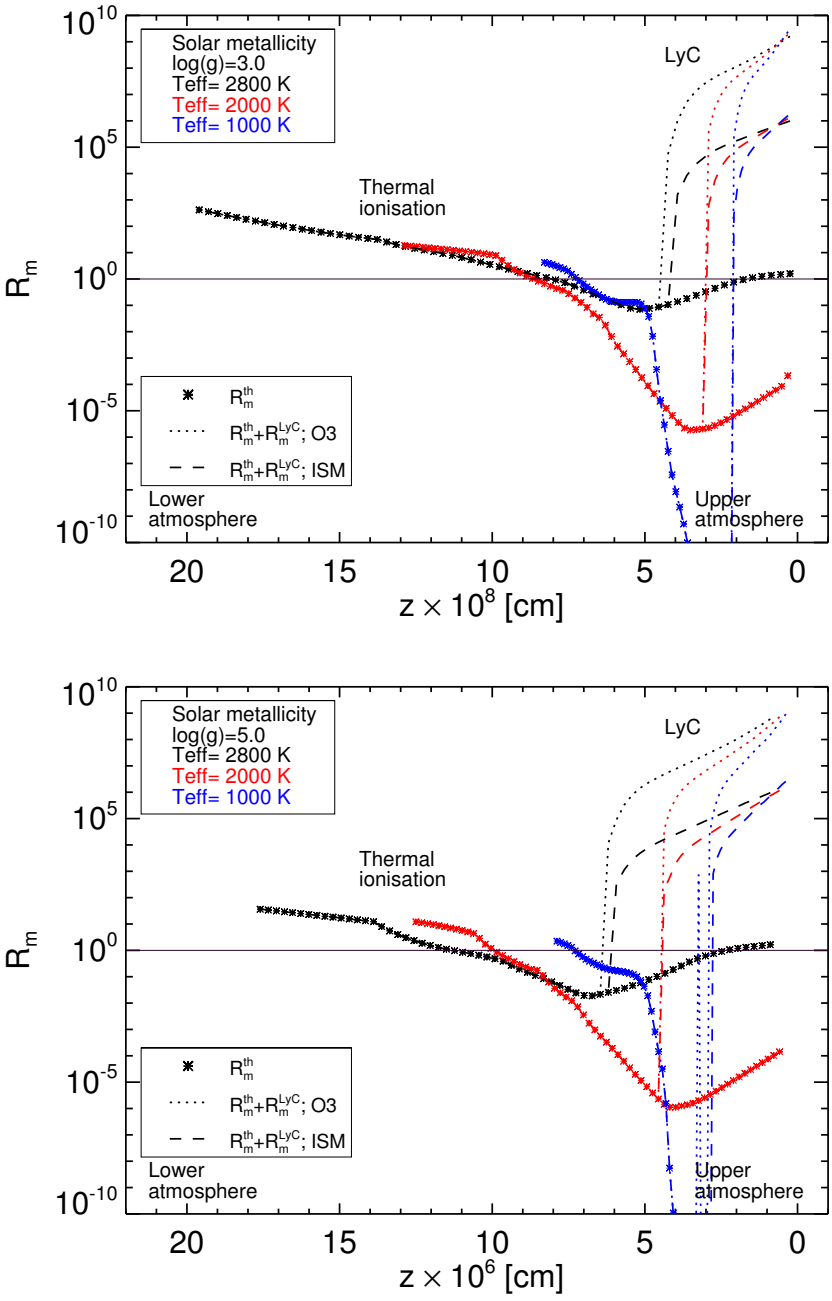

Figure 3.7: The magnetic Reynolds number, R_m, is calculated for atmospheres with T_{eff}=2000 K, 2800 K and with $\log(g) = 3.0, 5.0$ assuming a flow speed of $v_{flow} = 10^6$ cm s^{-1}. I consider a star forming region with an O3 star irradiating a brown dwarf at a distance of 0.5 pc and also the effect of the irradiation from the ISM. **Top:** Young brown dwarf atmospheres. **Bottom:** Old brown dwarf atmospheres.

3.3.2.5 The resulting luminosity from free-free emission

If I assume that the uppermost atmosphere of ionised brown dwarfs from the Lyman continuum irradiation is optically thin, the resulting luminosity from free-free emission can be estimated from the Eq. 3.2-3.4. Figure 3.8 shows the resulting luminosity from free-free emission of a brown dwarf that is ionised by Lyman continuum irradiation from an O3 star in a star forming region and from the ISM. The resulting luminosity produced might be enough to explain the observations from brown dwarfs at X-ray energies (Sicilia-Aguilar et al. 2008; Kashyap, Drake & Saar 2008; Forbrich & Preibisch 2007; Feigelson et al. 2003). The emissivity is very low if the emitting part of the atmosphere would be in LTE and emit with the local LTE gas temperature according to Fig. 2.1. Schmidt et al. (2015) present the H_α emission from of ultra cool (M7-L8) brown dwarfs and suggest that the understanding of these observations requires the presence of a chromosphere. Therefore, higher local gas temperatures are tested which maybe more representative for a chromosphere or corona: $T_{gas} = 10^5$ K (Schmidt et al. 2015) and $T_{gas} = 10^6$ K (Forbrich & Preibisch 2007). Sicilia-Aguilar et al. (2008) (their Table 2) and Forbrich & Preibisch (2007) (their Table 3) show the emitted X-ray luminosity at the range of energy of 0.2 ... 8 KeV of potential low mass and young stellar objects in the Coronet cluster (star forming region) being several of them identified as brown dwarfs. Forbrich & Preibisch (2007) suggest that the candidate brown dwarf B185839.6-365823 (Neuhäuser et al. 1999), with a $L_x \sim 2.7 \cdot 10^{28}$ erg s^{-1}, shows a high plasma temperature according with its fitted spectrum.

The M8.5 brown dwarf, B185831.1-370456, was observed and checked by Neuhäuser et al. (1999) resulting with a luminosity from free-free emission of $L_x \sim 8 \cdot 10^{26}$ erg s^{-1}. Neuhäuser & Comerón (1998) report a ~ 1 Myr old brown dwarf (Cha H_α 1) with a quiescent emission at X-ray (L_x=10^{28} erg s^{-1}) and also a list of brown dwarf candidates ($< 0.08\,M_\odot$) emitting at X-rays wavelengths. They predict that, as the interior of the brown dwarfs is quite close to the late type stars, a magnetic activity must be present to explain those observations. Feigelson et al. (2003) detect 525 objects in a massive cluster (Orion nebula) at the energies of 0.5 ... 8 KeV (X-rays); 144 of those objects observed are cataloged as brown dwarfs (logM $\leq$0.2 M$\odot$) (their Table 1) with an average of the X-ray emitted luminosity of log Lx $\approx$ 28.84 erg s^{-1}. *Those observations confirm the need of the presence of a chromosphere at the outermost part of the atmosphere of brown dwarfs*.

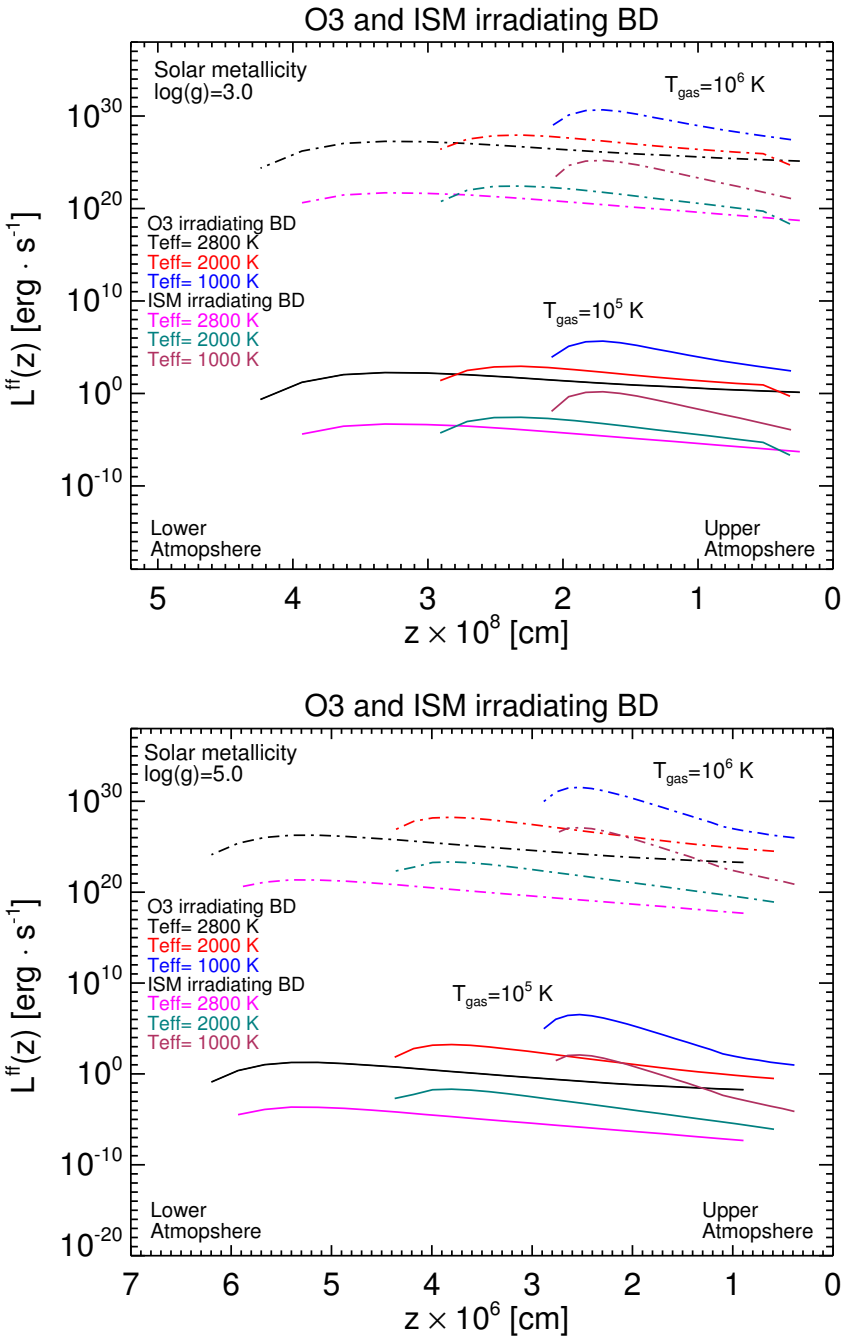

Figure 3.8: The luminosity, $L^{ff}(z)$ [erg s^{-1}], resulting from free-free emission in the energy interval 0.5 . . . 8 KeV (X-rays) in a star forming region with an O3 star irradiating a brown dwarf at a distance of 0.5 pc. Also the effect of the irradiation from the ISM is considered here. The results were calculated for two local gas temperatures: T_{gas}=10^5 K (**solid line**); T_{gas}=10^6 K (**dot-dash line**) which represent chromospheric and coronal temperatures, respectively. **Top:** Young brown dwarf atmospheres. **Bottom:** Old brown dwarf atmospheres.

Table 3.3: The X-ray resulting luminosity (upper limits) from free-free emission, L^{ff}_{tot} [erg s^{-1}] (Eq. 3.4), of a BD (T_{eff}=2800 K, 2000 K, 1000 K; log(g)=3.0, 5.0) irradiated from an O3 star for d= 0.5 pc in a star forming region, from a WD star for d=0.006 AU in a binary system and from the ISM at the interval energy 0.5 ... 8 KeV (X-rays). The local gas temperature has been considered as T_{gas} =10^5 K and T_{gas}=10^6 K assumed as chromospheric and corona temperatures.

L^{ff}_{tot} [erg s^{-1}]

Source	T_{eff} [K]	T_{gas}=10^5 K		T_{gas}=10^6 K	
		log(g)=3.0	log(g)=5.0	log(g)=3.0	log(g)=5.0
O3	2800	$1.79{\cdot}10^{2}$	$8.52{\cdot}10^{1}$	$7.03{\cdot}10^{27}$	$8.6{\cdot}10^{26}$
	2000	$3.39{\cdot}10^{3}$	$7.42{\cdot}10^{3}$	$3.43{\cdot}10^{28}$	$7.52{\cdot}10^{28}$
	1000	$1.57{\cdot}10^{6}$	$1.24{\cdot}10^{7}$	$1.59{\cdot}10^{31}$	$1.25{\cdot}10^{32}$
B0	2800	2.08	1.17	$2.11{\cdot}10^{25}$	$1.19{\cdot}10^{25}$
	2000	$3.51{\cdot}10^{1}$	$1.02{\cdot}10^{2}$	$3.56{\cdot}10^{26}$	$1.04{\cdot}10^{27}$
	1000	$5.66{\cdot}10^{3}$	$1.56{\cdot}10^{5}$	$5.73{\cdot}10^{28}$	$1.58{\cdot}10^{30}$
ISM	2800	$1.82{\cdot}10^{-3}$	$1.00{\cdot}10^{-3}$	$1.85{\cdot}10^{22}$	$1.02{\cdot}10^{22}$
	2000	$1.03{\cdot}10^{-2}$	$8.87{\cdot}10^{-2}$	$1.04{\cdot}10^{23}$	$8.98{\cdot}10^{23}$
	1000	5.24	$1.44{\cdot}10^{2}$	$5.3{\cdot}10^{25}$	$3.98{\cdot}10^{32}$
WD	2000	——	$8.31{\cdot}10^{12}$	——	$8.42{\cdot}10^{37}$
	1000	——	$2.52{\cdot}10^{16}$	——	$2.55{\cdot}10^{41}$

Table 3.3 provide the resulting luminosity from free-free emission, L^{ff}_{tot} , calculated along of the upper of atmosphere (where the effect of Lyman continuum irradiation is considered). The value of L^{ff}_{tot} (Eq. 3.4) for each brown dwarf atmosphere and for each local gas temperature T_{gas} is quite close to the upper limit of $L^{ff}(z)$ (Fig. 3.8) for the corresponding atmosphere. Figure 3.8 shows that the resulting luminosity from free-free emission in the energy interval 0.5 ... 8 KeV increases if:

- the object forms a chromosphere with a substantially increase temperature compared to LTE values.
- the T_{eff} decreases.
- the surface gravity increases.

The results of L^{ff}_{tot} for a given atmosphere structure can be comparable with the observations described above if the corona like temperature is $T_{gas} \geq 10^6$ K. That means that an additional mechanisms are required to heat the corona until reach such temperature even considering the Lyman continuum photoionisation. For $T_{gas} < 10^6$ K, the atmospheric gas shows a very low resulting X-ray luminosity, however, it might be able to emit at wavelengths longer than X-ray

(e.g mid-UV, IR, radio). *Therefore the most suitable brown dwarf / substellar object that may emit at X-ray energies, irradiated from an O3 star, a B0 star or from the ISM, are those that have formed a chromosphere/corona like temperature increase above the classical LTE (local thermal equilibrium) atmosphere*. The resulting X-ray luminosity for a white dwarf-brown dwarf binary system is higher than given for the irradiation from O/B stars or from the ISM. This case will be discussed in Sec. 3.3.3.4.

3.3.3 Application to a white dwarf - brown dwarf binary

The approach of Chapter 3 is to quantify how the ionisation structure of the rich hydrogen gas on brown dwarf atmospheres changes in different environments. In Sec. 3.3.1 and 3.3.2 was studied the influence of the ISM and from high mass stars on brown dwarf atmospheres. In this section, the effect of Lyman continuum photoionisation on the upper atmosphere of a brown dwarf irradiated from a white dwarf is study. As an example of a white dwarf-brown dwarf binary system, I have taken the binary system WD0837+185 composed by a cool white dwarf and an old brown dwarf with an orbital separation of d=0.006AU (Casewell et al. 2012). A binary system composed of a white dwarf and a low mass companion with a close orbital separation (<3 AU) are very rare. The lack of knowledge of a good number of these systems might be due to the formation mechanism involved (Casewell et al. 2013, 2012). Most of the substellar companions of Sun like stars are planets and/or some brown dwarfs. It is not very well known how a low mass companion survives to the evolution of its host star when becomes a red giant (Maxted et al. 2006). The chosen binary system WD0837+185 is one of the four white dwarf-brown dwarf binary system known until date (Casewell et al. 2015). The advantages in choosing this type of system is that brown dwarfs are well characterised and their atmosphere modelling are more advanced than for the exoplanets. Another advantage is the brown dwarfs are relatively bright even more than their white dwarfs in some wavelengths (e.g. K band and longer wavelengths) (Casewell et al. 2015).

3.3.3.1 The effect of Lyman continuum irradiation on the atmospheric electron budget

In this section, the effect of Lyman continuum irradiation from a white dwarf on the atmosphere of its brown dwarf companion is studied and compared to the effect from the ISM. Figure 3.9 (top panel) shows the degree of the ionised gas (see Eq. 2.1) quantified by the electrons produced from thermal ionisation and Lyman continuum irradiation. Figure 3.9 suggests

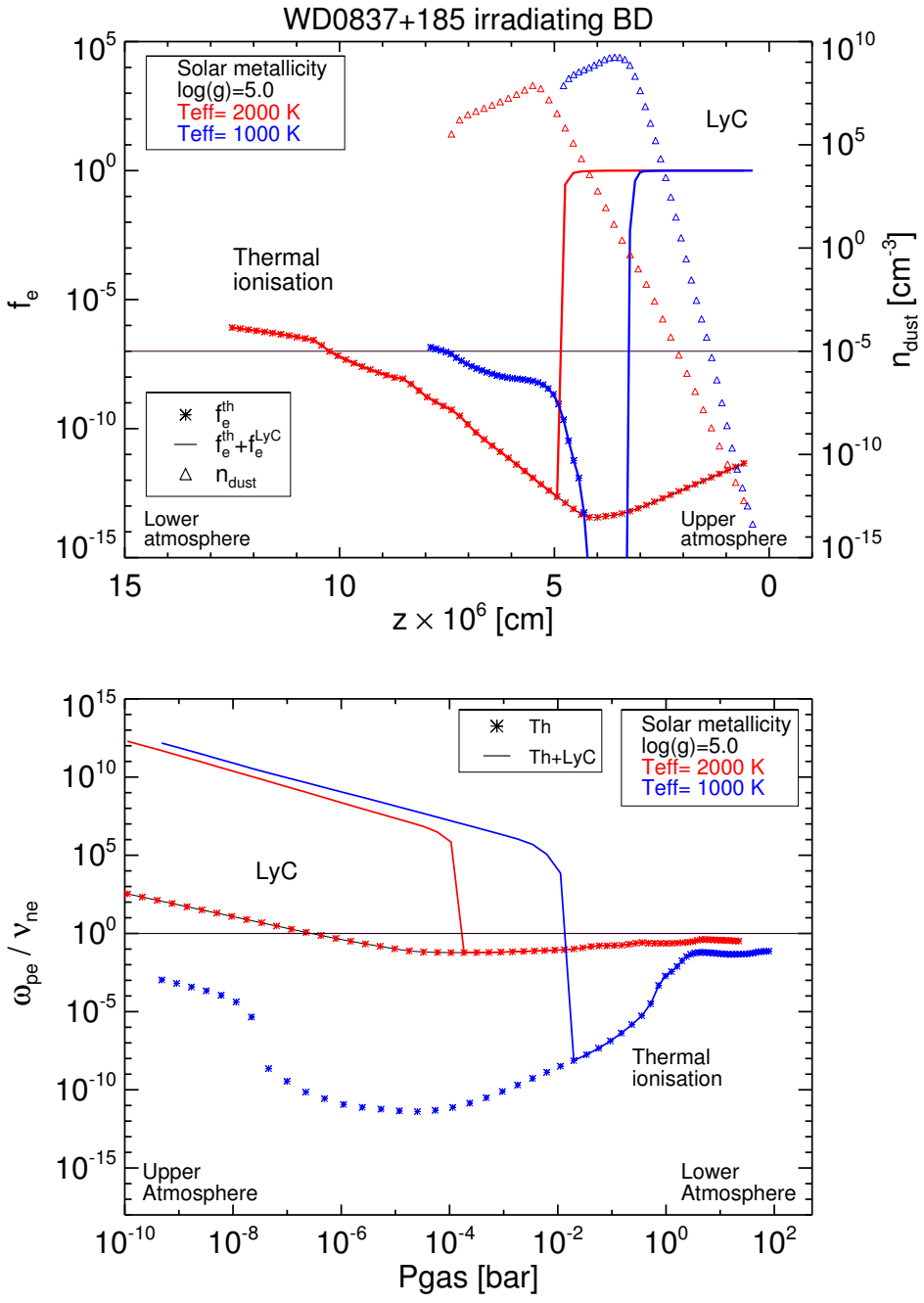

Figure 3.9: The effect of thermal ionisation and Lyman continuum irradiation on the brown dwarf atmospheres for different T_{eff} in a binary system irradiated from a WD star at a distance of d=0.006 AU. **Top:** Degree of thermal ionisation plus Lyman continuum irradiation (Eq. 2.1). Brown dwarf atmospheres can only be thermally ionised in deeper layers. However, brown dwarf upper layers can be easily ionised by Lyman continuum irradiation. **Bottom:** The ratio of plasma frequency of collisions between neutral particles and electrons. Electromagnetic interactions dominate over electron-neutral interactions if $\omega_{pe}/\nu_{ne} \gg 1$.

that at small geometrical extensions (counted from the top) of the atmosphere, the predominant ionisation process is Lyman continuum irradiation that ionises completely the upper atmosphere for T_{eff}=2000-1000 K (given a log(g)) and decreased at certain point (z=10^7 cm) of the atmosphere while thermal ionisation starts to ionise the atmospheric gas for z $> 7 \cdot 10^6$ cm (Sec. 2.3.1). Also Fig. 3.9 shows that dust cloud is not affected for the degree of ionisation and electron density at upper atmosphere. However, we can speculate how far Lyman continuum photoionisation could affect to the cloud charged particles by the strong effect of the local degree of ionisation. In that case, the cloud charged particles can be destroyed by Coulomb explosion if the electrostatics forces are larger than the bond energy inside the dust particles (Stark, Helling & Diver 2015). In this scenario, lightning may also be possible. Figure 3.10 shows the electron number density, n_e [cm^{-3}] for the same atmosphere structures and suggests that the effect of Lyman continuum irradiation is considerably larger than from the ISM (see Table 3.1).

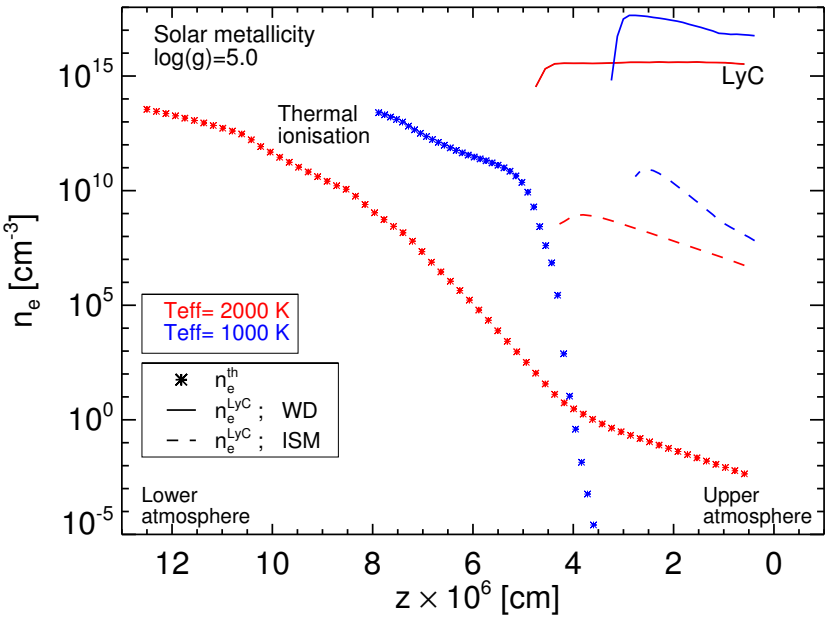

Figure 3.10: The electron number density as result of the Lyman continuum irradiation from a white dwarf a old brown dwarf in a white dwarf - brown dwarf system: **Solid lines** – Lyman continuum irradiation from a white dwarf at d=0.006 AU, **Dashed Lines** – Lyman continuum irradiation from the ISM, **Asterisks** – thermal ionisation. The thermal ionisation determines the electron density in the inner part of the brown dwarf atmosphere; the effect of Lyman continuum irradiation increases the electron density in the outer parts.

Table 3.4: The electron number density, n_e [cm^{-3}] as result of the effect of Lyman continuum irradiation from a WD star at a distance of d=0.006 AU in a binary system and from the ISM on a BD (T_{eff}=2000 K, 1000 K; log(g)=5.0).

Source	T_{eff} [K] log(g) = 5.0	n_e [cm^{-3}] max value
WD	2000	$3.59 \cdot 10^{14}$
	1000	$2.09 \cdot 10^{16}$
ISM	2000	$8.81 \cdot 10^{8}$
	1000	$4.77 \cdot 10^{10}$

3.3.3.2 Plasma parameter

As it was defined in Sec. 2.2, the plasma frequency $\omega_{p,e}$ quantifies the dominance of electromagnetic interactions over collisions. The results from Fig. 3.9 (bottom panel) demonstrates that the collective long-range electromagnetic interactions dominate over the collisions between electron and neutral particles at $p_{gas} \leq 10^{-4}$ bar for the atmosphere with T_{eff}=2000 K and at $p_{gas} \leq 10^{-2}$ bar for the coldest atmosphere with T_{eff}=1000 K. The comparison of those results with the results given by Sec. 2.3.2 shows that Lyman continuum irradiation increases the atmospheric volume where the collective long-range electromagnetic interactions dominate by six orders of magnitude in pressure, hence, expand the affected region higher in the atmosphere.

3.3.3.3 Magnetic parameters

The effect of Lyman continuum irradiation on the magnetic parameters is quantified to show how far the magnetic coupling changes by the effect of a WD-irradiation. For a gas to be magnetised, the cyclotron frequency of the electrons, $\omega_{c,e}$ needs to be larger than the collisional frequency, $\nu_{n,e}$. Figure 3.11 demonstrates that electrons can be magnetised in the brown dwarf and giant gas planet atmospheres.

- For atmospheres with T_{eff}=2000 K (covering brown dwarfs) the background magnetic field flux, B= 10^3 G can be magnetised the electrons at $p_{gas} < 5$ bar.
- For atmospheres with T_{eff}=1000 K (giant gas planets) the background magnetic field flux, B=10 G can be magnetised the electrons at $p_{gas} < 5 \cdot 10^{-2}$ bar.

Figure 3.12 shows the magnetic Reynolds number as the result of Lyman continuum irradiation by the irradiation of a WD and from the ISM compared to the effect of thermal ionisation:

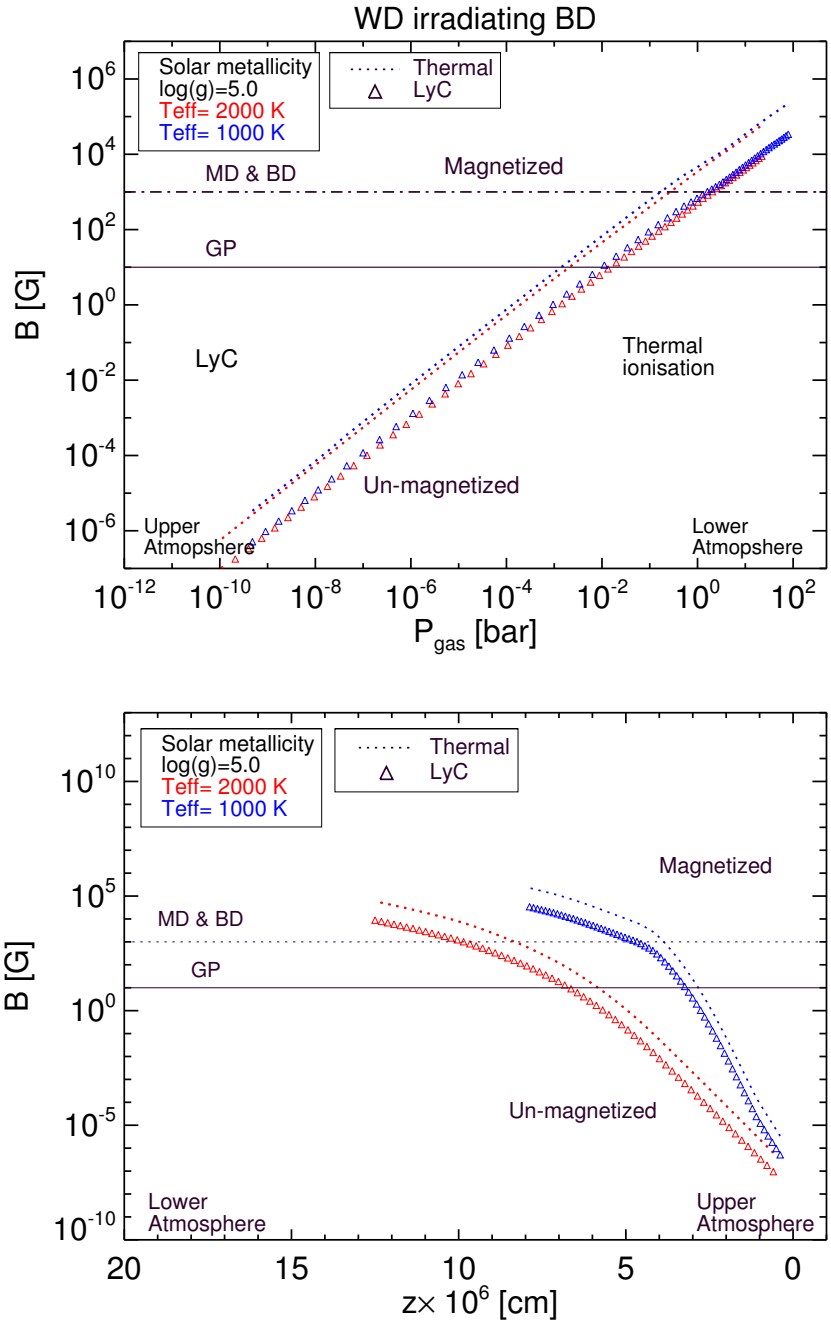

Figure 3.11: Magnetic flux density required for the electrons to be coupled with the background magnetic field present in the objects as a function of the local gas pressure, p_{gas} (**top**) and of the geometrical vertical coordinate, z (**bottom**). The effect of Lyman continuum irradiation (**Triangle**) is compared to the effect of the thermal ionisation (**Dot line**) in a binary system with a WD star irradiating a brown dwarf at a distance of d=0.006 AU.

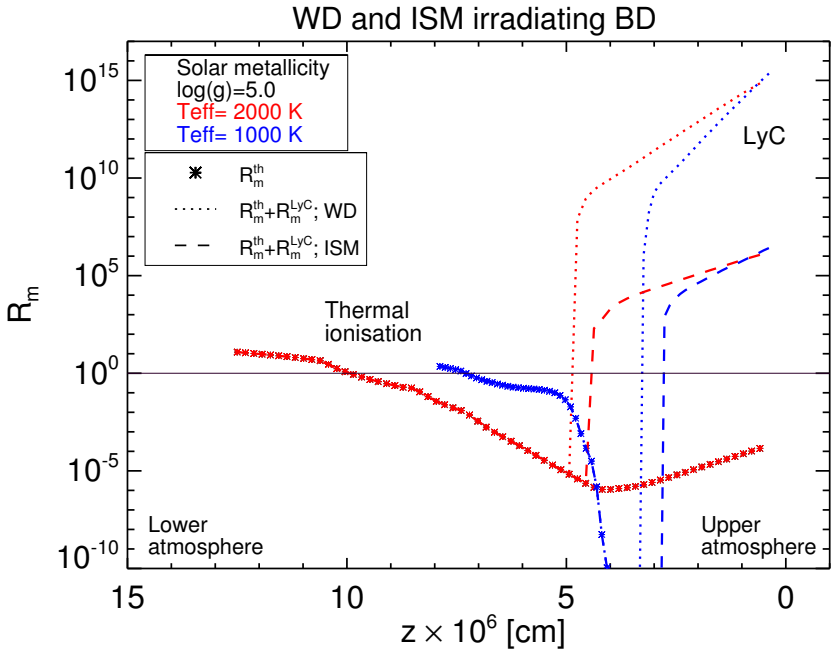

Figure 3.12: The magnetic Reynolds number R_m is calculated for atmospheres with T_{eff}=2000 K, 1000 K and $\log(g) = 3.0, 5.0$ assuming a flow speed of $v_{flow} = 10^6$ cm s^{-1}. I consider a binary system with a WD star irradiating a brown dwarf at a distance of d=0.006 AU and the effect of the irradiation of the ISM.

- A decrease of T_{eff}, for a given $\log(g)$ and [M/H], causes a decreasing of the geometrical extension of the effected atmosphere volume where $R_m > 1$ is fulfilled.

- An ideal MHD behaviour ($R_m > 1$) can be considered in the upper part of the atmosphere due to the significant increase of the electron density ($R_m \propto n_e$) by the effect of the Lyman continuum irradiation compared to the effect of thermal ionisation (in deeper parts of the atmosphere) (see Fig. 3.4).

3.3.3.4 Resulting luminosity from free-free emission

The resulting luminosity from free-free emission, $L^{ff}(z)$, from an optically thin ionised hydrogen gas can be derived from the Eq. 3.2 (Sec. 3.2). Figure 3.13 shows the results of the resulting luminosity from free-free emission (thermal Bremsstrahlung irradiation) of a brown dwarf that is ionised by Lyman continuum irradiation from a WD star in a white-dwarf-brown-dwarf system and from the ISM. This resulting luminosity might be enough to explain the observations from brown dwarfs at X-ray energies. In this study, the X-ray emission from non-accreting low mass objects is considered (Czesla, Schneider & Schmitt 2008; Stelzer et al. 2006). The emissivity is very low if the local atmospheric temperature is applied (Fig. 2.1):the atmosphere

models utilised here do not take into account the presence of a chromosphere/corona. In the calculations of the resulting luminosity from free-free emission, I have applied a higher temperature, which maybe more representative for a chromosphere/corona. The results from the Table 3.3 shows that L^{ff}_{tot} (Eq. 3.4) is larger in a white-dwarf-brown-dwarf system than in a considered star forming region or even in the ISM due to the close orbital separation between the white dwarf and the brown dwarf.

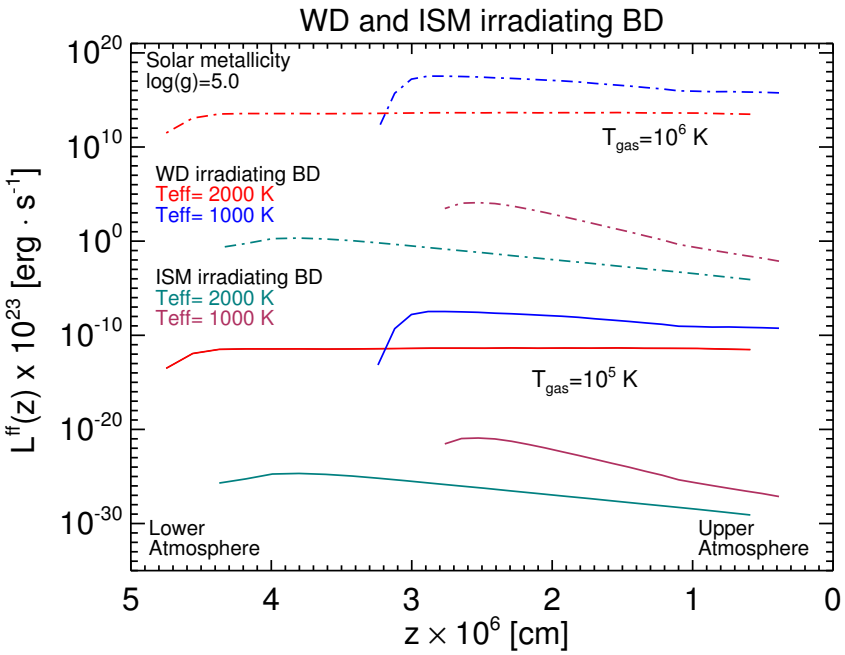

Figure 3.13: The resulting luminosity from free-free emission, $L^{ff}(z)$ integrated over the range of energies 0.5 . . . 8 KeV (X-rays). A binary system with a WD star irradiating a brown dwarf at a distance of d=0.006 AU and by the effect of the ISM irradiation are considered here. Results were calculated for two local gas temperatures: T_{gas}=10^5 K (**solid line**); $T_{gas} = 10^6$ K (**dot-dash line**) assumed as chromospheric/corona temperatures.

4

Discussion and conclusions

This section discuses the results presented in Chapters 2 and 3 with respect to previous publications. The conclusions reflect that ultra-cool atmospheres with high T_{eff}, high [M/H] and low $\log(g)$ have a large fraction of atmospheric volume where plasma processes occur, and are therefore the best candidates for radio, X-ray and H_α emissions. The results show that thermal ionisation is sufficient to produce a partially ionised gas in cool brown dwarfs and giant gas planets and a highly ionised gas in the hotter/younger brown dwarfs or M-dwarfs. However, for low effective temperatures and high surface gravities, an additional mechanisms are needed to ionise the upper atmosphere sufficiently such that X-ray and radio emission may become possible. This study supports the idea that cool objects as brown dwarfs could have a chromosphere/corona.

4.1 Observations in ultra-cool objects: the need of the existence of a chromosphere/corona.

Unexpected powerful emissions at radio, X-ray and H_α wavelengths from very low-mass objects (ultra-cool dwarfs) have been observed for different authors (e.g. Williams et al. 2014; Burgasser et al. 2013; Berger (2002); Route & Wolszczan 2012). A magnetised plasma and the presence of a chromosphere/corona seem required and must be sustained. In brown dwarfs, an efficienct dynamo mechanism must exist to generate a large-scale magnetic field in such ultra-cool objects (Cook, Williams & Berger, 2014). Sorahana, Suzuki & Yamamura (2014) and Schmidt et al. (2016, 2015) suggest the presence of chromospheres in brown dwarfs. They represent a potential chromospheric heating by an increased of the temperature structure of each object with a constant temperature. In this context and to keep the hydrostatic equilibrium, they assume a ideal gas in terms of gas pressure only, $p_{\text{gas}} = nkT(r)$ but, reducing the density of the gas in the upper atmosphere of their 1D model atmosphere which allows a considerably better data fit of their observation. Schmidt et al. (2015) use a comparable approach replacing the outer atmospheric temperature of BT-settle model atmospheres (Allard, Homeier & Freytag 2011) with a chromospheric temperature structure (see their Fig. 8). Nichols et al. (2012) study the properties of radio emissions in ultra-cool dwarfs with the concurrence of an auroral region. They suggest that the coupling between the present plasma and the magnetic field (magnetic coupling) has an effect on the angular velocity of high-latitude ionosphere regions reducing it and generating auroral processes. A loss of particles to the ionosphere is suggested in this process. Speirs et al. (2014) describe a theoretical approach for cyclotron radio emission from Earth's auroral region showing that the radiation results from a backward-wave cyclotron-maser emission process. Also Tanaka, Suzuki & Inutsuka (2014) support the formation of a chromosphere in brown dwarfs suggesting that energy from the convective part of the atmosphere might be transported through the upper atmosphere by magneto-convection processes by Alfvén wave heating (Mullan & MacDonald 2016; Reep & Russell 2016; Brady & Arber 2016).

4.1.1 Thermal ionisation in brown dwarf atmospheres

If the atmospheric gas is well coupled with the background magnetic field in brown dwarfs and giant gas planets, the kinetic energy carried by large-scale convective motions may be transported to the top of the atmosphere and could lead to the formation of a chromosphere or corona. Mohanty et al. (2002) carried out a study of magnetic field diffusivity and the magnetic coupling (quantified by the Reynolds number) to explain why the chromospheric H_α activity in brown dwarfs is lower than in early M-dwarfs. Mohanty et al. (2002) based their work on a grid of model atmospheres (mid-M and L dwarfs) in a parameter range $T_{eff} = 3000\,K..1500\,K$, $\log(g)$=5.0 and [M/H]=0.0. They explained why the observation of chromospheric levels activity are lower than early M-dwarfs, considering mid-M and L dwarfs as rapid rotators. In this work, I used an extended model atmosphere grid until $T_{eff} = 1000\,K$ and I include atmosphere structures with different values of $\log(g)$ and [M/H] (Table 2.1). A LTE is assumed in this work. Mohanty et al. (2002) affirm that the brown dwarf atmosphere is very resistive, quite neutral and with a large collisional neutral-charged particles rate that can dissipate the magnetic field generated at the deeper layers. However, in this work I have shown that also a partially ionised gas is enough to allow a magnetic coupling and that ultra-cool atmospheres could be ionised and treated as an ideal MHD gas only at deep layers.

The results of my study suggest that large volumes of the atmospheric gas are magnetised (Fig. 2.15) even for a low ionisation fraction of the gas (Fig. 2.8) although with a large dominance of electrostatic over neutral-charged particles interactions (Fig. 2.9). The results further suggest not only that higher effective temperatures (in agreement with Mohanty et al. (2002)) and higher metallicity atmospheres are the best candidates for forming a magnetised atmospheric plasma in support of radio, X-ray and H_α observations in ultra-cool objects also for low surface gravity atmospheres. While M-dwarfs have been shown to be fully magnetised, L-dwarfs and later brown dwarfs have smaller atmospheric volume that can be magnetised in an external magnetic field. This findings are related to the activity-vs-SpecT results in Schmidt et al. (2015) (e.g. their Fig. 6). The threshold of $T_{eff} = 2300\,K$ given in their Fig.6 is the Mohanty et al. (2002) threshold that points out the limit from which models fulfil $R_m > 1$ using v= 10^4 cms^{-1} and $10^{-2} \leq \tau_J \leq 10^2$ (convection zone) being τ_J the optical length in J band. In my work the threshold of $T_{eff} = 2300\,K$ is moved towards $T_{eff} = 1400\,K$ for the same value of flow velocity and same region suggesting that atmospheres cooler than $T_{eff} = 2300\,K$ may

be susceptible to be magnetised. Another criterion to consider a magnetised gas is $\omega_{ce} \gg \nu_{ne}$ (see Fig. 2.10). For all models considered in this study (Table 2.1)) the atmospheric gas fulfill $\omega_{ce} \gg \nu_{ne}$ for $p_{gas} < 1$ bar. Combining both criteria $\omega_{ce} \gg \nu_{ne}$ and $R_m > 1$, a large fraction of possible active objects are found for T_{eff}=3000 K-1400 K, log(g)=3.0, [M/H]=0.0 (Group1).

4.1.2 Lyman continuum irradiation in brown dwarf atmospheres

The effect of the irradiation from an external source could ionise the upper atmosphere of those ultracool objects and also allow X-ray emissions from their atmospheres. Feigelson et al. (2003) report the X-ray emission from some brown dwarfs in the Orion nebula. Also Sicilia-Aguilar et al. (2008) and Forbrich & Preibisch (2007) show an emitted X-ray luminosity of some potential low mass and young stellar objects in the Coronet cluster. Neuhäuser et al. (1999) (Table 5) and Neuhauser & Comeron (1998) (Table 1) report a list of brown dwarfs emitting at X-rays wavelengths in the Chameleon I star forming region. They predict that, as the interior of the brown dwarfs is quite close to the late type stars, a magnetic activity must be present to explain those observations. As the upper atmosphere is highly irradiated by an external source, the electron density achieve must be large. Osten et al. (2009) suggest that non-thermal processes are the most suitable for radio brown dwarf emissions, i.e gyro synchrotron. For the brown dwarf (M8) LP 349-25 a continuous particle supply is needed at high latitudes to explain the presence of the cyclotron maser ($n_e \geq 10^{14}$ cm^{-3} for $T_{gas} \sim 10^6$ K; B $\leq 10^2$ G). My results suggest that when an O3 star is irradiating a BD in a star forming region, the electron density for atmospheres with T_{eff}= 1000 K and log(g)= 5.0 is quite close to the electron density $n_e \approx 10^{14}$ cm^{-3} (Table 3.2, Fig. 3.4). Such electron density, $n_e \approx 10^{14}$ cm^{-3}, also is presented at the outer atmosphere when a white dwarf is irradiating a brown dwarf in a binary system (T_{eff}=2000 -1000 K, log(g)= 5.0; Fig. 3.10). However, the irradiation of a B0 star and from the ISM produce electron densities below of $n_e \approx 10^{14}$ cm^{-3} (see Table 3.2) .

An high electron density could also have an effect on the dust cloud layer on brown dwarf atmospheres. Helling et al. (2016) suggest that cloud particles can be destroyed if the electron temperature is $> 10^5$ K. This would occur if a chromosphere-like temperature increase would coincide with some part of the cloud layer where a strong gas ionisation is achieved (only the uppermost atmosphere, Fig. 3.3). Burgasser et al. (2013) suggest that the brown dwarf, 2MASS J13153094-2649513 (L7), emits electrons with temperature of $T \approx 10^9 - 10^{10}$ K and

with a constraint yield of L $\geq$ 1-3 R_{Jup} (L $\approx 10^6$ cm) obtaining an electron plasma density of $n_e \geq 10^9$-10^{10} cm^{-3}. Those values are comparable to my results suggest based on the Lyman continuum irradiation (Fig. 3.4). I have calculated the resulting luminosity from free-free emission (Fig. 3.8) using $T_{gas}=10^5$ K and $T_{gas}=10^6$ K as a corona gas temperatures assuming a length scale of the considered plasma as $L=10^3$ m (Helling et al. 2011b). Those assumed temperatures are lower than the electron temperature derived for 2MASS J13153 (Burgasser et al. (2013)). Another source of ionising photons was presented by Rimmer & Helling (2013) who study the effect of the cosmic rays (CR) on a brown dwarf atmospheres and giant gas planets driving the CR ionisation structure along of the atmosphere. The comparison of their results with my results suggests that Lyman continuum irradiation increases the electron density of the upper atmosphere more than the effect of the cosmic rays for the same model structure atmospheres. Also the magnetic Reynolds number is increased by the effect of Lyman continuum irradiation more than the effect of cosmic rays.

Bilíková et al. (2010) present the emitted X-ray luminosity of white dwarfs at the range of energies of 0.5 ... 8 KeV. In their Table 5 and 6 is shown the emitted X-ray luminosity of different white dwarfs with a given T_{eff} (WD1026+002, 17600 K, $L_x \sim 10^{27}$ erg s^{-1}; WD1347-129, 14220 K, $L_x \sim 10^{29}$ erg s^{-1}). The white-dwarf-brown-dwarf system of my study has a white dwarf with a T_{eff}=14748 K (Casewell et al. 2012) and with a emitted luminosity of $1.76 \cdot 10^{31}$ erg s^{-1} being capable to ionise the lower atmosphere of its companion. It has a extremely small orbital separation between both objects (d=0.006 AU). The white dwarf, WD0837+185, may emit in X-ray according to Bilíková et al. (2010). As WD0837+185 may emit high energy emissions, it is reasonable to expect that its companion, the brown dwarf WD0837+185 (T8), can received such amount of energy and re-emit it. Table 3.3 suggests that the resulting luminosity from free-free emission, L^{ff}_{tot}, for a considered brown dwarf irradiated from a white dwarf is $L_x \sim 10^{12}$ erg s^{-1} for a $T_{gas} = 10^5$ K and $L_x \sim 10^{37}$ erg s^{-1} for a $T_{gas} = 10^6$ K. It is reasonable not to expect a steady X-ray emission from a brown dwarf in a white dwarf-brown dwarf system. Maybe, the X-ray emissions are dominated for flare emissions instead of quiescent emission (Imanishi et al. 2003).

4.2 Conclusions

I present a reference study for late M-dwarfs, brown dwarfs and giant gas planet to identify which ultra-cool objects are most susceptible to atmospheric gas-phase plasma processes. Only thermal ionisation is considered for this reference study and the influence of dust beyond element depletion is neglected. I have shown that all the objects in the star-planet transition regime could potentially emit high-energy radiation if they have a large enough magnetic field and coupled with the atmospheric gas. The next step was to determine the effect of an additional process in order to explain the observed emission. In this study the effect of the Lyman continuum irradiation from an external source on the ionisation structure of brown dwarf atmospheres is discussed and compared to the effect of the thermal ionisation. Also the resulting X-ray luminosity from free-free emission has been calculated from a highly ionised chromospheric region at the top of an ultra-cool atmosphere.

4.2.1 The effect of thermal ionisation

Ultra-cool atmospheres with high $T_{\rm eff}$, high [M/H] and low $\log(g)$ have large fraction of atmospheric volume where plasma processes occur, and are therefore the best candidates for radio, X-ray and H_α emissions. M-dwarfs have a considerable degree of ionisation throughout the whole atmosphere, the degree of thermal ionisation for a L-dwarf is low, however, it might be enough to seed other local ionisation processes like Alfvén ionisation or lightning discharges. Electromagnetic interaction dominates over electron-neutral interactions also in regions of a very low degree of ionisation in most model atmospheres in my sample. The relevant length scales effected by electromagnetic interactions in the gas phase are larger in low-density regions of any atmosphere. The minimum threshold for the magnetic flux density required for electrons and ions to be magnetised is smaller than typical values of the global magnetic field strengths of a brown dwarf and a giant gas planet. A considerably lower magnetic flux density is required for magnetic coupling of the atmosphere in the rarefied upper atmosphere than in the dense inner atmosphere. Even the criterion $\omega_{c,e} \gg \omega_{p,e}$, the required condition for the electron-cyclotron maser instability to be the dominant mechanism to produce radio emission in ultracool dwarfs, is fulfilled at the upper atmosphere. Therefore it is not unreasonable to expect ultra-cool atmospheres (M-dwarfs and brown dwarfs) to emit H_α or even in radio wavelength as in particular the rarefied upper parts of the atmospheres fulfil

plasma criteria easily despite having low degrees of ionisation. Also it might be reasonable to expect the emerge of an ionosphere in brown dwarf and giant gas planet atmospheres and the built-up of a chromosphere.

4.2.2 The effect of the Lyman continuum irradiation

The main observable implication is that the probability of having a larger volume susceptible to emit at high energy levels (e.g at X-ray energies) has considerably increased compared to the thermal ionisation. The effect of the Lyman continuum irradiation have been studied in this work from the ISM, from a massive stars in a star forming region and from a white dwarf in a white dwarf- brown dwarf binary system. The results suggest that the irradiation from O/B stars on brown dwarf atmospheres increases the number of free electrons of the upper atmosphere sufficient to get a plasma and a magnetic coupling between the atmospheric gas and the background magnetic field. The effect of the interstellar radiation field is smaller than the effect of the OB stars, but still substantial compared to the effect of cosmic rays. The very close orbital separation of two bodies allows that the irradiation from the white dwarf on its companion increases the photoionisation of the upper brown dwarf atmosphere. All three cases suggest the presence of a highly ionised, magnetised upper atmosphere in which, for example, Alfvén waves could lead to the emergence of a chromosphere/corona. Given the high probability that such low-mass, ultra-cool atmospheres develop a chromospheric temperature increase above a cloud forming atmosphere, the resulting luminosity from free-free emission was derived and suggest that brown dwarfs/ free floating planets may emit at X-ray wavelengths assuming a local gas temperature of $10^5 \ldots 10^6$ K (chromospheric and corona temperatures). The combination of the effect of Lyman continuum irradiation plus those high coronal temperatures may provide the mechanism to understand the X-ray observation and radio emission from brown dwarf atmospheres. One mechanism that may reach those corona temperatures in brown dwarf atmospheres may be produced by Alfvén waves (Mullan & MacDonald 2016).

4.2.3 Potential observational tests for the proposed theoretical model

The search of brown dwarfs can provide the knowledge of how many brown dwarfs occur as free-floating objects, as part of binary systems and as member of a cluster with a stellar companion. A multi wavelength survey could be performed covering late M spectral type dwarfs and young/old brown dwarfs. One of those scenarios could be an undetected dynamical brown dwarf companion of a massive star in a cluster (whose spectrum suggests an object with a mass below the minimum stellar mass). As brown dwarfs change with the time (the effective temperature, surface gravity and metallicity change) its is reasonable to expect that they evolve as the cluster evolves too.

Figure 3.8 provides the luminosity, $L^{ff}(z)$ $[\mathrm{erg\,s^{-1}}]$, resulting from free-free emission in the energy interval $0.5 \ldots 8$ KeV (X-rays) in a star forming region with an O3 star irradiating a brown dwarf at a distance of 0.5 pc. Also the case of an isolated object in the field (effect of the irradiation from the ISM). The emitted luminosity of the brown dwarf may provide a probe of the evolution of the object (to cooler spectral types: L, T and Y type dwarfs) and also an idea about the evolution of the cluster. Therefore, the emitted luminosity from brown dwarfs depends on the amount of irradiation (emitted flux of the external source) that its atmosphere is receiving, on the distance between the source an the irradiated object and the global parameters of the irradiated object (T_{eff}, $\log(g)$, [M/H]).

It has been showed, how the impact of an external source can play an important role on the ionisation structure of a brown dwarf atmosphere. An observational test would be to observe at different clusters with different ages and different structures (if they content OB type stars or less massive) and check the effect of those parameters on different brown dwarf atmospheres. Currently, this observational test is possible to carry out with the existing resources.

5

Appendix

5.1 Input of model atmosphere simulations DRIFT-PHOENIX

The input quantities for DRIFT-PHOENIX are the following:

- *Effective temperature*, T_{eff} [K], quantifies the total energy output of a particular object. Formally, the effective temperature is defined as the temperature at which an object emits the same radiation of a black body at the temperature. The effective temperature is a variable in the radiative equation.

- *Surface gravity*, $\log(g)$ [$\mathrm{cm\,s^{-2}}$], is the gravitational acceleration measured at the surface of a particular object ($g \propto M/(R+r^2)$). Surface gravity can be used as an age indicator of a object. If the value of $\log(g)$ is small (young object), the extension of its atmosphere is larger than the atmosphere of a object with higher surface gravity (old object). Surface gravity is a variable in the hydrostatic equilibrium equation.

- *Elemental abundances* also called metallicity, [M/H], measures the relative abundances of 'metals' (i.e. elements heavier than H) in the respect to hydrogen. A metallicity of

[M/H]=0.0 corresponds to the same ratio of a heavy to light elements of our Sun (solar abundance). A higher metallicity (e.g. [M/H=+0.3]) indicates an environment richer of heavy elements than our Sun. A lower metallicity (e.g. [M/H=-0.3]) indicates an environment poorer of heavy elements than our Sun.

Besides these fundamental input quantities, there are other quantities (absorption coefficients for the radiative transfer, equilibrium constants for all molecules in the chemical equilibrium, ...) involved in the equations mentioned above. However, I focus on simulating the atmosphere of a particular object changing only the T_{eff}, $\log(g)$ and [M/H].

Bibliography

Allard F., Homeier D., Freytag B., 2011, in Astronomical Society of the Pacific Conference Series, Vol. 448, 16th Cambridge Workshop on Cool Stars, Stellar Systems, and the Sun, Johns-Krull C., Browning M. K., West A. A., eds., p. 91

Antonova A., Hallinan G., Doyle J. G., Yu S., Kuznetsov A., Metodieva Y., Golden A., Cruz K. L., 2013, A&A, 549, A131

Benz A. O., Güdel M., 1994, A&A, 285, 621

Berger E., 2002, ApJ, 572, 503

Berger E. et al., 2010, ApJ, 709, 332

Berger E. et al., 2008, ApJ, 676, 1307

Bilíková J., Chu Y.-H., Gruendl R. A., Maddox L. A., 2010, AJ, 140, 1433

Biller B. A. et al., 2013, ApJL, 778, L10

Boss A. P., 2011, ApJ, 731, 74

Boyd T., Sanderson J., 2003, The physics of plasmas (cambridge)

Brady C. S., Arber T. D., 2016, ArXiv e-prints

Buenzli E., Apai D., Radigan J., Reid I. N., Flateau D., 2014, ApJ, 782, 77

Burgasser A. J., Kirkpatrick J. D., Reid I. N., Liebert J., Gizis J. E., Brown M. E., 2000, AJ, 120, 473

Burgasser A. J., Melis C., Zauderer B. A., Berger E., 2013, ApJL, 762, L3

Burgasser A. J., Putman M. E., 2005, ApJ, 626, 486

Burrows A., Hubbard W. B., Lunine J. I., Liebert J., 2001, Rev. Mod. Phys., 73, 719

Casewell S. L., Burleigh M. R., Lawrie K. A., Maxted P. F. L., Dobbie P. D., Napiwotzki R., 2013, Mem. Societa Astronomica Italiana, 84, 1022

Casewell S. L. et al., 2012, ApJL, 759, L34

Casewell S. L. et al., 2015, MNRAS, 447, 3218

Chabrier G., Küker M., 2006, A&A, 446, 1027

Christophorou L. G., Olthoff J. K., 2004, Fundamental electron interactions with plasma processing gases. Springer

Cook B. A., Williams P. K. G., Berger E., 2014, ApJ, 785, 10

Cooper C. S., Showman A. P., 2005, in Bulletin of the American Astronomical Society, Vol. 37, AAS/Division for Planetary Sciences Meeting Abstracts #37, p. 671

Cravens T. E., 1997, Physics of Solar System Plasma. Cambridge University Press

Crossfield I. J. M. et al., 2014, Nature, 505, 654

Cushing M. C., 2014, in Astrophysics and Space Science Library, Vol. 401, 50 Years of Brown Dwarfs, Joergens V., ed., p. 113

Czesla S., Schneider P. C., Schmitt J. H. M. M., 2008, A&A, 491, 851

Dinklage A., 2005, Plasma physics: confinement, transport and collective effects, Vol. 670. Springer

Diver D. A., 2001, A plasma formulary for physics, technology, and astrophysics. Wiley-VCH

Donati J.-F. et al., 2008, MNRAS, 390, 545

Durney B. R., De Young D. S., Roxburgh I. W., 1993, solphys, 145, 207

Duru F., Gurnett D. A., Morgan D. D., Modolo R., Nagy A. F., Najib D., 2008, Journal of Geophysical Research (Space Physics), 113, 7302

Fazio G. G. et al., 2004, ApJS, 154, 10

Feigelson E. D., Broos P., Gaffney, III J. A., Garmire G., Hillenbrand L. A., Pravdo S. H., Townsley L., Tsuboi Y., 2002, ApJ, 574, 258

Feigelson E. D., Gaffney, III J. A., Garmire G., Hillenbrand L. A., Townsley L., 2003, ApJ, 584, 911

Flaccomio E., Damiani F., Micela G., Sciortino S., Harnden, Jr. F. R., Murray S. S., Wolk S. J., 2003, ApJ, 582, 398

Forbrich J., Preibisch T., 2007, A&A, 475, 959

Fridman A., 2008, Plasma chemistry. Cambridge University Press

Gibson N. P. et al., 2012, MNRAS, 422, 753

Gizis J. E., Burgasser A. J., Berger E., Williams P. K. G., Vrba F. J., Cruz K. L., Metchev S., 2013, ApJ, 779, 172

Green S., Williams I., McDonnell T., McBride N., 2002, Dust in the Solar System and Other Planetary Systems, Cospar. Elsevier Science

Güdel M., Benz A. O., 1993, ApJL, 405, L63

Hallinan G., Antonova A., Doyle J. G., Bourke S., Brisken W. F., Golden A., 2006, ApJ, 653, 690

Hallinan G., Antonova A., Doyle J. G., Bourke S., Lane C., Golden A., 2008, ApJ, 684, 644

Hauschildt P. H., Baron E., 1999, Journal of Computational and Applied Mathematics, 109, 41

Helling C., Casewell S., 2014, arXiv, 22, 80

Helling C., Dehn M., Woitke P., Hauschildt P. H., 2008, ApJL, 675, L105

Helling C., Jardine M., Stark C., Diver D., 2013, ApJ, 767, 136

Helling C., Jardine M., Witte S., Diver D. A., 2011a, ApJ, 727, 4

Helling C., Jardine M., Witte S., Diver D. A., 2011b, ApJ, 727, 4

Helling C., Rimmer P. B., Rodriguez-Barrera I. M., Wood K., Robertson G. B., Stark C. R., 2016, ArXiv e-prints

Helling C., Woitke P., 2006, A&A, 455, 325

Helling C., Woitke P., Thi W.-F., 2008, A&A, 485, 547

Heng K., Showman A. P., 2014, ArXiv e-prints

Hills J. G., 1973, A&A, 28, 63

Hollenbach D. J., Tielens A. G. G. M., 1999, Reviews of Modern Physics, 71, 173

Huang X., Cumming A., 2012, ApJ, 757, 47

Imanishi K., Nakajima H., Tsujimoto M., Koyama K., Tsuboi Y., 2003, PASJ, 55, 653

Inan U. S., Golkowski M., 2010, Principles of Plasma Physics for Engineers and Scientists. Cambridge University Press

Jardine M., Collier Cameron A., Donati J.-F., Gregory S. G., Wood K., 2006, MNRAS, 367, 917

Jess D. B., Mathioudakis M., Crockett P. J., Keenan F. P., 2008, ApJL, 688, L119

Kashyap V. L., Drake J. J., Saar S. H., 2008, ApJ, 687, 1339

Kremer J. P., Pedersen T. S., Lefrancois R. G., Marksteiner Q., 2006, Phys. Rev. Lett., 97, 095003

Kuzmychov O., Berdyugina S. V., Harrington D., 2015, in Cambridge Workshop on Cool Stars, Stellar Systems, and the Sun, Vol. 18, 18th Cambridge Workshop on Cool Stars, Stellar Systems, and the Sun, van Belle G. T., Harris H. C., eds., pp. 441–444

Lang K., 1974, Astrophysical formulae: a compendium for the physicist and astrophysicist. Springer

Luque A., Dubrovin D., Gordillo-Vázquez F. J., Ebert U., Parra-Rojas F. C., Yair Y., Price C., 2014, Journal of Geophysical Research (Space Physics), 119, 8705

Lynch C., Mutel R. L., Güdel M., 2015, ApJ, 802, 106

Maxted P. F. L., Napiwotzki R., Dobbie P. D., Burleigh M. R., 2006, Nature, 442, 543

McCaughrean M. J., Rayner J. T., Zinnecker H., 1994, ApJL, 436, L189

McLean M., Berger E., Reiners A., 2012, ApJ, 746, 23

Menou K., Rauscher E., 2009, ApJ, 700, 887

Mohanty S., Basri G., Shu F., Allard F., Chabrier G., 2002, ApJ, 571, 469

Morin J., 2012, in EAS Publications Series, Vol. 57, EAS Publications Series, Reylé C., Charbonnel C., Schultheis M., eds., pp. 165–191

Mullan D. J., MacDonald J., 2016, ApJ, 818, 154

Nakajima T., Oppenheimer B. R., Kulkarni S. R., Golimowski D. A., Matthews K., Durrance S. T., 1995, Nature, 378, 463

Neuhäuser R. et al., 1999, A&A, 343, 883

Neuhauser R., Comeron F., 1998, Science, 282, 83

Nichols J. D., Burleigh M. R., Casewell S. L., Cowley S. W. H., Wynn G. A., Clarke J. T., West A. A., 2012, ApJ, 760, 59

Oppenheimer B. R., Kulkarni S. R., Stauffer J. R., 2000, Protostars and Planets IV, 1313

Osten R. A., Phan-Bao N., Hawley S. L., Reid I. N., Ojha R., 2009, ApJ, 700, 1750

Osterbrock D., Ferland G., 2006, Astrophysics of Gaseous Nebulae and Active Galactic Nuclei. University Science Books

Parker E. N., 1955, ApJ, 122, 293

Parker E. N., 1975, Annals of the New York Academy of Sciences, 257, 141

Perna R., Menou K., Rauscher E., 2010, ApJ, 724, 313

Pineda J. S., Hallinan G., Kirkpatrick J. D., Cotter G., Kao M. M., Mooley K., 2016, ArXiv e-prints

Pont F., Knutson H., Gilliland R. L., Moutou C., Charbonneau D., 2008, MNRAS, 385, 109

Poppenhaeger K., Robrade J., Schmitt J. H. M. M., 2010, A&A, 515, A98

Preibisch T. et al., 2005a, ApJS, 160, 401

Preibisch T. et al., 2005b, ApJS, 160, 582

Rauscher E., Kempton E. M. R., 2014, ApJ, 790, 79

Rauscher E., Menou K., 2013, ApJ, 764, 103

Rebolo R., Zapatero Osorio M. R., Martín E. L., 1995, Nature, 377, 129

Reep J. W., Russell A. J. B., 2016, The Astrophysical Journal Letters, 818, L20

Reid N., Hawley S. L., eds., 2000, New light on dark stars: red dwarfs, low mass stars, brown dwarfs

Reiners A., Basri G., 2010, ApJ, 710, 924

Reiners A., Christensen U. R., 2010, A&A, 522, A13

Reynolds R. J., 1984, ApJ, 282, 191

Rimmer P. B., Helling C., 2013, ApJ, 774, 108

Rimmer P. B., Helling C., 2015, ArXiv e-prints

Rodríguez-Barrera M. I., Helling C., Stark C. R., Rice A. M., 2015, MNRAS, 454, 3977

Route M., Wolszczan A., 2012, ApJL, 747, L22

Route M., Wolszczan A., 2016, ArXiv e-prints

Schmidt S. J., Hawley S. L., West A. A., Bochanski J. J., Davenport J. R. A., Ge J., Schneider D. P., 2015, AJ, 149, 158

Schmidt S. J. et al., 2016, ArXiv e-prints

Shulyak D., Seifahrt A., Reiners A., Kochukhov O., Piskunov N., 2011, MNRAS, 418, 2548

Sicilia-Aguilar A., Henning T., Juhász A., Bouwman J., Garmire G., Garmire A., 2008, ApJ, 687, 1145

Siess L., Dufour E., Forestini M., 2000, A&A, 358, 593

Sing D. K. et al., 2014, ArXiv e-prints

Sorahana S., Suzuki T. K., Yamamura I., 2014, MNRAS, 440, 3675

Speirs D. C., Bingham R., Cairns R. A., Vorgul I., Kellett B. J., Phelps A. D. R., Ronald K., 2014, Phys. Rev. Lett., 113, 155002

Stark C. R., Helling C., Diver D. A., 2015, A&A, 579, A41

Stelzer B., Micela G., Flaccomio E., Neuhäuser R., Jayawardhana R., 2006, A&A, 448, 293

Sternberg A., Hoffmann T. L., Pauldrach A. W. A., 2003, ApJ, 599, 1333

Tanaka Y. A., Suzuki T. K., Inutsuka S.-i., 2014, ApJ, 792, 18

Tarter J. C., 1975, PhD thesis, California Univ., Berkeley.

Testa P., Saar S., Drake J., 2015, ArXiv e-prints

Trotignon J. G., Séran H.-C., Béghin C., Meyer-Vernet N., Manning R., Grard R., Laakso H., 2001, -, 49, 155

Tsuboi Y., Maeda Y., Feigelson E. D., Garmire G. P., Chartas G., Mori K., Pravdo S. H., 2003, ApJL, 587, L51

Ulmschneider P., Musielak Z., 2003, in Astronomical Society of the Pacific Conference Series, Vol. 286, Current Theoretical Models and Future High Resolution Solar Observations: Preparing for ATST, Pevtsov A. A., Uitenbroek H., eds., p. 363

Williams P. K. G., Berger E., Irwin J., Berta-Thompson Z. K., Charbonneau D., 2014, ArXiv e-prints

Williams P. K. G., Berger E., Zauderer B. A., 2013, ApJL, 767, L30

Witte S., Helling C., Barman T., Heidrich N., Hauschildt P. H., 2011, A&A, 529, A44

Witte S., Helling C., Hauschildt P. H., 2009, A&A, 506, 1367

Woitke P., Helling C., 2003, A&A, 399, 297

Woitke P., Helling C., 2004, A&A, 414, 335

Wood K., Loeb A., 2000a, ApJ, 545, 86

Wood K., Loeb A., 2000b, ApJ, 545, 86

Wright E. L., Mainzer A., Gelino C., Kirkpatrick D., 2011, ArXiv e-prints

Yaroshenko V. V., Miloch W. J., Vladimirov S., Thomas H. M., Morfill G. E., 2011, Journal of Geophysical Research (Space Physics), 116, 12218

Zohm H., 2005, Plasma Physics: Confinement, Transport and Collective Effects, Dinklage A., Klinger T., Marx G., Schweikhard L., eds., Springer Berlin Heidelberg, Berlin, Heidelberg, pp. 75–93